Influence of insulin-induced oxidative stress in genotoxicity and disease

Einfluss von insulininduziertem oxidativem Stress auf Genotoxititität und Krankheit

Doctoral thesis for a doctoral degree at the

Graduate School of Life Sciences (GSLS)

Julius-Maximilians-University of Wuerzburg

Section Biomedicine

Submitted by

Geema Kodandaraman

from

Chennai, India

Wuerzburg, 2021

Submitted on: ……..

Office stamp

Members of the Thesis Committee

Chairperson: Prof. Dr.rer.nat. Christian Janzen

Primary Supervisor: Prof. Dr.rer.nat. Helga Stopper

Supervisor (Second): Prof. Dr.rer.nat. Thomas Haaf

Supervisor (Third): PD. Dr.rer.nat. Robert Hock

Date of Public Defence: ……

Date of Receipt of Certificates: ……

Contents

1. **Introduction** ---------- 1

1.1. Genomic damage and hormones ---------- 1

1.2. Effect of PTEN inhibition on insulin induced genotoxicity. ---------- 8

1.3. Effect of proliferative stress on micronucleus induction ----------10

1.4. Genotoxic outcomes in obese patients with diabetes ----------12

2. **Objective** ----------14

3. **Methods** ----------15

3.1. Cell culture ----------15

3.2. Cytokinesis block micronucleus assay ----------16

3.3. Western blotting ----------17

3.4. Ferric reducing/antioxidant power (FRAP) Assay ----------17

3.5. Reverse transcription polymerase chain reaction (RT-PCR) ----------18

3.6. Mitochondrial membrane potential ----------18

3.7. Oxidative stress microscopic quantification ----------19

3.8. Animal model and treatment ----------20

3.9. Live-cell microscopy ----------20

3.10. Scratch wound healing assay with live cell microscopy ----------22

3.11. Human study ----------22

3.12. Advanced oxidation protein products (AOPP) ----------23

3.13. Statistics ----------23

4. **Results** ----------24

4.1. *In vitro* genotoxicity of insulin in combination with adrenaline ----------24

4.2. Effect of PTEN inhibition on insulin induced genotoxicity ----------36

4.3. Effect of proliferative stress on micronucleus induction ----------45

4.4. Genotoxic outcomes in obese patients with diabetes---57

5. **Discussion**---64

5.1. *In vitro* genotoxicity of insulin in combination with adrenaline---64

5.2. Effect of PTEN inhibition on insulin induced genotoxicity---68

5.3. Effect of proliferative stress on micronucleus induction---71

5.4. Genotoxic outcomes in obese patients with diabetes---74

5.5. Conclusion---76

6. **Summary**---77

7. **Bibliography**---81

Acknowledgements---91

Appendix---93

Permissions for the use of published data in this dissertation---94

Publications---97

CV / Resume---98

Affidavit---101

List of Figures

Figure 1. Insulin and adrenaline signaling pathways and their mechanistic crosstalk. ____ **3**

Figure 2. Schematic diagram of the analysis of the toxicity of mixtures. ____ **5**

*Figure 3. PTEN mediated negative regulation of AKT signalling after insulin stimulation.*____ **9**

*Figure 4. Micronucleus induction in HL60 cells with 100nM insulin and 10µM adrenaline and their combination*____ **24**

Figure 5. Micronucleus induction in HL60 cells with 100nM insulin and 100µM MMS and their combination ____ **25**

*Figure 6. AKT phosphorylation in HL60 cells with 100nM insulin and10µM adrenaline and their combination detected by western blotting*____ **26**

Figure 7. AKT phosphorylation in HL60 cells by western blotting with insulin 100nM and MMS 100µM and their combination ____ **27**

*Figure 8. Micronucleus induction in HL60 cells with insulin 100nM and MK-2206 10nM and their combination*____ **28**

Figure 9. AKT phosphorylation in HL60 cells by western blotting with insulin 100nM and MK-2206 10nM and their combination ____ **28**

Figure 10. Expression of insulin receptor (IR) (340 basepairs) and β2 adrenergic receptor (β2AR) (281 basepairs); Beta actin (116 basepairs) was used as a loading control, as detected by RT-PCR in HL60 cells. ____ **30**

Figure 11. Micronucleus induction in HL60 cells with insulin 100nM, adrenaline 10µM and their combination with the hormone receptor blockers at HNMPA (AM_3) 10nM, propranolol 10µM, respectively. ____ **30**

Figure 12. FRAP assay to test the antioxidant activity of hormone receptor blockers HNMPA(AM3) 10nM, propranolol 10µM and tempol 50µM as positive control. ____ **31**

Figure 13. Micronucleus induction in HL60 cells with insulin 100nM, adrenaline 10µM and their combination with the mitochondrial complex I blocker, rotenone 10nM ____ **32**

*Figure 14. Expression of NOX 1 (293 basepairs), NOX 2 (526 basepairs) and NOX 4 (248 basepairs); Beta actin (116 basepairs) was used as a loading control, as detected by RT-PCR in HL60 cells.*____ **33**

*Figure 15. Micronucleus induction in HL60 cells with insulin 100nM, adrenaline 10µM and their combination with the total NOX assembly blocker, VAS2870 1µM*____ **33**

Figure 16. Micronucleus induction in HL60 cells with insulin 100nM, adrenaline 10µM and their combination with an antioxidant N-acetyl cysteine (NAC), NAC 5mM ____ **34**

*Figure 17. Micronucleus induction in HL60 cells with the mitochondrial complex III blocker Antimycin A (0-10nM)*____ **35**

*Figure 18. Expression of Heat shock protein 70 (HSP70) in wildtype and PTEN Ko mice detected by western blotting*____ **36**

Figure 19. Expression of Hemeoxygenase-1 (HO-1) detected by western blotting in wildtype and PTEN Ko mice ___ ***37***
Figure 20. Micronucleus induction in NRK cells with 100nM insulin (Ins) and 50nM VO-Ohpic and their combination ___ ***38***
Figure 21. DHE fluorescence to measure the ROS induction in NRK cells treated with insulin 100nM and VO-Ohpic 10nM and their combination ___ ***39***
Figure 22. TMRE fluorescence to measure the change in mitochondrial membrane potential in NRK cells treated with insulin 100nM and VO-Ohpic 10nM and their combination ___ ***40***
Figure 23. Micronucleus induction in LLCPK-1 cells with insulin 100nM and VO-Ohpic 50nM and their combination ___ ***41***
Figure 24. DHE fluorescence to measure the ROS induction in LLCPK-1 cells treated with insulin 100nM and VO-Ohpic 50nM and their combination ___ ***42***
Figure 25. TMRE fluorescence to measure the change in mitochondrial membrane potential in LLCPK-1 cells treated with insulin 100nM and VO-Ohpic 2µM and their combination ___ ***44***
Figure 26. Micronucleus induction in Hela-H2B-GFP cells with insulin 2µM and VO-Ohpic 2µM and their combination ___ ***45***
Figure 27. Live cell imaging and scoring micronuclei in Hela-H2B-GFP treated with insulin 2µM and MMS 200µM as positive control ___ ***46***
Figure 28. Scoring the period of mitosis in Hela-H2B-GFP treated with insulin 2µM and MMS 200µM as positive control ___ ***47***
Figure 29. The total number of mitosis in Hela-H2B-GFP treated with insulin 2µM and MMS 200µM as positive control ___ ***48***
Figure 30. Live imaging of the different stages of mitosis after treatment with insulin 2µM and solvent control ___ ***49***
Figure 31. Live imaging of scratch wound healing in Hela-H2B-GFP cells with insulin 2µM and VO-Ohpic 2µM and their combination ___ ***50***
Figure 32. Live imaging of scratch wound healing in Hela-H2B-GFP cells with insulin 2µM and VO-Ohpic 2µM and their combination ___ ***50***
Figure 33. Live imaging of scratch wound healing in Hela-H2B-GFP cells with insulin 2µM and VO-Ohpic 2µM and their combination ___ ***51***
Figure 34. Live imaging of scratch wound healing in Hela-H2B-GFP cells with insulin 2µM and VO-Ohpic 2µM and their combination ___ ***52***
Figure 35. Live imaging of scratch wound healing in Hela-H2B-GFP cells with insulin 2µM and NAC 5mM and their combination ___ ***53***
Figure 36. Live imaging of scratch wound healing in Hela-H2B-GFP cells with insulin 2µM and NAC 5mM and their combination ___ ***54***

Figure 37. DHE fluorescence to measure the ROS induction in Hela-H2B-GFP cells treated with insulin 2µM and VO-Ohpic 2µM and their combination **55**
Figure 38. TMRE fluorescence to measure the ROS induction in Hela-H2B-GFP cells treated with insulin 2µM and VO-Ohpic 2µM and their combination **56**
Figure 39. The graph shows the bodyweight distribution (in kg) of control and obese patients used in this study, n = 10 and n = 27, respectively. **58**
Figure 40. Bodyweight distribution (in kg) of control and obese patients with pre-existing conditions used in this study. **58**
Figure 41. The graph shows the body mass index (BMI) distribution (in kg/m^2) of control and obese patients used in this study, n = 10 and n = 27, respectively. **59**
Figure 42. Body mass index (BMI) distribution (in kg/m^2) of control and obese patients with pre-existing conditions used in this study. **60**
Figure 43. Genotoxicity assessment by alkaline comet assay in peripheral blood mononuclear cells of the control and obese patients, n = 10 and n = 27, respectively. **61**
Figure 44. Genotoxicity assessment by comet assay in peripheral blood mononuclear cells of the control and obese patients with glycated hemoglobin (HbA1C) levels higher than 6 **61**
Figure 45. Genotoxicity assessment by alkaline comet assay in peripheral blood mononuclear cells of the control and obese patients with different pre-existing conditions. **62**
Figure 46. Detection of advanced oxidation protein products as µmoles/mL equivalents of Chloramine-T in the plasma of the control and obese patients used in this study, n = 10 and n = 27, respectively **63**
Figure 47. Detection of advanced oxidation protein products as µmoles/mL equivalents of Chloramine-T in the plasma of the control and obese patients used in this study with pre-existing conditions **63**
Figure 48. Correlation analysis performed in obese patients between: **93**

List of tables

Table 1. List of primer sequences, annealing temperatures, and amplicon size used in RT-PCR for gene expression. 18
Table 2. Characteristics of subjects used in the human study. 57
Table 3. Glycated hemoglobin HbA1C levels in obese subjects. 57
Table 4. Correlation analysis performed between the physiological characteristics and the DNA damage levels among the obese patients used in the human study. 93

1. Introduction

1.1. Genomic damage and hormones

Genotoxicity

DNA damage in germline cells leads to permanent hereditary mutations, while in somatic cells it can lead to malignant transformations and carcinogenesis [1]. The chemicals/agents that induce this kind of damage are genetic toxicants or genotoxins. There are different types of DNA or genomic damage that can be induced, such as breakage of DNA (single or double stranded), DNA adduct formation, DNA oxidation, cross-links and replicative errors [2]. Several techniques for the *in vitro* and *in vivo* evaluation of genomic damage induction are available. In this study, we focus predominantly on the induction of micronuclei (MN), which are extra-nuclear structures that contain chromosome fragments and/or whole chromosomes surrounded by a nuclear membrane [3]. These extra-nuclear fragments are remnants that did not segregate into the daughter nuclei after cell division. MN can be induced by defects in the cell repair machinery and accumulation of DNA damage and chromosomal aberrations.

Endogenous hormones - insulin and adrenaline

Endogenous hormones, produced within the body (e.g., insulin, adrenaline, thyroxine, estrogen, etc.) are desirable in routine cellular metabolic functions and signaling cascades [4]. However, when there is an imbalance in the production and usage of these hormones, they lead to conditions such as high blood sugar, hyperinsulinemia, high blood pressure, growth and developmental defects, cancer progression and so on [5]. Previous studies in *in vitro* and *in vivo* models have shown that insulin and adrenaline mediated DNA damage takes place through the overproduction of reactive oxygen species, causing oxidative DNA damage [6, 7]. Some pathologies related to high insulin levels are hyperinsulinemia, (early) type-2 diabetes mellitus (T2DM), and obesity [8], while hypoglycaemia, haemorrhagic hypotension, and high stress associated cancer progression are associated to high adrenaline levels [9].

Insulin signalling

Insulin signalling influences the overall growth and development in the body, by regulating the molecular pathways involved in protein synthesis, lipid and glucose storage, glycogen synthesis and at the same time preventing ketogenesis and gluconeogenesis. Insulin signalling starts with the binding of insulin molecules to the membrane bound insulin receptor (IR). Then, the insulin receptor substrate (IRS) is phosphorylated which acts on the downstream effector and adaptor proteins, as shown in figure 1 [10]. IRS activates the PI3K and the AKT proteins, which plays a central role in the regulation of glucose transport, protein and lipid synthesis and mitogenic responses. The insulin signalling pathway is especially responsible for pro-proliferative/ anti-apoptotic effects in a variety of cell types. [11] Insulin signalling dysfunction leads to insulin resistance, defective glucose homeostasis and other pathologies which are accompanied by oxidative stress, mitochondrial dysfunction, genomic instability, and inflammation.

Adrenaline signalling

Adrenaline and noradrenaline are catecholamine hormones that are essential for the body's fight or flight response though vasoconstriction, regulation of blood pressure and stimulation of cardiac function. These catecholamine hormones act through transmembrane G protein coupled receptors called the adrenergic receptors: α and β-adrenergic receptors. [12] There are 2 subtypes of the α-adrenergic receptor (α1 and α2) and 3 subtypes of the β-adrenergic receptor (β1, β2 and β3) based on their structure and signalling mechanisms [9]. Indeed, epidemiological studies have shown an association of β2AR genetic polymorphism with obesity, diabetes, and hyperlipidemia [13]. Similarly, the work by [14] has shown that adrenergic stress causes ROS accumulation via the activation of the β2AR receptor signalling leading to DNA damage induction in embryonic stem cells. The β2AR is widely expressed in several tissues including the vasculature, liver, skeletal muscle, adipocytes and cardiac muscle, and therefore participates in cardiac function and body metabolism. The signalling starts with the binding of ligands to the transmembrane β-adrenergic receptor, causing conformational changes, which then binds to a specific G protein, that activates the cyclic adenosine monophosphate (cAMP)-PKA mediated intracellular signalling. [15]

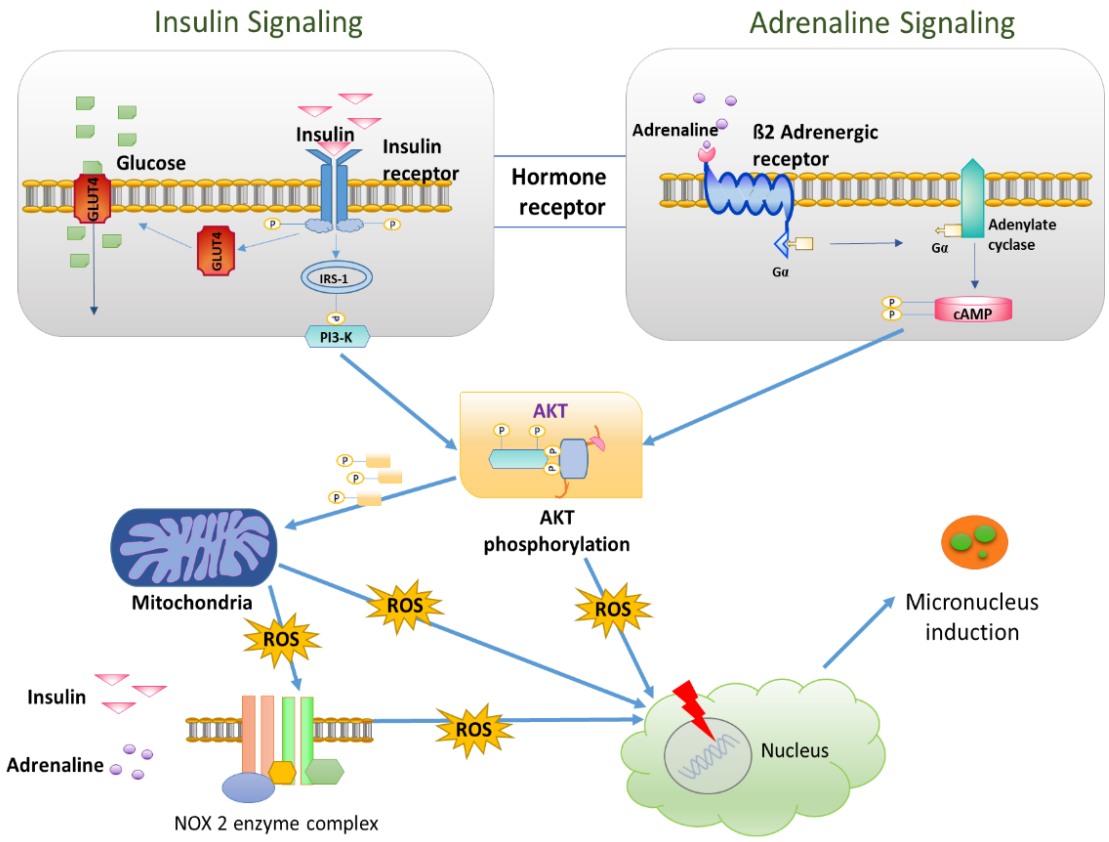

Figure 1. Insulin and adrenaline signaling pathways and their mechanistic crosstalk.

Own creation based on the figures described in [15, 16]

Insulin resistance, Obesity and Type-2 diabetes mellitus

Insulin resistance is characterized by the lack of suppression of glucose production and the failure of glucose uptake, metabolism and storage. In the case of T2DM and obesity, insulin resistance presents defective glucose transport to the adipocytes and skeletal muscles and impaired hepatic glucose release. [17] The conditions associated with these are hyperinsulinemia, hyperglycaemia and dyslipidemia. In case of obesity, dyslipidemia leads to higher ROS formation and lower antioxidant enzymes causing oxidative stress and genomic instability [18]. Mitochondrial dysfunction and impaired fatty acid beta-oxidation can be a direct mechanism by which excessive lipid supply leads to oxidative stress in metabolic syndrome and T2DM [19]. Overall glucose and lipid metabolism are related to the mitochondria through the Citric acid/Krebs cycle and the oxidative phosphorylation pathways, thus leading to energy production and their dysfunction becomes crucial for disease development [20].

Analysis of toxicity of mixtures

The analysis of toxicity of mixtures is necessary to understand the effects of individual substances and the effects of their combinations. Theoretically, at effect saturating substance levels, the system producing the effect is working at its upper maximal limit and if more of the same substance or another substance, which uses the same effect producing system is added, the cellular response cannot increase further. Therefore, combination of two substances using concentrations at which their dose response levels are saturated may provide information whether they both use the same cellular effect producing system. If they do, the effect of the combination should be equal to that of each of the substances, and if they are additive, they exert their effects by a different mode of action. [21-23]

Based on the type of effect produced we can classify three outcomes: additive effect, non-additive effect and an inhibitory effect. (e.g., figure 2). When there is an additive effect from combining the saturated concentrations of two compounds it indicates the different modes of action for the individual components of the mixture. A non-additive effect from combining the saturated concentrations of two compounds implies the exhaustion of the capacity of the effect producing system, thus causing no further increase in effect beyond the effect produced by the saturated concentration. Inhibitory effect shows a downregulation of the response from the mixture, where one compound blocks the action of the other. [24] Therefore, it was one of the aims of this work, in which we tested the combination effect of insulin and adrenaline *in vitro*, at the saturation concentration taken from each of the compounds' *in vitro* dose response curves for micronucleus induction.

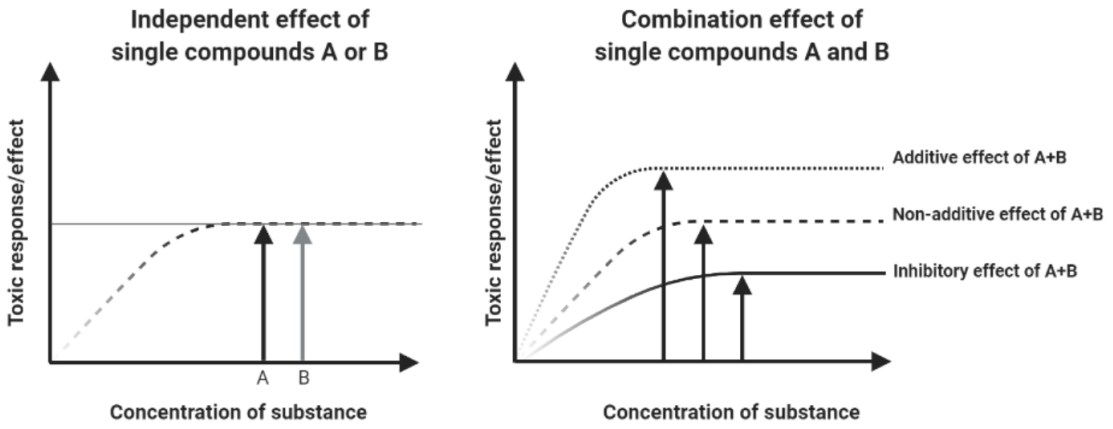

Figure 2. Schematic diagram of the analysis of the toxicity of mixtures.

Own creation, based on the figures from [21]

Mechanistic overlap of insulin and adrenaline signalling

Insulin and adrenaline are essential hormones with heterologous signalling pathways activating different cellular functions. The action of insulin in skeletal muscles requires the protein AKT/PKB while the adrenaline action requires cAMP and PKA [25]. Adrenaline influences the PKB activation by itself and enhances the insulin mediated activation of the PKB [26]. Similarly, the IR and β2AR interact with each other, form complexes, and regulate the insulin and catecholamine-signalling pathways [27]. This is however dependent on the cell type, its physiological function and the type of adrenergic receptor expressed. For example, in human leukemia HL60 cells, the β2AR is involved in adrenaline signalling via G-protein coupled receptors, cAMP and PKA signalling [28]. Thus, for insulin and adrenaline, PKB/AKT is a common signalling step. This is further supported by the fact that the overstimulation of the βAR's leads to impaired glucose uptake and insulin resistance in skeletal, adipocyte and heart tissues. [12]

Oxidative stress and reactive oxygen species (ROS)

Oxidative stress and DNA oxidative damage are pathological conditions that arise due to increased levels of reactive oxygen species (ROS) and reactive nitrogen species (RNS). The mitochondria and the enzyme NAPDH oxidase (NOX) are the two major and well-studied sources of cellular ROS formation. [29] ROS are also required at low concentrations as cellular signalling molecules, but if dysregulated and present at high concentrations, they

lead to irreversible changes to macromolecules contributing to aging, cancer and cell death [30].

Mitochondria

The mitochondria are the power houses of the cell and are essential in ATP production through oxidative phosphorylation, Ca^{2+} regulation, ROS production and scavenging actions. Under normal conditions, they produce only minimal amounts of ROS necessary for the signalling functions, due to their strong antioxidant enzyme equipment. [29] The electrons fed by the tricarboxylic acid (TCA) cycle are transferred across the inner mitochondrial membrane by the mitochondrial electron transport chain (ETC). The ETC transfers electrons across the 5 complexes (I-V) of the mitochondrial inner membrane. The complexes I, II and IV pump protons from the mitochondrial matrix to the mitochondrial intermembrane space, leading to the formation of an electrochemical gradient across the membrane yielding the membrane potential which generates ATP from ADP at the mitochondrial complex V. [31] However, under certain pathologies an overproduction of ROS and escape from radical scavenging systems can lead to ROS leakage into the cytoplasm. Damage and dysfunction of the mitochondria causes the depolarization of the mitochondrial membrane and leakage of ROS, which leads to activation of proapoptotic signals (cytochrome c), which in turn activates the caspases and initiate protein degradation and cell death response. [32] Mitochondrial ROS released into the cytosol can influence the production of ROS from the NOX complex, through the redox-sensitive PKC protein [33]. Mitochondrial function is impaired during insulin resistance, which is associated with the development of metabolic diseases, which are shown to have a reduction in respiration, mitochondrial number, ATP production and increased oxidative stress. [31, 34]

NADPH oxidase (NOX)

NADPH oxidases of the NOX family proteins are the enzymatic sources of cellular ROS, to be used in hormone synthesis, host defence mechanisms and redox signalling. These are transmembrane proteins with cytosolic subunits and there are 7 different isoforms of the NOX enzymes encoded by the human genome: NOX1-5, DUOX 1 and DUOX 2. These isoforms differ by the type of ROS released, organ specific function, expression level and their regulation. The physiological functions of NOX are essential for health, but their excess may lead to pathologies such as fibrotic diseases, neurodegenerative diseases and cardiovascular conditions [35]. In T2DM, NOX 2 and 4 isoforms are known to play a role in insulin induced NOX activation and ROS generation [36]. NOX 2/ gp91(phox) (where phox refers to phagocyte oxidase) is the catalytic membrane subunit of the granulocyte NADPH oxidase complex involved in host defence mechanisms. The NOX 2 protein complex catalyses the reduction of oxygen to superoxide anion, generating large quantities of intracellular ROS. [32] NOX 2 derived ROS contributes to pro-inflammatory cytokine induction, stress kinase activation and mitochondrial dysfunction leading to metabolic stress and T2DM [35].

1.2. Effect of PTEN inhibition on insulin induced genotoxicity.

Tumor suppressor gene – phosphatase and tensin homolog (PTEN)

PTEN is a tumor supressor protein encoded by the PTEN gene, which is important for cell cycle regulation, cell proliferation, apoptosis, aging, DNA damage response and more. It is both a nuclear and cytoplasmic protein, and in most differentiated tissues it is found in the nuclear region. The lipid phosphatase PTEN acts on the PI3K/AKT signaling pathway by catalyzing the conversion of PIP_3 to PIP_2 and leads to the negative feedback regulation of the mitogenic signaling pathway. [37] Paradoxically, PTEN regulated metabolic functions can also influence the insulin sensitivity, tumor growth and metabolism. In humans, PTEN mutations have been identified in several pathologies such as autism, Cowdens syndrome, hamartomas, diabetes and cancer [38]. The inactivation of PTEN is seen in many types of cancers (skin, brain, endometrium and prostate) and this is caused by genomic alterations such as point mutations, deletions and epigenetic modifications [39].

PTEN in AKT signalling

The AKT protein is a central molecule in cell proliferative signalling. High levels of ROS causes both, the hyperactivation of AKT signalling and the inhibition of PTEN tumor suppresor function (figure 3) [40]. All three isoforms of the AKT protein are downregulated by the PTEN action [41]. Sporadic tumors have also been reported for the presence of various types of PTEN missense, deletion and protein instability mutations [42]. The signalling pathway due to the lack of PTEN regulation causes the hyperphosphorylation of the AKT protein which has been shown to result in endometrial, skin and prostate cancers [37, 43]. Studies have reported PTEN polymorphisms in insulin resistance and T2DM [44, 45]. PTEN depletion also causes replicative stress and disrupts the mitotic spindle formation, leading to the formation of lagging chromosomes and the accumulation of numerical and structural chromosomal aberrations [42]. The PTEN protein regulates chromosome segregation through the mitotic arrest deficient 2 (MAD2) protein, which is an essential component of the spindle asembly checkpoint (SAC) protein in mitosis control and its dysregulation can lead to cancer cell proliferation [46].

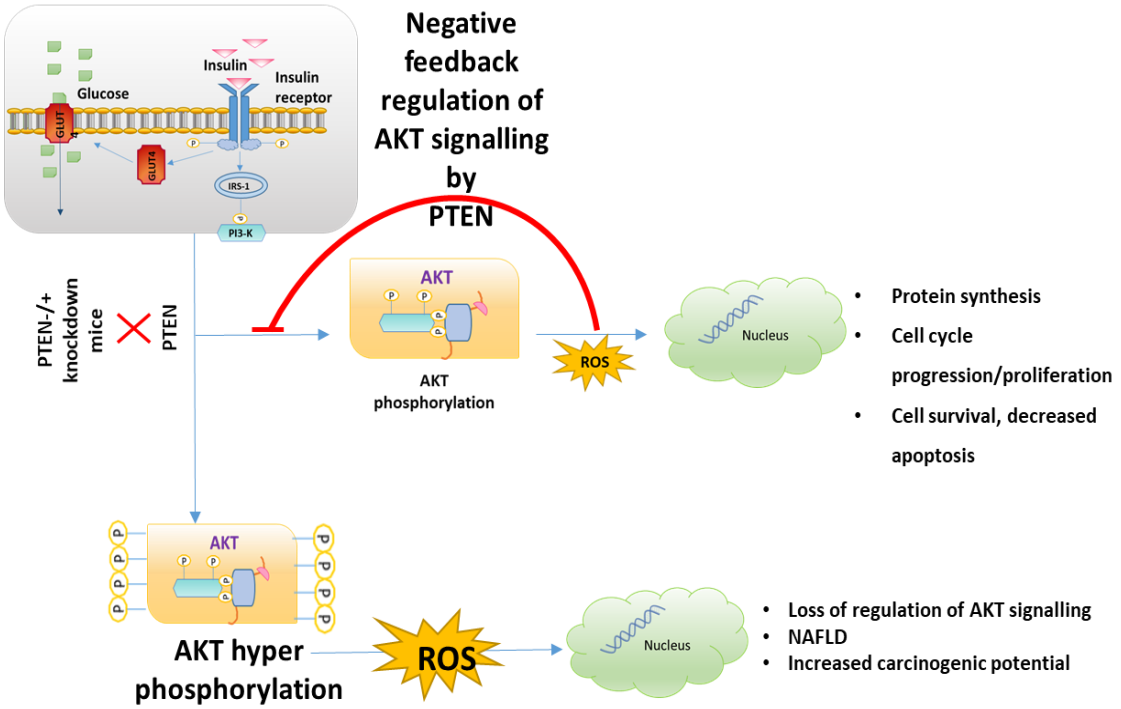

Figure 3. PTEN mediated negative regulation of AKT signalling after insulin stimulation.

Own creation.

Role of PTEN in cancers

PTEN protein is regulated by sub-cellular processes such as ubiquitilation, nitrosylation, transcription, translation, phosphorylation and oxidation. The oxidation of the PTEN protein by ROS causes the inactivation of the lipid phosphatase (tumor supressor) activity. [47] The PI3K/AKT is essential for NOX activation and the upregulation of PTEN causes modulations in AKT signalling which reduces the ROS generation in cells [40]. NOX derived ROS are known to be involved in cancer progression and metastasis. Since high levels of ROS can regulate PTEN function through direct oxidation, there has been a causal relationship established between NOX derived ROS and PTEN inhibition in cancers, but their underlying mechanisms are not well known [48]. The metabolic regulation functions of PTEN are especially realized when there is a heterozygous deletion of the gene and this mutation leads to a loss of tumor suppressor functions and has also been shown to cause tumor development in several tissues in animal models (prostate, ovarian and brain). [39]

1.3. Effect of proliferative stress on micronucleus induction

Replicative stress

Any event that blocks DNA replication and prevents cells from completing genome duplication before mitosis is considered as replicative stress [49]. Replicative stress is a complex phenomenon with severe consequences to the genome integrity, cell survival and maintenance. The origin of replicative stress may be due to oncogene activation, nucleotide pool imbalance and a conflict between replication and transcription. [50] Numerical chromosomal aneuploidy is also a consequence of DNA replicative stress. Several exogenous and endogenous threats can lead to replicative stress, including DNA lesions or adducts induced by chemical compounds, UV or ionizing radiation, reactive oxygen species (ROS), by-products of cellular metabolism, nucleotide pool imbalances or a shortage of replication factors. [50]

Genomic instability caused by replicative stress

Cells carrying DNA damage in their genomes can undergo mitotic errors leading to the formation of genomic instability, which could be a consequence of chromosome lagging, missegregation and breaks [51]. This has been observed in Hela-H2B-GFP cells after treatment with hydroxyurea, which led to abnormal mitosis (multipolar mitosis, chromatin bridges and buds) resulting in micronucleated cells which had an early chromatin condensation and nuclear fragmentation during the mitosis and therefore may contain entire chromosomes or lagging chromosome fragments [52]. Studies have shown that a mild replicative stress poses a particular threat to the genome stability, as the interphase checkpoint proteins may overlook the problem, leading to genomic damage accumulation [53, 54].

Replicative and oxidative stress

Replicative and oxidative stresses are both well-known endogenous genotoxic assaults, which cause genomic instability. These two stressors are closely linked, and their imbalance generates the induction of micronuclei. Oxidative stress can lead to DNA lesions, which can evoke cancer-promoting mutations. [55] When the oxidative stress induced DNA lesions are left unrepaired and the cells enter into the next mitosis, it leads

to the induction of replicative stress causing the stalling and collapse of the DNA replication forks, resulting in the formation of micronuclei and nuclear buds [56, 57].

Mitotic checkpoints

During mitosis, the genetic material must be equally distributed for the genome maintenance. In the prophase of the cell division, a bipolar spindle is formed. From prophase to pro-metaphase to metaphase, the microtubules bind to the kinetochores of the chromosomes. [58] As the cells enter anaphase, the sister chromatids are pulled apart, leading to equal distribution of genetic material under normal conditions. The checkpoint proteins involved during mitosis are the spindle assembly checkpoint (SAC) and the anaphase-promoting complex (APC). The SAC monitors the microtubule-kinetochore binding during metaphase, and it is activated especially when there is a lagging chromosome or lack of tension between sister kinetochores to pull them apart during anaphase. The SAC acts on the mitotic checkpoint complex, thereby initiating mitotic arrest, cell death pathway and regulates APC function. [56] The APC is a large protein complex which ubiquitinates the cyclin B protein. The degradation of cyclin B leads to the downregulation of cdk1, which is the primary protein that maintains the mitotic state. [59] Checkpoint proficient cell lines undergo apoptotic cell death upon exposure to mitotic spindle poisons, while the checkpoint defective cells are resistant to checks and accumulate abnormal chromosomal aberrations. In addition, the checkpoint defective cells exit mitosis prematurely which may lead to chromosome missegregation. [56]

Several studies have observed the dynamics of mitosis using live cell time-lapse imaging technique in fluorescence-tagged cells [e.g., Hela with a green fluorescent protein tag on the histone 2B (Hela-H2B-GFP)]. By using the histone 2B, we can efficiently monitor the movement, location and condensation rate of the chromosomes along with other mitotic events. Frequently reported abnormalities in Hela-H2B-GFP include the presence of lagging chromosomes and multipolar mitotic spindles which are defects arising from defective checkpoint proteins and mitotic errors. [60, 61]

1.4. Genotoxic outcomes in obese patients with diabetes

Obesity

Obesity is a major risk factor for increased cardiovascular mortality in patients with type 2 diabetes mellitus. A strong positive correlation is found between obesity and ischemic heart disease, hypertension, and stroke, through its role in the development of insulin resistance and its associated complications. [62] Obesity is characterized by abnormal and increased body weight along with dyslipidemia and an increased body mass index (BMI); higher than 30. Obesity related chronic tissue inflammation triggers the pro-inflammatory signals and oxidative stress in the body leading to the development of diseases such as type 2 diabetes mellitus, metabolic syndrome and cancer. [63]

Obesity, insulin resistance and cancer

Obesity has been associated with the increased incidence of tumour development, which could be due to the metabolic and hormonal alterations. High circulating insulin levels and insulin resistance are a common characteristic of obese patients. The hyperinsulinemia itself contributes to the tumour cell growth and development, by increasing the availability of free insulin-like growth factors (IGF) through the inhibition of IGF binding proteins, which favours carcinogenesis. Insulin and IGF mediated carcinogenesis may occur through the AKT signalling pathway. [64] An increased body mass index (BMI) amongst overweight individuals has been shown to be associated with the increased risk of oxidative stress induced DNA damage and cardiovascular disease [65]. In general, impaired DNA repair, reduction of telomere length, inflammation and hormonal effects are postulated as reasons for the induction of DNA damage in obese patients [66].

Obesity and oxidative DNA damage

Many studies have shown the relationship between pro-inflammatory cytokines and high BMI values, impaired insulin signalling and insulin resistance. Elevated levels of intracellular ROS and oxidative stress in adipocytes leads to mitochondrial dysfunction and subsequent insulin resistance due to attenuated insulin signalling. [67] Oxidative stress and inflammation occurring during obesity can accumulate DNA damage and enhance the occurrence of mutations along with inhibiting the DNA repair mechanisms

[68]. During early stages of obesity, increased intake of glucose and fatty acids activate the NOX4 enzyme mediated ROS production in the adipocytes. Chronic inflammation signals the intracellular cytokines to active the NOX2 mediated ROS production in the immune cells. [68] T2DM patients have an elevated oxidative DNA damage, measured by 8-oxo-7,8-dihydro-2'-deoxyguanosine (8-oxodG) as a biomarker of oxidative DNA damage detected in the urine of patients. [69] Under normal conditions, it is essential that free radical induced damage as well as mitochondrial and nuclear DNA damage is repaired. However, when the antioxidant system is overwhelmed in T2DM and obesity, the increasing levels of insulin leads to increased free radical activity and accumulation of DNA damage. [70]

Glycated haemoglobin (HbA1c) and Type-2 diabetes mellitus

Glycated haemoglobin (HbA1c) is a chronic biomarker of hyperglycaemia associated with T2DM. Chronic hyperglycemia has been shown to induce oxidative stress, insulin resistance, chronic inflammation and T2DM. HbA1c reflects the average plasma glucose levels over the previous 8 to 12 weeks. [71, 72] The cut-off values for HbA1c are ≤ 5.5% for healthy individuals, 5.6-6.5% for individuals who are in a pre-diabetic state, and ≥ 6.5% for patients suffering from T2DM. [73]

2. Objective

Hormones are essential components in the body and their imbalance leads to pathological consequences. T2DM, insulin resistance and obesity are the most commonly occurring lifestyle diseases in the past decade. Also, an increased cancer incidence has been strongly associated with obese and T2DM patients.

Therefore, our aim was to study the influence of high insulin levels in accumulating DNA damage in *in vitro* models and patients, through the induction of oxidative stress. The primary goal of this study was to analyze the genotoxicity induced by the combined action of two endogenous hormones (insulin and adrenaline) with *in vitro* models, through the induction of micronuclei and to see if they cause an additive increase in genomic damage. This is important for multifactorial diseases having high levels of more than one hormone, such as metabolic syndrome and conditions with multiple pathologies (e.g., T2DM along with high stress levels).

Furthermore, the combination of insulin and the pharmacological inhibition of the tumor suppressor gene: PTEN, was to be tested in *in vitro* models for their genotoxic effect and oxidative stress inducing potential. As the tumor suppressor gene: PTEN is downregulated in PTEN associated syndromes and when presented along with T2DM and insulin resistance, this may increase the potential to accumulate genomic damage.

The consequences of insulin action were to be further elucidated by following GFP-expressing cells in live cell-imaging to observe the ability of insulin, to induce micronuclei and replicative stress. Finally, the detrimental potential of high insulin levels in obese patients with hyperinsulinemia and pre-diabetes was to be studied by analyzing markers of oxidative stress and genomic damage. In summary, the intention of this work was to understand the effects of high insulin levels in *in vitro* and in patients to understand its relevance for the development of genomic instability and thus an elevated cancer risk.

3. Methods

3.1. Cell culture

HL60 human myeloblastic leukaemia cells were grown suspended in RPMI-1640 medium supplemented with 10% fetal bovine serum, 1% L-glutamine, 0.4% penicillin/streptomycin under sterile conditions at 37°C and 5% CO_2. For experiments, the cells were plated at a density of 300,000 cells/3mL of growth medium per well on a 6-well tissue culture plate and treated after 24h. All experiments were performed up to 50 passages after thawing.

LLC-PK1 pig kidney epithelial cells were grown adhered to cell culture flasks in low glucose (1g/L) DMEM medium supplemented with 10% fetal bovine serum, 1% L-glutamine, 0.4% penicillin/streptomycin, 2.5% hepes buffer under sterile conditions at 37°C and 5% CO_2. For the experiments, the cells were plated one-day prior at a density of 300,000 cells/3mL growth medium per well on a 6-well tissue culture plate and treated after 24h. The cells were then washed in warm phosphate buffered saline (PBS), harvested by trypsin/EDTA treatment for 8-10min at 37°C and then resuspended in fresh medium. All experiments were performed up to 15-20 passages after thawing.

NRK primary rat kidney epithelial cells were grown adhered to culture flask in high glucose (4.5g/L) DMEM medium supplemented with 10% fetal bovine serum, 1% L-glutamine, 0.4% penicillin/streptomycin, 2.5% hepes buffer under sterile conditions at 37°C and 5% CO_2. For experiments, cells were plated one day prior at a density of 300,000 cells/3mL growth medium per well on a 6-well tissue culture plate and treated after 24h. The cells were then washed in warm PBS, harvested by trypsin/EDTA treatment for 5-7min at 37°C and resuspended in fresh medium. All experiments were performed up to 15-20 passages after thawing.

HeLa-H2B-GFP human immortalized epithelial cells, derived from the cervical adenocarcinoma of a female patient was obtained from Noriaki Shimizu, Graduate School of Integrated Sciences for Life, Hiroshima University, Japan by the working

group of Dr. Hintzsche. These cells were stably transfected with the green fluorescence protein (GFP) at the histone2B position. The cells were grown as a monolayer in DMEM high glucose (4.5g/L) medium without phenol red, supplemented with 10% (v/v) fetal bovine serum, 1% (w/v) L-glutamine, 1% (w/v) 10,000 units/mL of penicillin/10mg/mL streptomycin; 1% hepes buffer, 1% sodium pyruvate and under sterile conditions at 37°C and 5% CO_2. The cells divided at a cell cycle duration of 18-20h. For cell proliferation experiments, the cells were plated at a density of 250,000 cells/2mL growth medium per well, on a 12-well tissue culture plate and treated after 24h.

3.2. Cytokinesis block micronucleus assay

The cells seeded for experiments were treated for 4h with hormones at concentrations taken from the saturation level of previously established dose-response curves, individually and in their combinations. In case of the treatment with inhibitors (MK-2206, N-acetyl cysteine, rotenone, VAS2870) or receptor blockers (HNMPA (AM_3) and propranolol), these substances were added 30min prior to the hormone treatment, unless mentioned otherwise. At the end of the 4h treatment, the culture medium was discarded and 3mL of fresh medium with 3 µg/mL of cytochalasin B was added for another 24h to yield binucleated (BN) cells. The cells were sampled at a time equivalent of about 1.4 cell cycle durations after the beginning of the treatment, spread onto microscopic slides by CytoSpin centrifugation (30,000 cells/slide at 1000 rpm for 5min) and fixed in methanol at -20°C for at least two hours. The slides were air-dried, stained with gel green (diluted to 1:100 in double-distilled water) and mounted with the mounting medium DABCO (1, 4- diazabicyclo [2.2.2] octane). For each test, two replicate slides were scored using a fluorescence microscope with fluorescein isothiocyanate (FITC) filter at 40x magnification. For each slide, 1000 binucleated cells were scored for micronuclei, along with the number of mononucleated, binucleated, multinucleated, mitotic and apoptotic cells. The cytokinesis block proliferation index (CBPI) was assessed as a criterion for determining the cytotoxicity (cytostatic effect) using the given formula. [19]

$$CBPI = \frac{number\ of\ (1 * mono + 2 * bi + 3 * multi)\ nucleated\ cells}{total\ number\ of\ (mono + bi + multi)\ nucleated\ cells}$$

3.3. Western blotting

The treated cells were washed twice in ice cold PBS and the pellet was aspirated 8-10 times with 1mL syringe in 80µl of radio-immune precipitation assay (RIPA) buffer supplemented with sodium fluoride (1mM), sodium orthovanadate (1mM) and protease inhibitor cocktail (10µL/mL). The amount of protein was estimated by Bradford's method spectrophotometrically and 30µg of protein was heat denatured and separated by sodium dodecyl sulphate-polyacrylamide gel electrophoresis (SDS-PAGE). The proteins were then transferred to Immobilon® polyvinylidene fluoride (PVDF) blotting membrane, blocked overnight in 5% non-fat dry milk powder dissolved in tris buffered saline containing 0.05% tween 20 (TBS-T). The membranes were probed with the primary antigen (anti-p-AKT 1:2000, anti-pan-AKT 1:1000, anti HO-1 1:100, anti HSP70 1:500, anti-G-beta 1:5000 and anti-beta actin 1:5000), followed by the secondary detection antibody linked to horse radish peroxidase (anti-immunoglobulin G -IgG HRP linked 1:5000) and developed enzymatically using clarity western ECL (enhanced chemiluminescence) substrate to observe the chemiluminescence. The protein bands were quantified using Image J analysis software. Beta actin was used as the protein loading control.

3.4. Ferric reducing/antioxidant power (FRAP) Assay

The FRAP assay was used to measure the reductive antioxidant capacity of a substance based on the following principle: at low pH, the ferric (Fe III) -2,4,6-tripyridyl-s-triazine (TPTZ) complex was reduced to the ferrous (Fe II) form, developing a blue colour, which was indicative of the antioxidant capacity of the substance. This blue colour development had a maximum absorption at 593nm using UV-vis spectrum. Different concentrations of ferrous sulphate solution were used as calibration standards and the colour development acted as an indicator of reducing/antioxidant capacity as

described by [74]. As a positive control, the synthetic substance tempol with characteristics like the naturally occurring superoxide dismutase was used.

3.5. Reverse transcription polymerase chain reaction (RT-PCR)

The gene expression analysis was performed by the RT-PCR method. RNA was isolated from cultivated HL60 cells using RNeasy Mini Kit (Qiagen) and quantified using NanoDrop. From that, 3µg of RNA was used to synthesize the cDNA using RevertAid First Strand cDNA Synthesis Kit (Thermo Scientific). The PCR was performed in a thermocycler, using REDTaq ReadyMix reaction mixture (Sigma-Aldrich) with the gene specific primers as listed below in table 1 and the amplicons visualized on agarose gel electrophoresis.

Gene	PCR Primer		PCR product size (bp)	Annealing temperature (°C)
IR	Forward	5′ AGA CGT CCC GTC AAA TAT TGC 3′	340	58.5
	Reverse	5′ ACT CGT TGA CCG TCT TCA CC 3′		
β2AR	Forward	5′ ACC AAC TAC TTC ATC ACT TCA C 3′	281	51
	Reverse	5′ GAC ACA ATC CAC ACC ATC AG 3′		
NOX 1	Forward	5′ ATC CTG CTT CCT GTG TGT CG 3′	293	56
	Reverse	5′ GTC GTG TTT CGG GAC TGG AT 3′		
NOX 2	Forward	5′ TGG GCC GTC CAT ACA AAG TC 3′	526	56
	Reverse	5′ TTT ACA CTG ACA TCC GCC CC 3′		
NOX 4	Forward	5′ ACC CCA TCG CTA CTA AAA ATA C 3′	248	50
	Reverse	5′ GCC GAC TAC TAA ACA AAA TCA C 3′		
Beta actin	Forward	5′ CTC TTC CAG CCT TCC TTC CT 3′	116	55
	Reverse	5′ AGC ACT GTG TTG GCG TAC AG 3′		

Table 1. List of primer sequences, annealing temperatures, and amplicon size used in RT-PCR for gene expression.

3.6. Mitochondrial membrane potential

To evaluate the change in the mitochondrial membrane potential, the cell-permeable fluorogenic probe tetra methyl rhodamine ethyl ester (TMRE) was used. TMRE is a positively charged molecule, which binds to the negatively charged healthy mitochondrial membrane. When there is a damage to the mitochondria, there is a

blockage of the electron transfer function that causes a depolarization of the membrane leading to a net positive charge, therefore TMRE dye does not bind to the membrane. [75] For the experiment, $3x10^5$ cells were seeded on 24mm cover slips in a 6-well plate with 3mL medium and left overnight. After adhering, the cells were treated first with the PTEN inhibitor VO-Ohpic for 15min and then treated for another 15min with insulin. TMRE (10nM final concentration in the culture) was added to the cells and incubated in the dark at 37°C for 30min. After washing the cells thrice with cold PBS, the cover slips were inverted onto the microscopic slides and observed under an Eclipse 55i microscope (Nikon GmbH, Duesseldorf, Germany) and a Fluoro Pro MP 5000 camera (Intas Science Imaging Instruments GmbH, Goettingen, Germany) at a 200-fold magnification with TRITC filter. All the images of the TMRE staining were taken using the same exposure time. Quantification was done by measuring grey values of 200 cells per treatment with ImageJ software 1.40g (http://rsb.info.nih.gov/ij/).

3.7. Oxidative stress microscopic quantification

To evaluate the formation of ROS, the cell-permeable fluorogenic probe dihydroethidium (DHE) was used. The DHE dye is specific for the detection of the superoxide radicals, through which they are oxidised to form the intermediate product (2-dihydroxyethidium), which emits fluorescence at Ex/Em: 500-530/590-620nm. [76] For the experiment, $3x10^5$ cells were seeded on 24mm cover slips in a 6-well plate with 3mL medium and left overnight. After adhering, the cells were first treated with the PTEN-inhibitor VO-Ohpic for 15min and then treated for another 15min with insulin. The DHE dye (10µM final concentration) was added to the cells and incubated in the dark at 37°C for 30min. After washing the cells thrice with PBS, the cover slips were inverted onto a microscopic slide and observed under an Eclipse 55i microscope (Nikon GmbH, Duesseldorf, Germany) and a Fluoro Pro MP 5000 camera (Intas Science Imaging Instruments GmbH, Goettingen, Germany) at 200-fold magnification using TRITC filter. All the images of the DHE staining within one experiment were taken using the same exposure time. Quantification was done by measuring grey values of 200 cells per treatment with ImageJ software 1.40g (http://rsb.info.nih.gov/ij/).

3.8. Animal model and treatment

Dr. Ezgi Eylül Bankoglu, obtained the organ samples from mice with whole-body targeted deletion of PTEN from the lab of Pier P. Pandolfi (Beth Israel Deaconess Medical Center, Harvard Medical School, Boston, MA) [77]. In the mice model, the wildtype control and the haplodeficient PTEN knockout (Ko) mice were fed either with a standard diet (Kliba 3336, 5.5% fat content) or a high fat diet (Kliba 2126, 23.6% fat content) for a duration of 20 weeks. The animals were sacrificed after 32 weeks and the tissue samples were collected and snap frozen, which we received for further analysis from our collaborators. The tissues were stored at -80°C until they were used. The animal experiments were performed in accordance with Swiss Federal Animal Regulation and approved by the Veterinary Office of Zurich, Switzerland (No: 35/2009 and 222/2012). [77, 78] In the present work, kidney tissues were homogenised with the protease inhibitor cocktail and the extracted protein content was estimated by using Bradford's method. All further steps of western blotting were performed similar to the description in paragraph 3.3 of the methods section. Here G-Beta was used as a protein loading control.

3.9. Live-cell microscopy

For the live imaging of MN induction, the Hela-H2B-GFP cells were plated at a low density of 15,000 cells/2mL medium in a 12-well glass bottomed black-coated plate (Cellvis P12-1.5-N). After the treatment of the cells with the test substance, the medium was changed, and the cells were placed in the plate chamber of a Nikon Ti–S fluorescence microscope equipped with a motorized table and an incubation envelope (Okolab) to maintain the temperature, CO_2 and humidity for optimal growth conditions. The system was controlled by the software NIS-Elements Advanced Research version 5.10.01 (Nikon). The positions of the chosen micronucleated cells were saved using the software. Images were taken every 10min for 24h, covering the time taken for at least one cell cycle (18-20h). A 40×0.75 numerical aperture (NA) objective (Nikon) and an Andor Luca S (Andor Technology) camera with neutral density filter (ND) 32 and an exposure time of 90ms were used without binning. The

experiment was repeated three times and in total, 1000 cells were screened, and the occurrence of MN, mitosis and apoptosis were recorded. The cell death (apoptosis) was recorded based on the increase in signal intensity and subsequent fragmentation of the nucleus. The duration of mitosis was recorded from the start of the prophase until telophase, with images taken at every 2 minutes for 100 cells with an exposure time of 200ms and ND 4. For the evaluation of the different stages of mitosis, we used the following criteria as represented in image 1. From the sequence shown in image 1, A-C represents the interphase cells, D-E represents the prophase where the condensed chromatids start to appear clearly, F represents the pro-metaphase where the condensed chromatids start to align together near an equatorial plane, G represents the metaphase alignment of the chromosomes, H-J represents the anaphase movement of the chromosomes towards opposite ends and K-L represents the telophase where the chromosomes move farthest from each other and chromosome decondensation is observed as the individual chromatids are no longer visible. All cells, which blurred or moved away from focus, were excluded from the data analysis. [79]

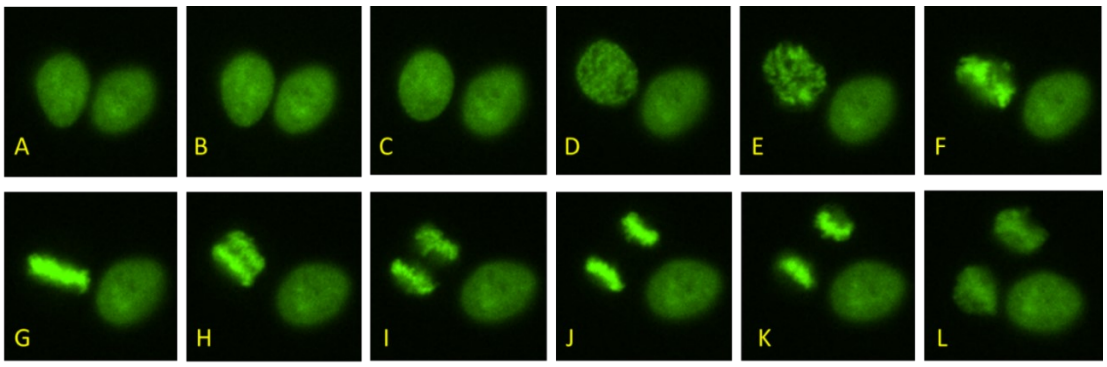

Image 1. Live cell time lapse imaging of mitosis in Hela -H2B-GFP cells

The representative images show representative pictures of the different stages of mitosis snapped at 2 min intervals for 24h, A-C interphase, D-E prophase, F pro-metaphase, G-metaphase, H-J anaphase and K-L show telophase.

3.10. Scratch wound healing assay with live cell microscopy

For the scratch wound-healing assay, the Hela-H2B-GFP cells were plated at a high density of 250,000 cells/2mL medium in a 12-well glass bottomed black-coated plate (Cellvis P12-1.5-N). After 24h, a straight longitudinal scratch was introduced using a 10µL pipette tip and the sides of the scratch were marked with a glass marker at the bottom of the plate. The medium containing the floating cells and debris from the scratch was discarded and the well was washed once with fresh medium and then refilled with 2mL of fresh medium. The cells were treated with the test substance and placed in the plate chamber of a Nikon Ti–S fluorescence microscope with favourable growth conditions as mentioned in section 4.11. Images were taken at every 30min intervals for 10 points along the length of the scratch with an exposure time of 200ms and ND 4, for 24h. The change in scratch area and width was quantified using ImageJ Software 1.40g (http://rsb.info.nih.gov/ij/). After the live imaging, the medium was discarded, the well was washed twice with PBS and the cells were fixed in the wells with ice-cold methanol at -20°C for atleast 2h. Then, the fixed cell monolayer was stained with gel green and scored for MN, apoptosis and mitosis in 1000 mononuclear cells along the length of the scratch using a fluorescence microscope. [80]

3.11. Human study

The blood samples were collected by the Department of Surgery and Endocrinology, University Hospital of Wuerzburg. Blood samples were collected into commercially available EDTA tubes from obese patients before undergoing bariatric surgery. The peripheral blood mononuclear cells (PBMCs) were isolated by using histopaque density gradient centrifugation and then cryopreserved by diluting 1×10^6 PBMCs/mL of freezing medium (RPMI 1640 medium containing 1% FBS, 1% L-glutamine, 10% DMSO). Aliquots were frozen overnight in a cryobox with isopropanol at −80 °C and transferred to regular storage containers after 2 days and stored at −80 °C until further use. The cryopreserved samples from 27 obese patients and 10 healthy controls were assessed for DNA damage and plasma oxidation products. The Ethics Committee of the University of Wuerzburg approved this study (Study No: 186/14) and for the

control subjects (Study No: 279/18). The PBMC's were subjected to comet assay with a 12-gel system and the images were evaluated using the Komet 5 software. (Dr. Ezgi Eyluel Bankoglu, Ms. Johanna Gerber and Ms. Franziska Stipp performed the processing of blood samples and the preparation of the samples for comet assay analysis. The DNA damage analysis in the comet assay and analysis of the plasma advanced oxidation protein products was performed by the author for the present thesis).

3.12. Advanced oxidation protein products (AOPP)

The protein content of the plasma samples was estimated spectrophotometrically by Bradford's method. Then the plasma was diluted at 1:10 dilution in PBS and 200µL was added in triplicates to a 96-well microplate. The assay standard was chloramine-T, which was added at 200µL/well in triplicates from 0-100µM concentration. All the substances were pipetted on ice. Finally, potassium iodide (KI 1.16M, 10µL) was added to all the wells and after 2min, 20µL of glacial acetic acid was added to initiate the reaction. The optical density was immediately measured at 340nm using a spectrophotometer. Chloramine-T equivalents of plasma AOPP were calculated by plotting the standard curve of the absorbance values. [81]

3.13. Statistics

All experiments were carried out as atleast three independent experiments and the data was presented as mean ± standard error. Graphical visualization and arithmetic calculations were performed using MS-Excel 2016. The results of western blotting were graphically shown as relative to the mean of the negative control values set to 1.0 and the experimental values were calculated as the fold increase over the control. The data distribution was tested for frequency distribution and statistical significance was considered when the p-value was ≤ .05 as tested by the T-Test or Kruskal-Wallis Test using IBM SPSS 25 software. The live cell time-lapse imaging was cumulative of three experiments with observations of 1000 individual living cells.

4. Results

4.1. *In vitro* genotoxicity of insulin in combination with adrenaline

To test the genotoxicity of hormone combinations, insulin and adrenaline were combined at concentrations in which a maximum induction of MN was observed from their individual dose response curves, as taken from previously published literature [23, 82, 83]. Prior permission had been obtained from the journal *Toxicology In Vitro* for the work published by the author of this thesis, to use the contents of the publication [23] in this dissertation (permission attached in Appendix). The results showed a significant increase in MN induction in the HL60 cells, after treatment with insulin (100nM) and adrenaline (10µM) as compared to the solvent control as seen in Figure 4.

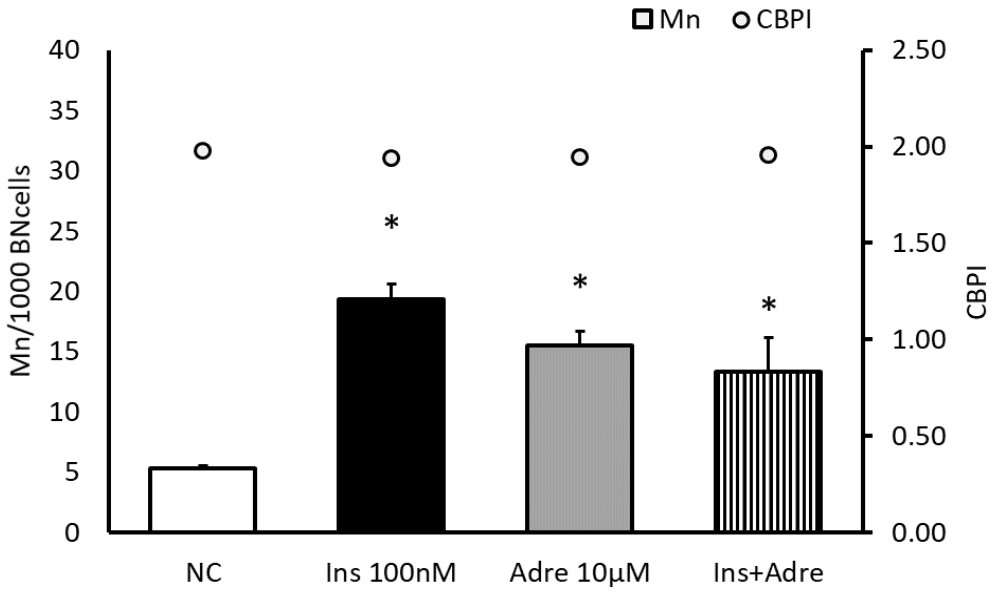

Figure 4. Micronucleus induction in HL60 cells with 100nM insulin and 10µM adrenaline and their combination

The HL60 cells were treated for 4h with insulin 100nM and adrenaline 10µM, followed by the addition of cytochalasin B 3µg/mL for 20-22h and the micronucleus number was counted per 1000 binucleated cells. Cell proliferation (cytokinesis block proliferation index [CBPI] (unfilled

*dots) is shown on the secondary y-axis. * significantly different from control with p≤.05. BN = binucleated, Mn = micronuclei; NC = negative control, Ins = insulin, Adre = adrenaline.*

The combined treatment showed a significant increase against the control, but no additive increase to the effects seen in the individual hormone treatment. We used MMS (100µM) as a positive control for MN induction, which showed a significant increase in MN induction both independently and in combination with insulin (Figure 5).

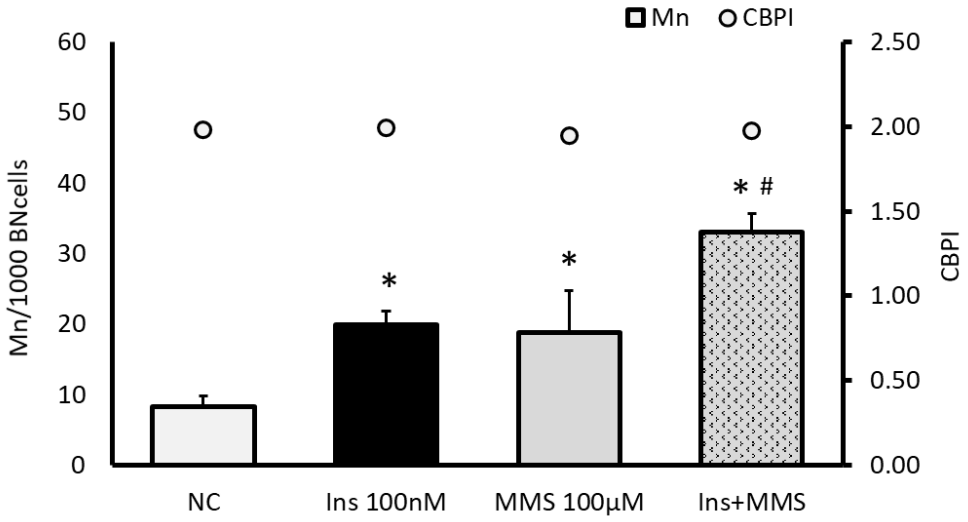

Figure 5. Micronucleus induction in HL60 cells with 100nM insulin and 100µM MMS and their combination

*The HL60 cells were treated for 4h with insulin 100nM and MMS 100µM, followed by the addition of cytochalasin B 3µg/mL for 20-22h and the micronucleus number was counted per 1000 binucleated cells. Cell proliferation (cytokinesis block proliferation index [CBPI] (unfilled dots) is shown on the secondary y-axis. * significantly different from control, # significantly different from insulin with p≤.05. BN = binucleated, Mn = micronuclei; NC = negative control, Ins = insulin, MMS = methyl methane sulfonate.*

We further investigated the mechanistic role of the hormone action in the insulin-signalling pathway by testing AKT phosphorylation in the HL60 cells. There was a significant increase in AKT phosphorylation after the insulin treatment and no increase in AKT phosphorylation after the adrenaline treatment as compared to the untreated control (Figure 6). Similarly, we tested MMS and it caused no increase in AKT

phosphorylation as compared to control, whereas its combination with insulin showed a significant increase in AKT phosphorylation as compared to the control. (Figure 7).

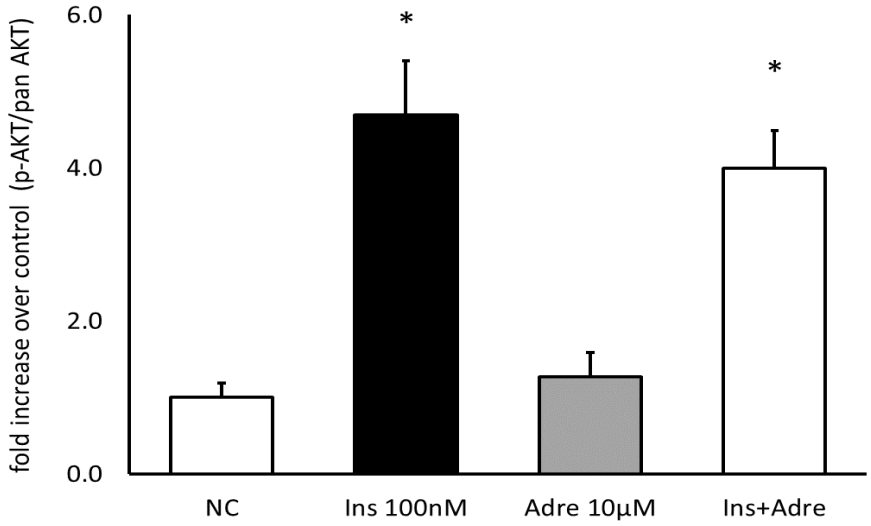

Figure 6. AKT phosphorylation in HL60 cells with 100nM insulin and10µM adrenaline and their combination detected by western blotting

*HL60 cells were treated for 4h with insulin 100nM and adrenaline 10µM, followed by protein isolation and western blotting with anti-phospho-AKT (60KDa), anti-pan AKT (60KDa) and beta actin (45KDa) antibodies. * significantly different from control, with p≤.05. NC = negative control, Ins = insulin, Adre = adrenaline.*

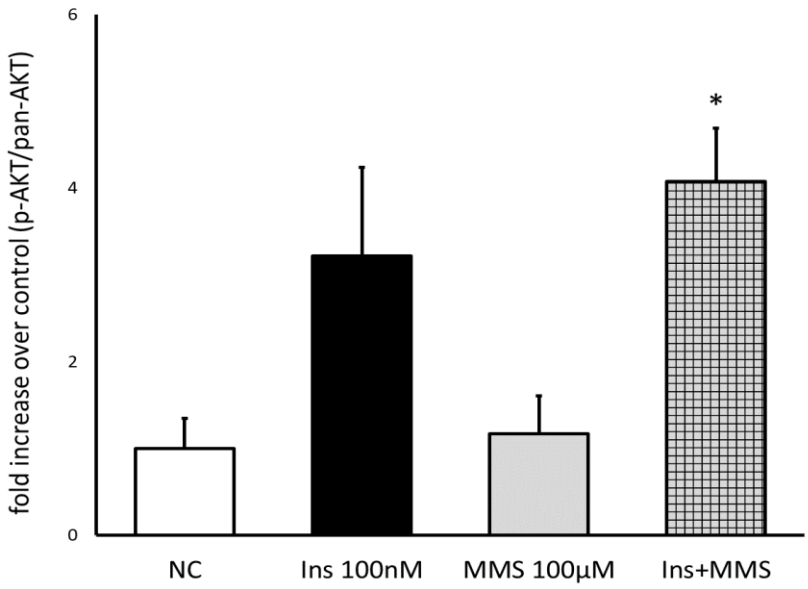

Figure 7. AKT phosphorylation in HL60 cells by western blotting with insulin 100nM and MMS 100µM and their combination

*HL60 cells were treated for 4h with insulin 100nM and MMS 100µM, followed by protein isolation and western blotting with anti-phospho-AKT (60KDa), anti-pan AKT (60KDa) and beta actin (45KDa) antibodies. * significantly different from control, with p≤.05. NC = negative control, Ins = insulin, MMS = methyl methane sulfonate.*

We tested the role of AKT phosphorylation and activation in MN induction by treating the cells with an inhibitor of AKT phosphorylation (MK-2206) (10nM) and saw a significant decrease in the MN number with the insulin treated HL60 cells (Figure 8). We verified this by western blot, where the AKT inhibitor decreased the phosphorylation of AKT when combined with insulin (Figure 9).

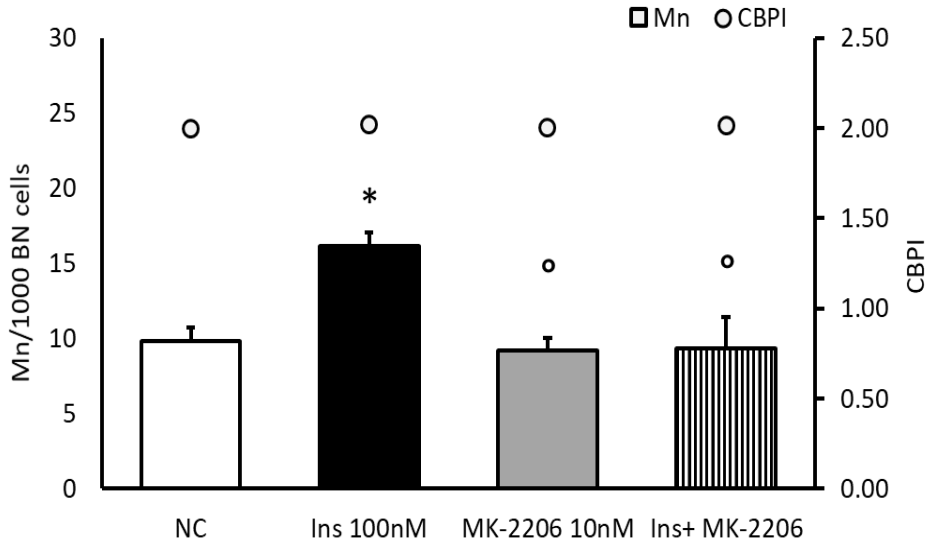

Figure 8. Micronucleus induction in HL60 cells with insulin 100nM and MK-2206 10nM and their combination

*The HL60 cells were treated for 4h with insulin 100nM and with MK-2206 10nM, an inhibitor of AKT phosphorylation, followed by the addition of cytochalasin B 3µg/mL for 20-22h and the micronucleus number was counted per 1000 binucleated cells. Cell proliferation (cytokinesis block proliferation index [CBPI] (unfilled dots) is shown on the secondary y-axis. * significantly different from control, # significantly different from insulin with p≤.05. BN = binucleated, Mn = micronuclei; NC = negative control, Ins = insulin, MK-2206 = AKT inhibitor.*

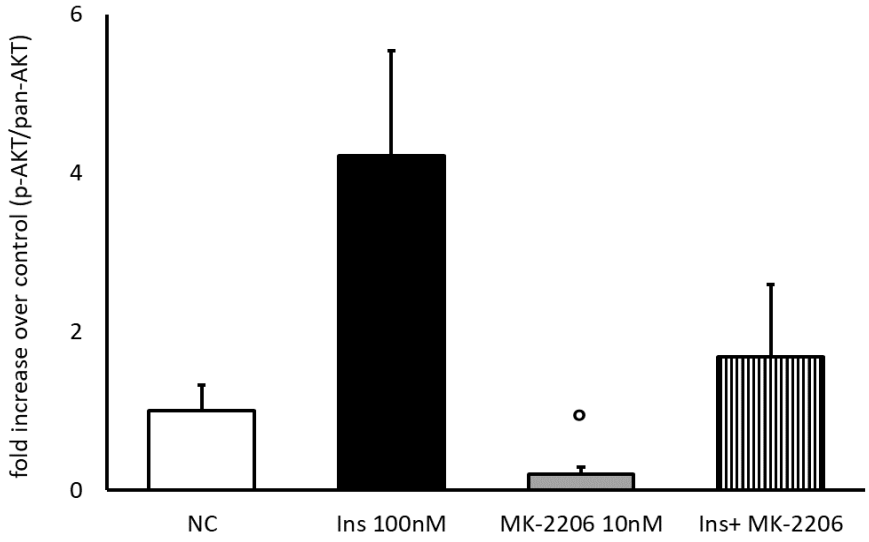

Figure 9. AKT phosphorylation in HL60 cells by western blotting with insulin 100nM and MK-2206 10nM and their combination

HL60 cells were treated for 4h with insulin 100nM and MK-2206 AKT inhibitor 10nM, followed by protein isolation and western blotting with anti-phospho-AKT (60KDa), anti-pan AKT (60KDa) and beta actin (45KDa) antibodies. ° significantly different from insulin, with p≤.05. NC = negative control, Ins = insulin, MK-2206 = AKT inhibitor.

It has been well known that the binding of growth factors to their respective cell surface receptors activates the PI3K, which then initiates the signalling events, leading to the phosphorylation of AKT protein. We confirmed the presence of the cell surface receptors for both insulin and adrenaline in our HL60 cells, using RT-PCR (Figure 10.). Then, we used hormone receptor specific inhibitors (insulin and adrenaline receptors blocked by 10nM HNMPA $(AM)_3$ and 10µM propranolol respectively), to see their effect on MN induction. In both cases, a significant decrease in MN number was seen after blocking the corresponding hormone receptors (Figure 11). We performed a FRAP assay and showed that in this assay, both the hormone receptor blockers, HNMPA $(AM)_3$ and propranolol, had no antioxidant capacity as compared to the positive control tempol (50µM) (Figure 12).

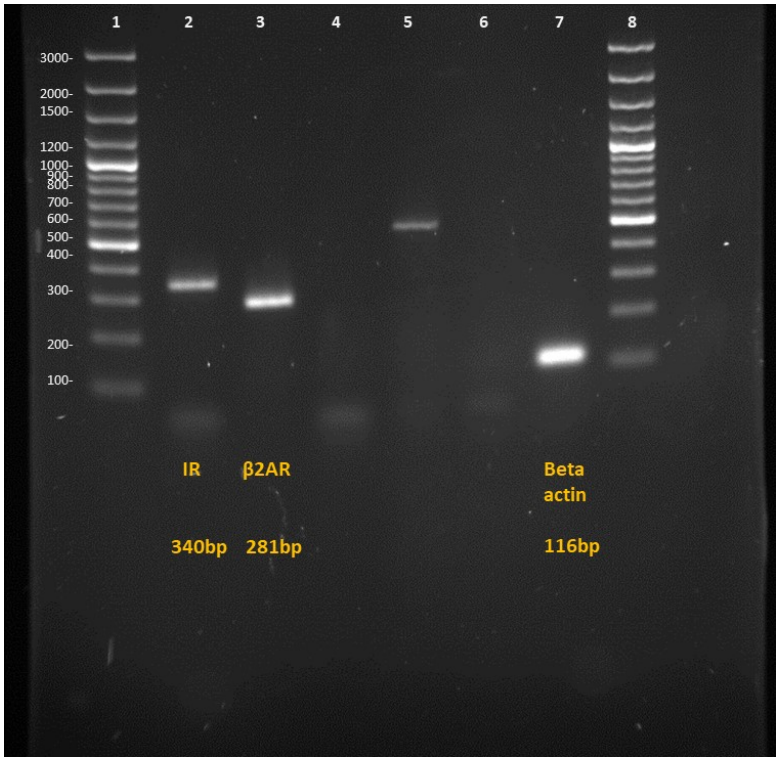

Figure 10. Expression of insulin receptor (IR) (340 basepairs) and β2 adrenergic receptor (β2AR) (281 basepairs); Beta actin (116 basepairs) was used as a loading control, as detected by RT-PCR in HL60 cells.

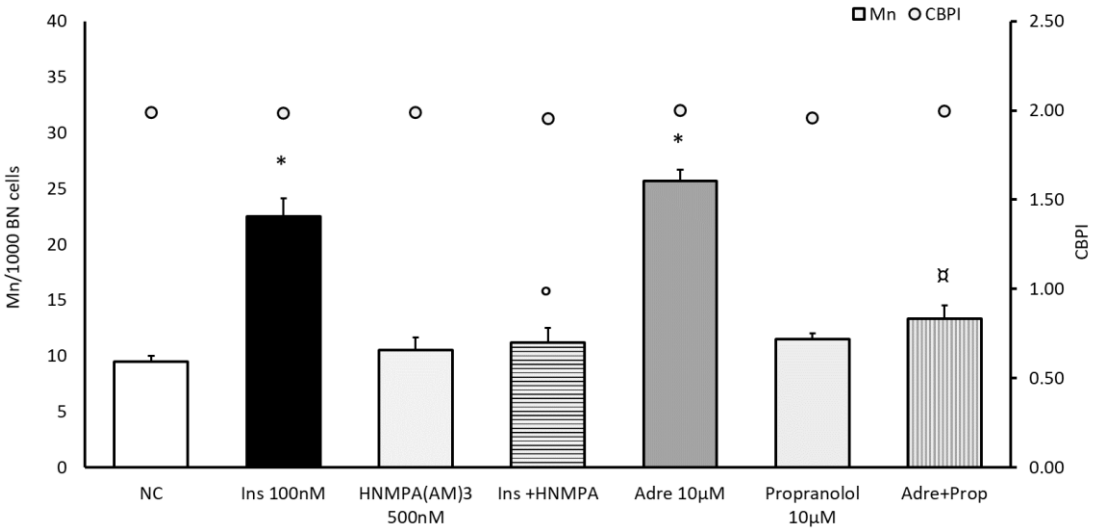

Figure 11. Micronucleus induction in HL60 cells with insulin 100nM, adrenaline 10μM and their combination with the hormone receptor blockers at HNMPA (AM_3) 10nM, propranolol 10μM, respectively.

*The HL60 cells were treated for 30min with the hormone-specific receptor blockers, HNMPA (AM_3) 10nM and propranolol 10µM, then treated with insulin 100nM and adrenaline 10µM for 4h respectively, followed by the addition of cytochalasin B 3µg/mL for 20-22h and the micronucleus number was counted per 1000 binucleated cells. Cell proliferation evaluated by cytokinesis block proliferation index [CBPI] (unfilled dots) is shown on the secondary y-axis. * significantly different from control, ° significantly different from insulin and ¤ significantly different from adrenaline with p≤.05. BN = binucleated, Mn = micronuclei; NC = negative control, Ins = insulin, HNMPA = HNMPA (AM_3) (insulin receptor blocker), Adre = adrenaline, Prop = propranolol (adrenaline receptor blocker).*

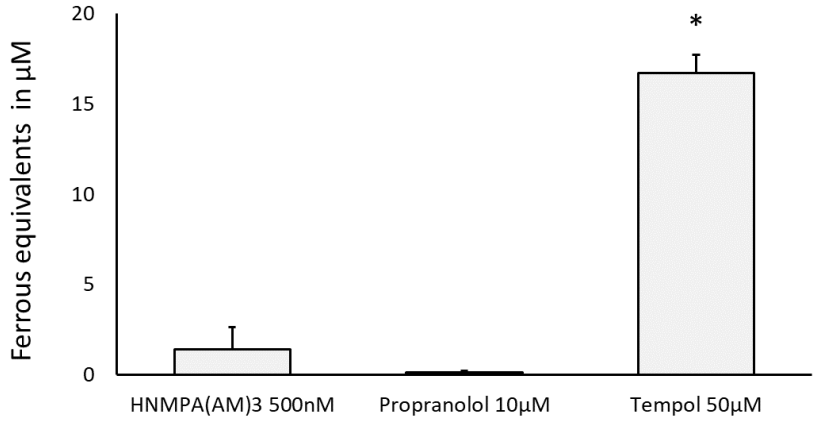

Figure 12. FRAP assay to test the antioxidant activity of hormone receptor blockers HNMPA(AM3) 10nM, propranolol 10µM and tempol 50µM as positive control.

** significantly different from control, with p≤.05*

We checked the role of mitochondria and NOX induced ROS in MN induction by treating the cells with rotenone (10nM) (a mitochondrial complex I inhibitor) and VAS2870 (1µM) (a general NOX enzyme assembly blocker). The results showed a significant decrease in MN induction after applying insulin to rotenone pre-treated cells, as compared to the control. The combination of adrenaline and rotenone showed a non-significant decrease in micronuclei (Figure 13). We confirmed the presence of different NOX isoforms (NOX 1,2 and 4) in our HL60 cells, using RT-PCR (Figure 14.). The combination of NOX inhibition with VAS2870 and the hormones showed a significant reduction with insulin and a non-significant reduction with adrenaline in the number of micronuclei (Figure 15).

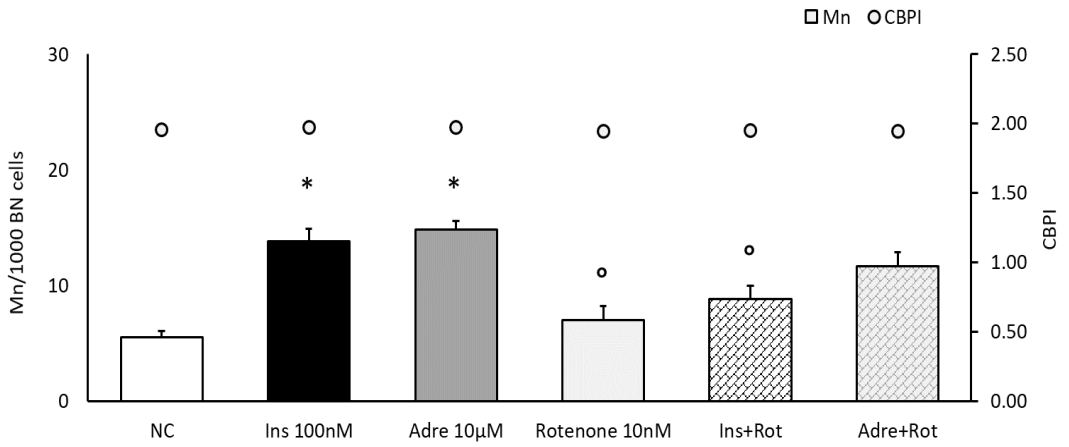

Figure 13. Micronucleus induction in HL60 cells with insulin 100nM, adrenaline 10µM and their combination with the mitochondrial complex I blocker, rotenone 10nM

*The HL60 cells were treated for 30min with the mitochondrial complex I blocker, rotenone 10nM and then treated with insulin 100nM and adrenaline 10µM for 4h respectively, followed by the addition of cytochalasin B 3µg/mL for 20-22h and the micronucleus number was counted per 1000 binucleated cells. Cell proliferation evaluated by cytokinesis block proliferation index [CBPI] (unfilled dots) is shown on the secondary y-axis. * significantly different from control, ° significantly different from insulin with p≤.05. BN = binucleated, Mn = micronuclei; NC = negative control, Ins = insulin, Adre = adrenaline, Rot = Rotenone.*

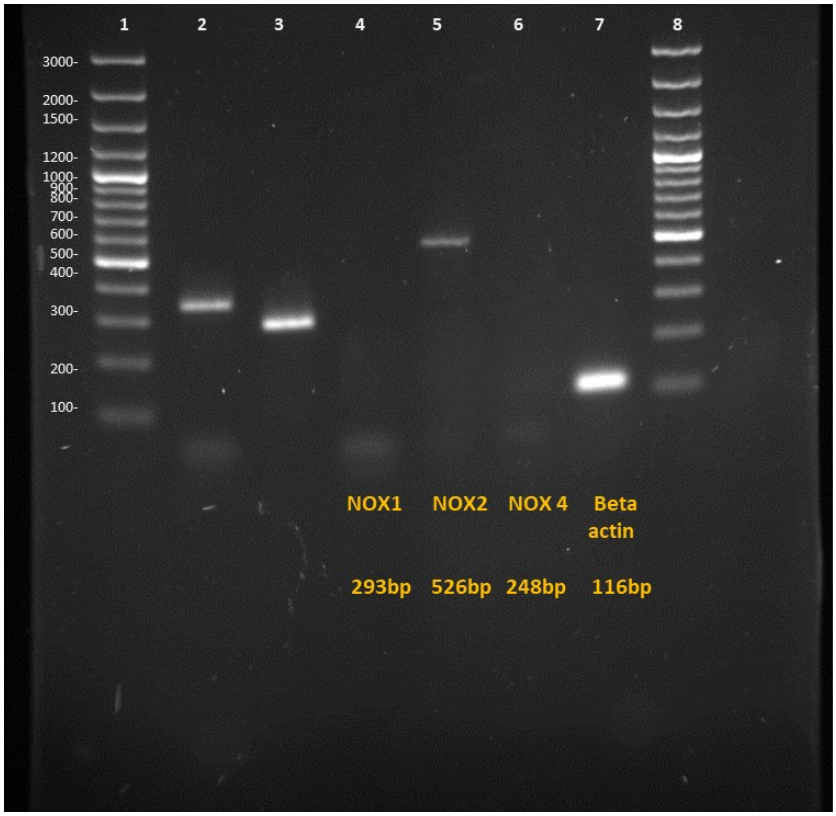

Figure 14. Expression of NOX 1 (293 basepairs), NOX 2 (526 basepairs) and NOX 4 (248 basepairs); Beta actin (116 basepairs) was used as a loading control, as detected by RT-PCR in HL60 cells.

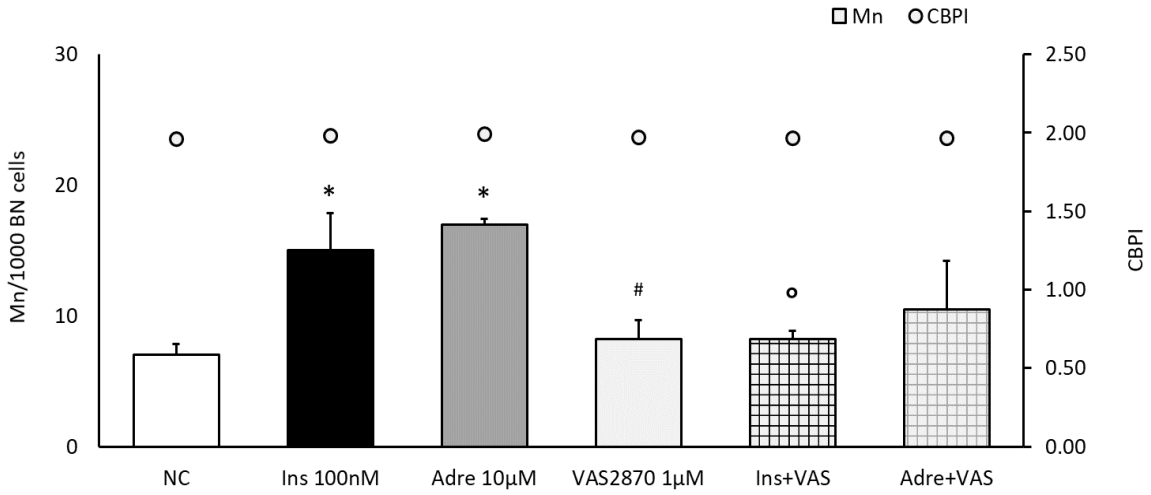

Figure 15. Micronucleus induction in HL60 cells with insulin 100nM, adrenaline 10µM and their combination with the total NOX assembly blocker, VAS2870 1µM

The HL60 cells were treated for 30min with the total NOX assembly blocker, VAS2870 1µM and then treated with insulin 100nM and adrenaline 10µM for 4h respectively, followed by the

*addition of cytochalasin B 3µg/mL for 20-22h and the micronucleus number was counted per 1000 binucleated cells. Cell proliferation evaluated by cytokinesis block proliferation index [CBPI] (unfilled dots) is shown on the secondary y-axis. * significantly different from control, ° significantly different from insulin, # significantly different from insulin and adrenaline with p≤.05. BN = binucleated, Mn = micronuclei; NC = negative control, Ins = insulin, Adre = adrenaline, VAS = VAS2870.*

We then confirmed that the MN induction was due to oxidative stress by treating the cells with the antioxidant N-acetyl cysteine (5mM) which yielded a significant decrease in MN number after combining it with insulin and adrenaline (Figure 16).

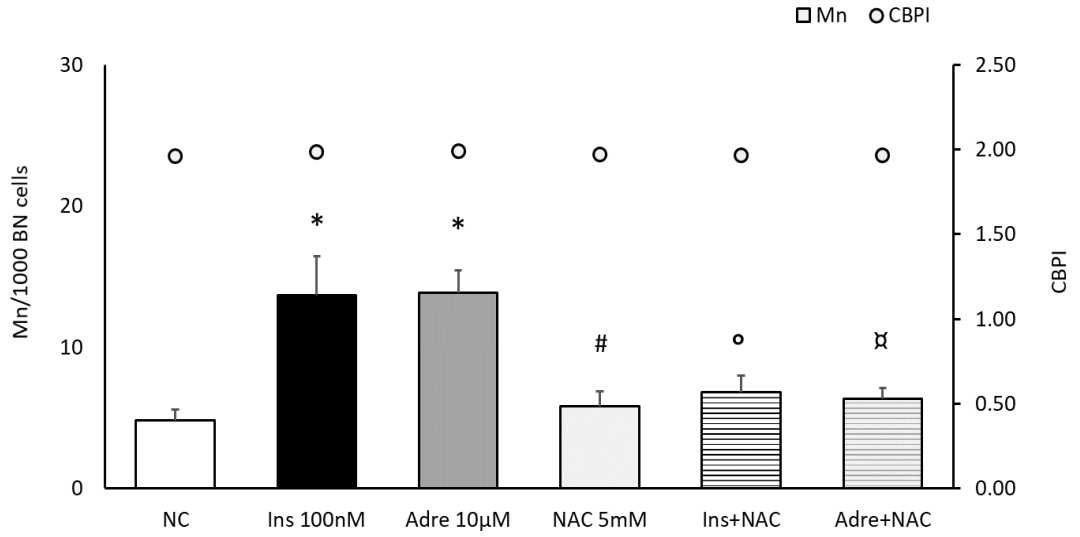

Figure 16. Micronucleus induction in HL60 cells with insulin 100nM, adrenaline 10µM and their combination with an antioxidant N-acetyl cysteine (NAC), NAC 5mM

*The HL60 cells were treated for 30min with the antioxidant N-acetyl cysteine (NAC) 5mM and then treated with insulin 100nM and adrenaline 10µM for 4h respectively, followed by the addition of cytochalasin B 3µg/mL for 20-22h and the micronucleus number was counted per 1000 binucleated cells. Cell proliferation evaluated by cytokinesis block proliferation index [CBPI] (unfilled dots) is shown on the secondary y-axis. * significantly different from control, ° significantly different from insulin, ¤ significantly different from adrenaline, # significantly different from insulin and adrenaline with p≤.05. BN = binucleated, Mn = micronuclei; NC = negative control, Ins = insulin, Adre = adrenaline, NAC = N-acetyl cysteine.*

We then further tested the effect of mitochondrial ROS in the MN induction of HL60 cells. The treatment with antimycin A, which was known to cause superoxide-release from mitochondria, showed a dose dependent decrease in the MN number, with a significant increase in cytotoxicity shown by the reduction in cytokinesis block proliferation index (Figure 17).

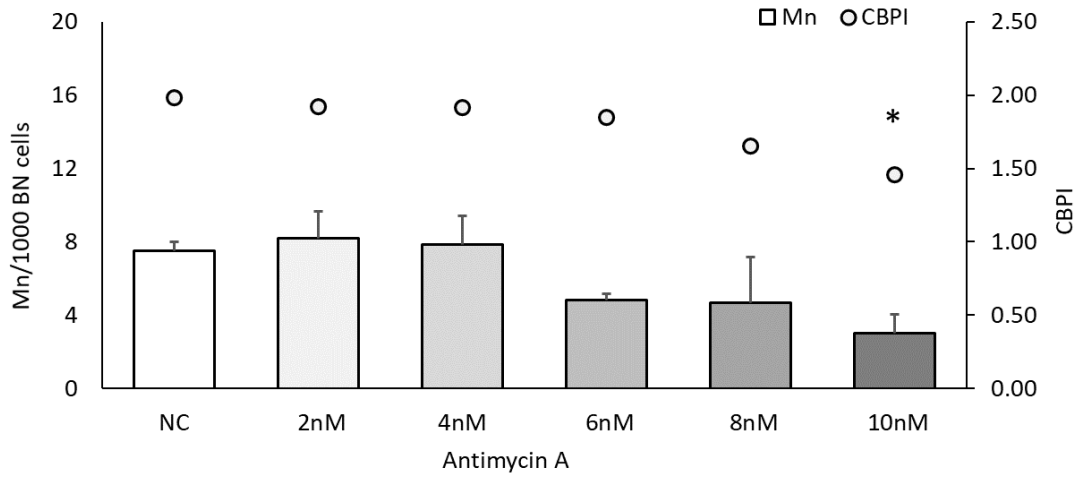

Figure 17. Micronucleus induction in HL60 cells with the mitochondrial complex III blocker Antimycin A (0-10nM)

*The HL60 cells were treated for 4h with a mitochondrial complex III blocker Antimycin A (0-10nM), followed by the addition of cytochalasin B 3µg/mL for 20-22h and the micronucleus number was counted per 1000 binucleated cells. Cell proliferation evaluated by cytokinesis block proliferation index [CBPI] (unfilled dots) is shown on the secondary y-axis. * significantly different from control, with p≤.05. BN = binucleated, Mn = micronuclei.*

4.2. Effect of PTEN inhibition on insulin induced genotoxicity

Based on our findings regarding the relevance of the AKT-signalling cascade for the induction of genomic damage by insulin, we next investigated the role of PTEN: a controlling step of the AKT-signalling cascade in healthy cells. For this purpose, the kidney tissue from PTEN Ko and control wildtype mice that had received a normal or a high fat diet was used to perform western blotting. The PTEN expression in this animal model was tested in our previous study and it showed a 40% reduction in PTEN expression in the PTEN Ko as compared to the wild type mice. [77]

At first, the expression of heat shock protein 70 (HSP70) was analysed, which showed a non-significant increase in the PTEN Ko as compared to the wild type mice. There was a slight increase in the HSP70 expression among the high fat diet group as compared to that of the normal diet group in the wild type mice, but no such difference was seen in the PTEN Ko model (Figure 18).

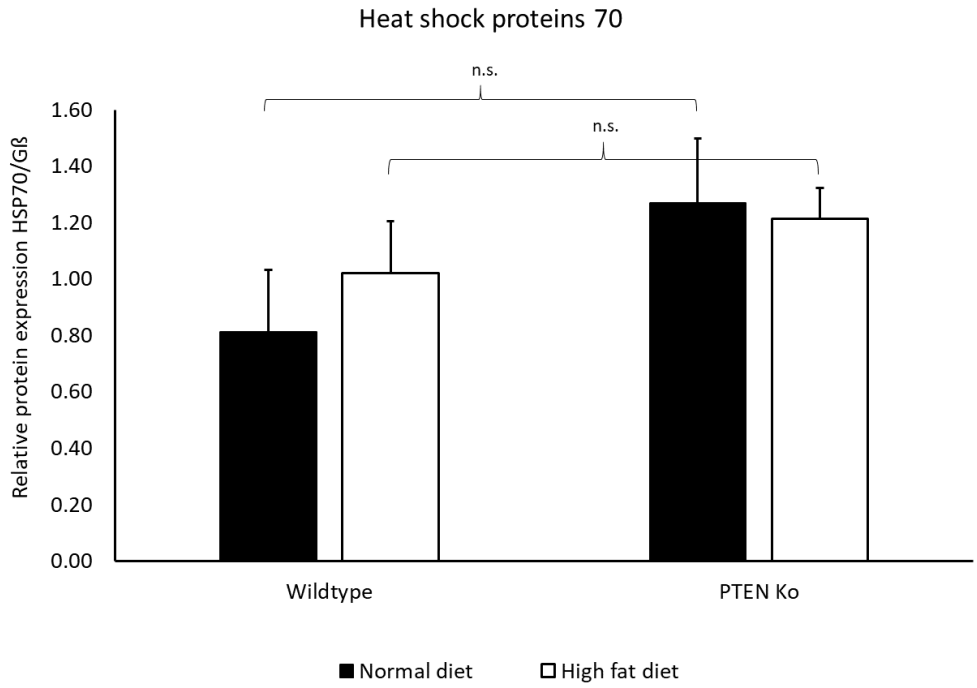

Figure 18. Expression of Heat shock protein 70 (HSP70) in wildtype and PTEN Ko mice detected by western blotting

Kidney tissue of mice groups with wildtype and a haplodeficient single allele knockout of the PTEN gene, fed with a normal diet or a high fat diet, probed with anti-HSP70 antibodies through western blotting. The anti-G-beta (Gβ) was used as the loading control. The n.s. indicates no significant difference between the different groups.

Similarly, the tissue was probed for the heme oxygenase HO-1 protein and the results showed a non-significant increase in HO-1 expression in the PTEN Ko group of mice. By comparing the two types of diets, a slight increase in oxidative stress was observed in the wild type mice, whereas no such effect was observed among the PTEN Ko animals (Figure 19).

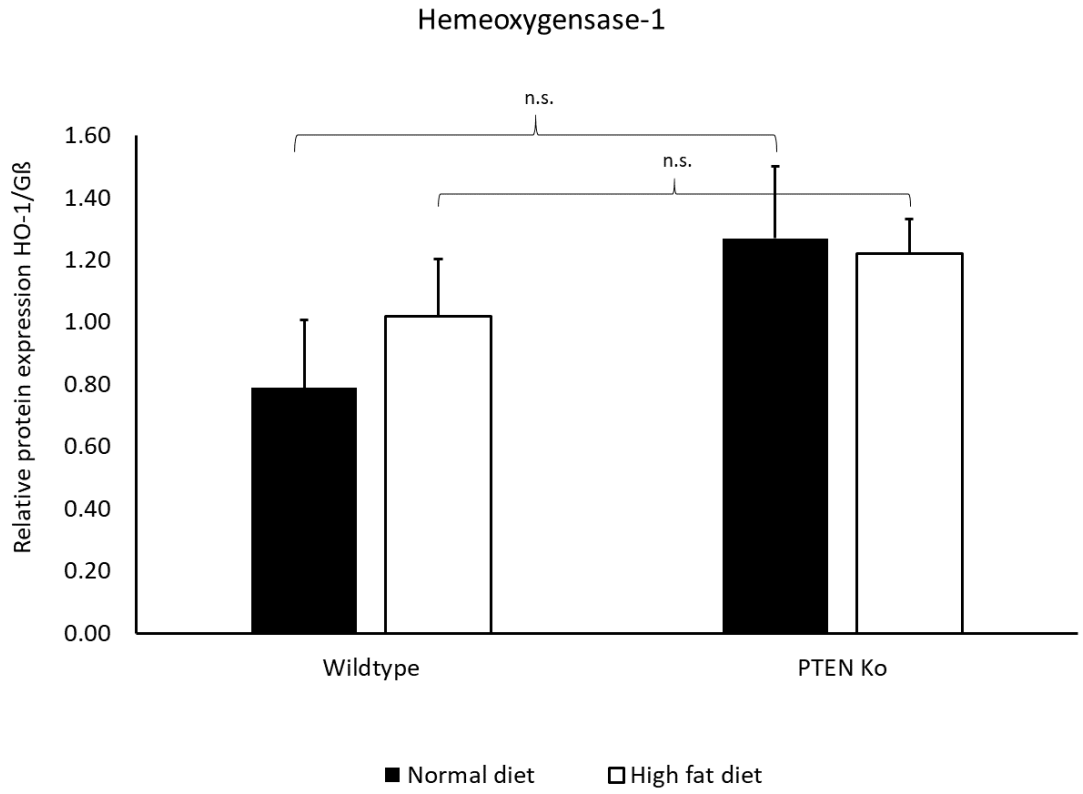

Figure 19. Expression of Hemeoxygenase-1 (HO-1) detected by western blotting in wildtype and PTEN Ko mice

Kidney tissue of mice groups with wildtype and a haplodeficient single allele knockout of the PTEN gene, fed with a normal diet or a high fat diet, probed with anti-HO-1 antibodies through western blotting. The anti-G-beta (Gβ) was used as the loading control. The n.s. indicates no significant difference between the different groups.

To further analyse the effect of PTEN inhibition in insulin mediated oxidative stress and genomic damage, we tested this *in vitro* in mammalian kidney cell lines (NRK and LLC PK1). The *in vitro* MN test was conducted in the NRK cells with the combination of insulin and the pharmacological PTEN inhibitor VO-Ohpic 50nM (IC_{50} value-50nM). The results showed a significant increase in MN induction as compared to the control with insulin and its combination with VO-Ohpic (Figure 20).

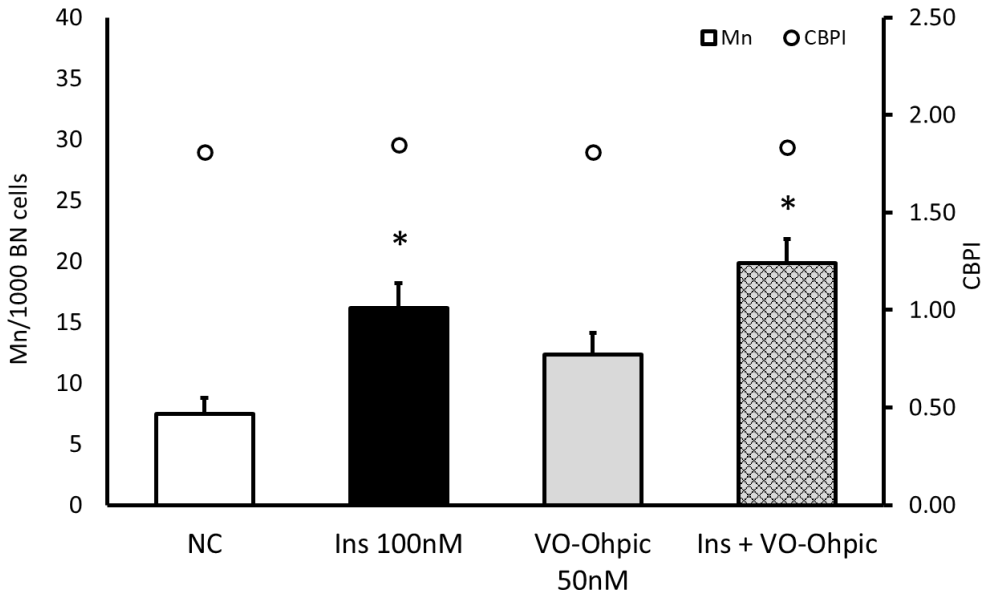

Figure 20. Micronucleus induction in NRK cells with 100nM insulin (Ins) and 50nM VO-Ohpic and their combination

*NRK cells were treated for 30min with the PTEN inhibitor VO-Ohpic 50nM and then for 4h with insulin 100nM, followed by the addition of cytochalasin B 3µg/mL for 20-22h and the micronucleus number was counted per 1000 binucleated cells. Cell proliferation (cytokinesis block proliferation index [CBPI] (unfilled dots) is shown on the secondary y-axis. * significantly different from control with p≤.05. BN = binucleated, Mn = micronuclei, Ins = insulin.*

A test for oxidative stress induction using ROS detection was performed by measuring the DHE fluorescence in NRK cells treated with insulin, VO-Ohpic and their combination. Antimycin A was used a positive control for ROS induction (Figure 21A). The results showed a significant increase in ROS induction after insulin treatment, while VO-Ohpic alone and its combination with insulin did not show an increase in ROS formation (Figure 21B).

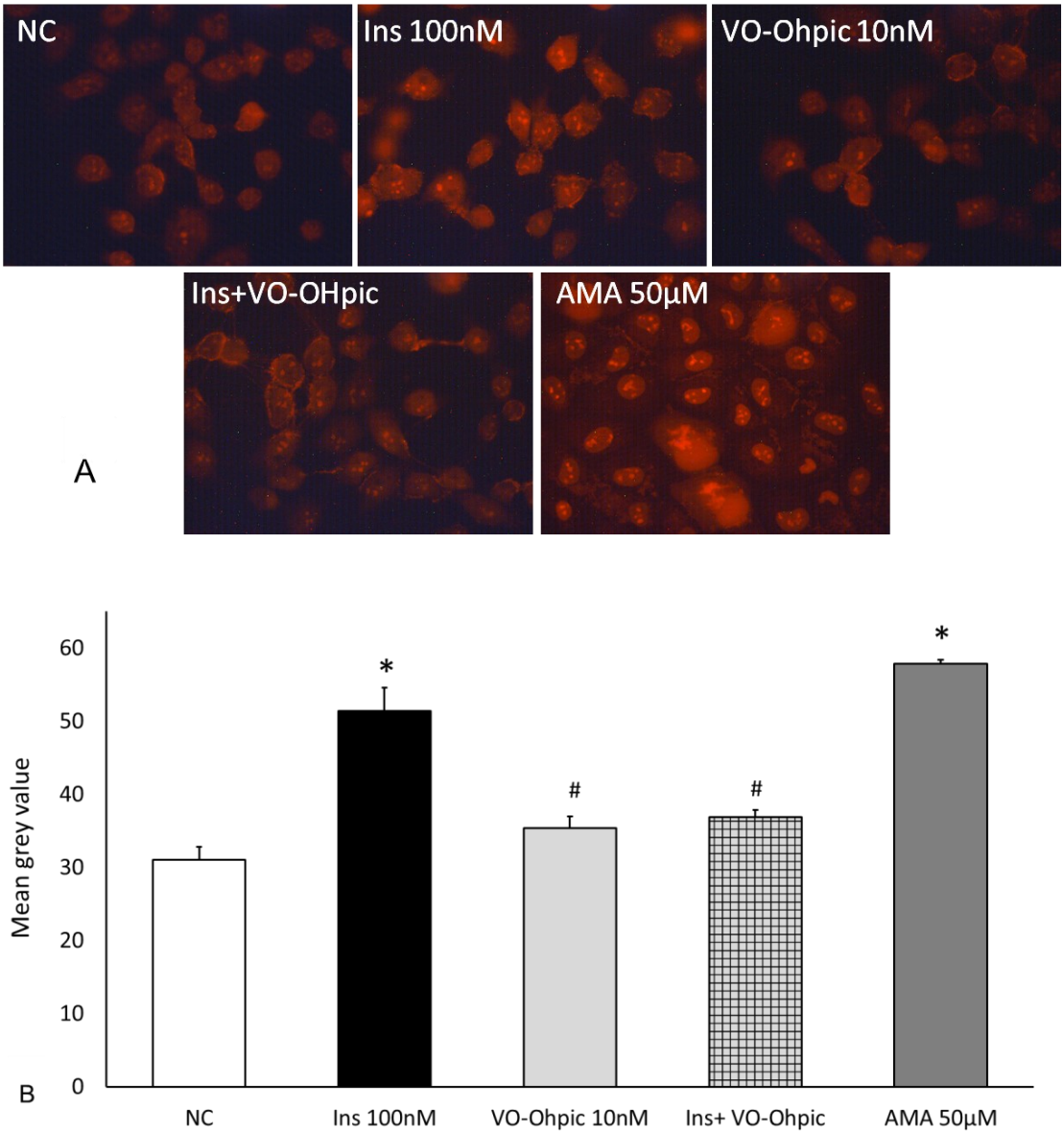

Figure 21. DHE fluorescence to measure the ROS induction in NRK cells treated with insulin 100nM and VO-Ohpic 10nM and their combination

*A. NRK cells treated for 30min with the PTEN inhibitor VO-Ohpic 10nM and then for 30min with insulin 100nM, along with 10µM DHE dye. Antimycin A 50µM was used as the positive control. B. The graph shows the DHE fluorescence measured as the mean grey value using the Image J software. * significantly different from control, # significantly different from insulin with p≤.05. Ins = insulin, AMA = antimycin A.*

We then tested the role of mitochondrial dysfunction through the changes in the mitochondrial membrane potential as the reason for the oxidative stress and ROS leakage. This was tested by staining NRK cells treated with insulin, VO-Ohpic and their

combination with TMRE dye to detect the depolarized state of the mitochondrial membrane (Figure 22A). The results showed a significant reduction in mitochondrial membrane potential in the insulin treated cells. The VO-Ohpic treatment also showed significantly lower mitochondrial membrane potential compared to the control, however it was also significantly higher than after the insulin treatment. The combination of insulin and VO-Ohpic yielded a significantly lower mitochondrial membrane potential as compared to the control (Figure 22B). Here we again used antimycin A as a positive control for mitochondrial toxicity.

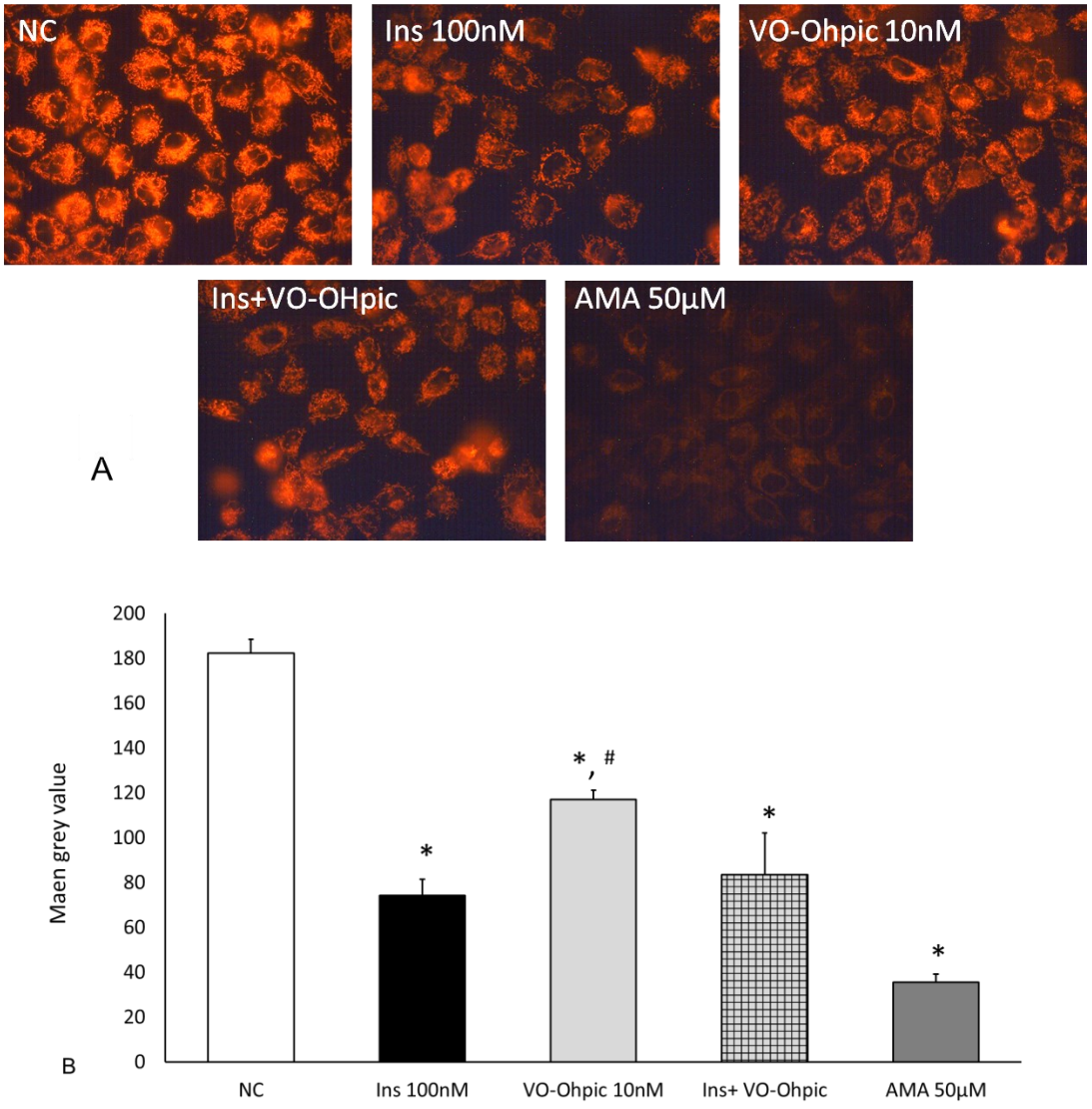

Figure 22. TMRE fluorescence to measure the change in mitochondrial membrane potential in NRK cells treated with insulin 100nM and VO-Ohpic 10nM and their combination

*A. NRK cells treated for 30min with the PTEN inhibitor VO-Ohpic 10nM and then for 30min with insulin 100nM, along with 10nM TMRE dye. Antimycin A 50µM was used as positive control. B. The graph shows the TMRE fluorescence measured as the mean grey value using the Image J software. * significantly different from control, # significantly different from insulin with p≤.05. Ins = insulin, AMA = antimycin A.*

The results from the micronucelus test conducted in LLCPK1 cells showed a significant increase in MN induction with insulin, as compared to that of the control and the combination of insulin with the pharmacological PTEN inhibitor VO-Ohpic (Figure 23).

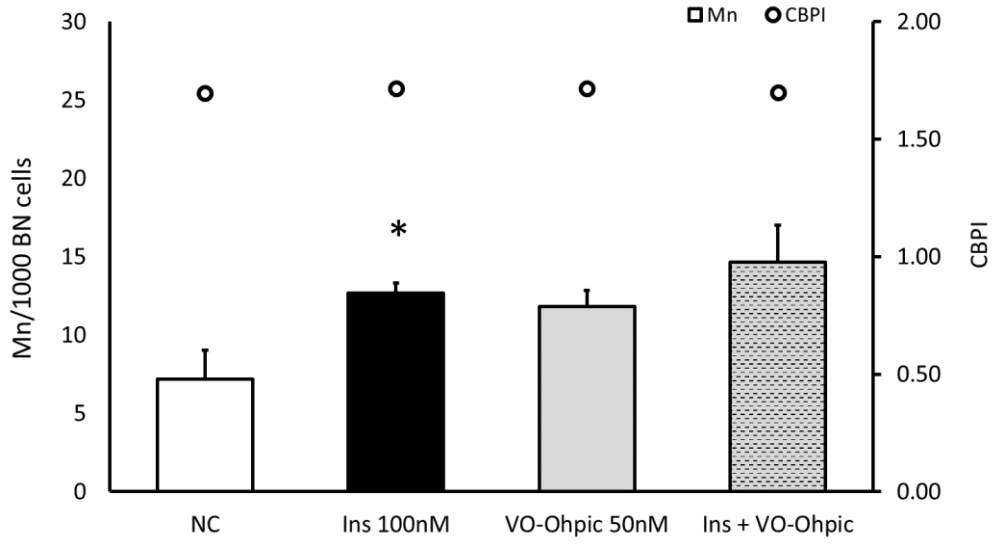

Figure 23. Micronucleus induction in LLCPK-1 cells with insulin 100nM and VO-Ohpic 50nM and their combination

*LLCPK-1 cells were treated for 30min with the PTEN inhibitor VO-Ohpic 50nM and then for 4h with insulin 100nM, followed by the addition of cytochalasin B 3µg/mL for 20-22h and the micronucleus number was counted per 1000 binucleated cells. Cell proliferation (cytokinesis block proliferation index [CBPI] (unfilled dots) is shown on the secondary y-axis. * significantly different from control with p≤.05. BN = binucleated, Mn = micronuclei; Ins = insulin*

A test for the oxidative stress induction using ROS detection was performed by measuring DHE fluorescence in LLCPK-1 cells treated with insulin, VO-Ohpic and their combination. Antimycin A was used a positive control for ROS induction (Figure 24A). The results showed a slight increase in ROS induction after insulin treatment, but VO-

Ohpic alone and its combination with insulin did not show an increase in ROS formation (Figure 24B).

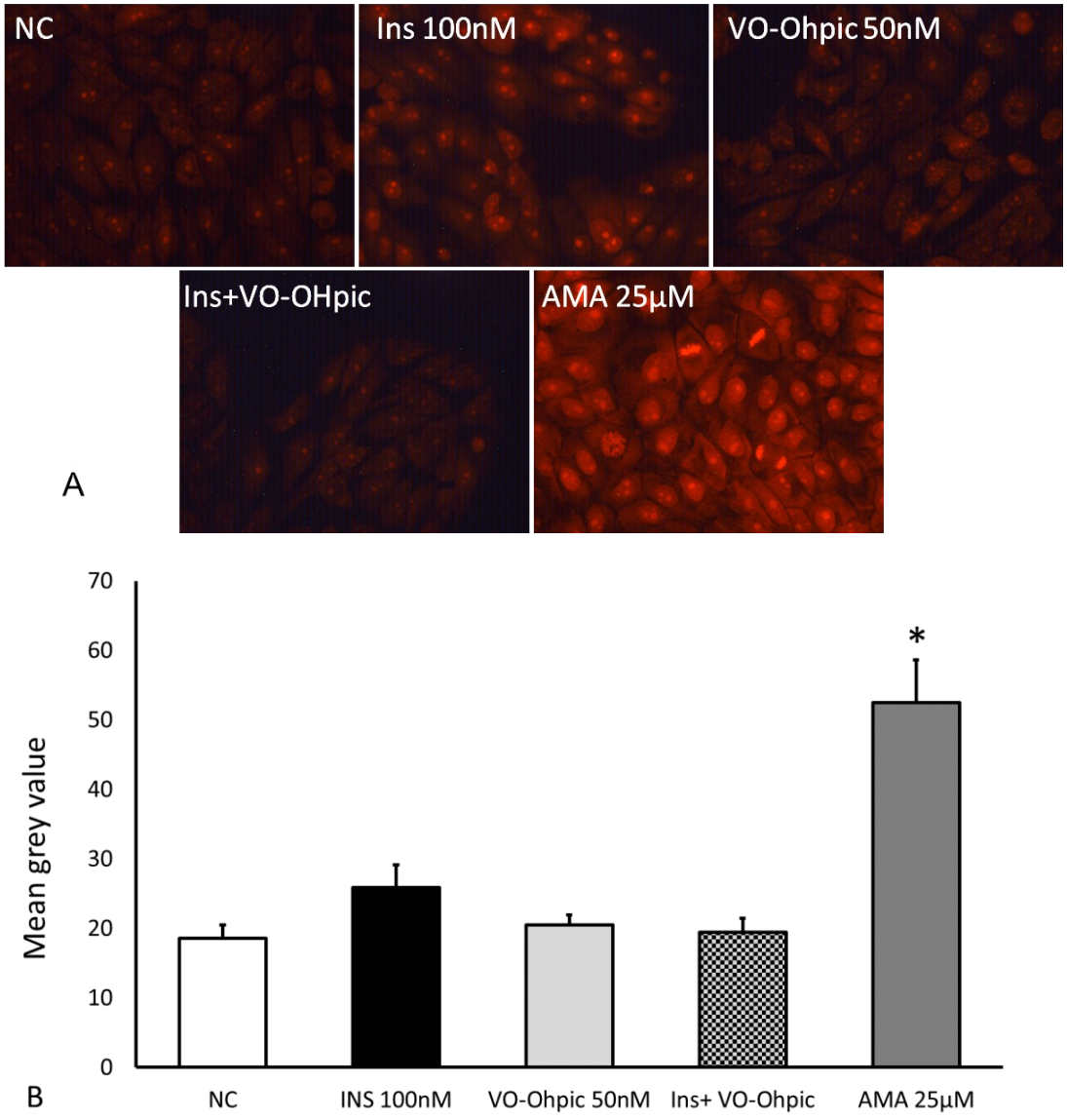

Figure 24. DHE fluorescence to measure the ROS induction in LLCPK-1 cells treated with insulin 100nM and VO-Ohpic 50nM and their combination

A. LLCPK-1 cells treated for 30min with the PTEN inhibitor VO-Ohpic 50nM and then for 30min with insulin 100nM, along with 10µM DHE dye. Antimycin A 25µM was used as positive control.

*B. The graph shows the DHE fluorescence measured as the mean grey value using the Image J software. * significantly different from control, # significantly different from insulin with p≤.05. Ins = insulin, AMA = antimycin A.*

We then tested the role of mitochondrial dysfunction through the changes in the mitochondrial membrane potential as the reason for the oxidative stress and ROS leakage. This was tested by staining the LLCPK-1 cells treated with insulin, VO-Ohpic and their combination with TMRE dye to detect the depolarized state of the mitochondria membrane (Figure 25A). The results showed a non-significant reduction in the mitochondrial membrane potential in the insulin treated cells as compared to the control. The VO-Ohpic treatment also showed a slightly lower mitochondrial membrane potential as compared to the control. The combination of insulin and VO-Ohpic showed a significantly lower mitochondrial membrane potential as compared to the control (Figure 25B). Here we again used antimycin A as a positive control for mitochondrial toxicity.

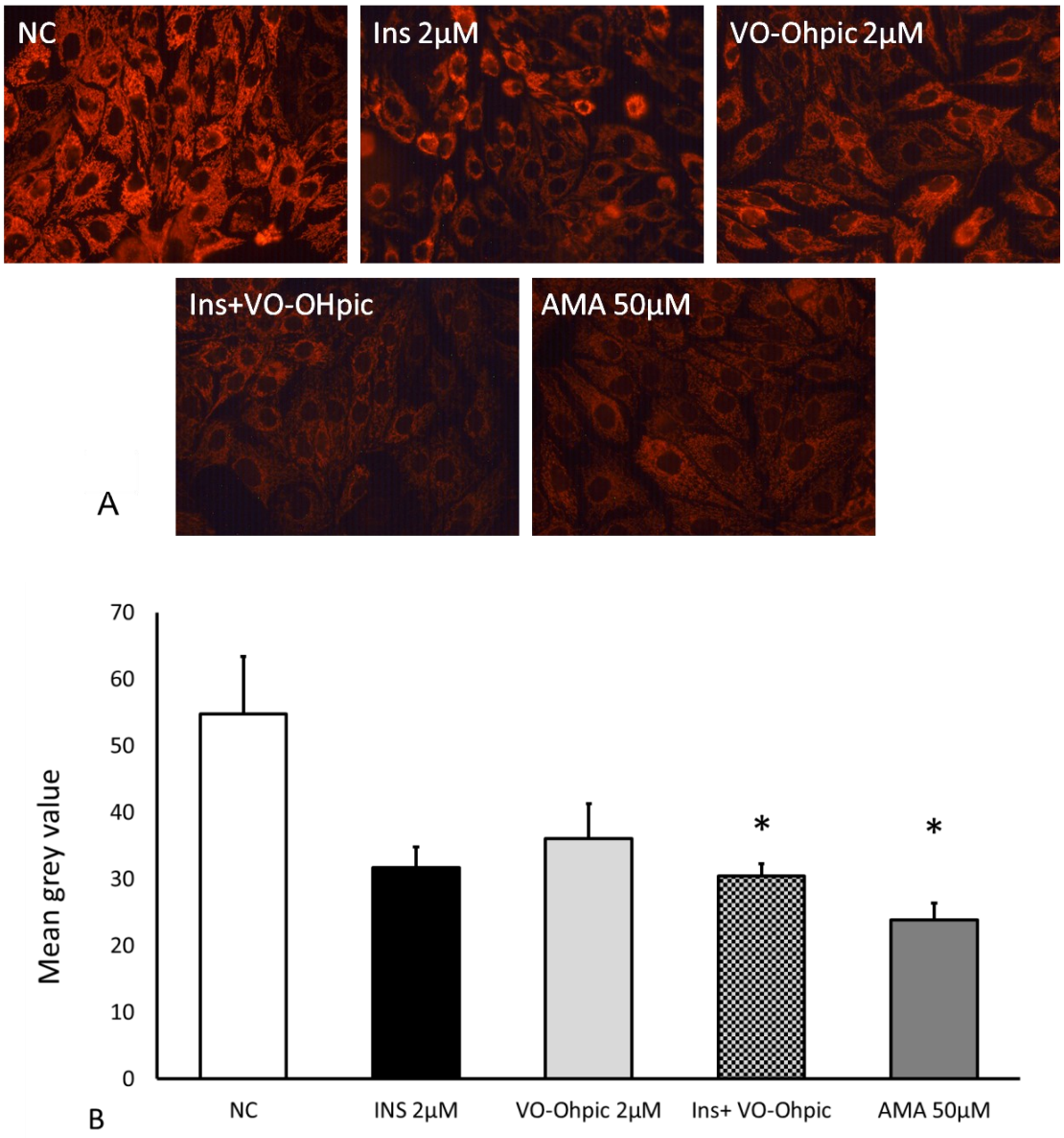

Figure 25. TMRE fluorescence to measure the change in mitochondrial membrane potential in LLCPK-1 cells treated with insulin 100nM and VO-Ohpic 2µM and their combination

A. LLCPK-1 cells treated for 30min with the PTEN inhibitor VO-Ohpic 2µM and then for 30min with insulin 100nM, along with 10nM TMRE dye. Antimycin A 50µM was used as the positive control.

*B. The graph shows the TMRE fluorescence measured as the mean grey value using the Image J software. * significantly different from control with p≤.05. Ins = insulin, AMA = antimycin A.*

4.3. Effect of proliferative stress on micronucleus induction

We further studied the influence of PTEN suppression on MN and oxidative stress induction as seen in section 4.2, by investigating the effect of insulin on the proliferation and the genomic damage induction in Hela-H2B-GFP cells. Here, we combined the treatment of insulin with the pharmacological PTEN inhibitor VO-Ohpic and checked for their effect on MN induction and proliferation. The CBMN assay showed a non-significant, slight increase in MN induction and a non-significant reduction with the combination of insulin and VO-Ohpic as compared to the control (Figure. 26).

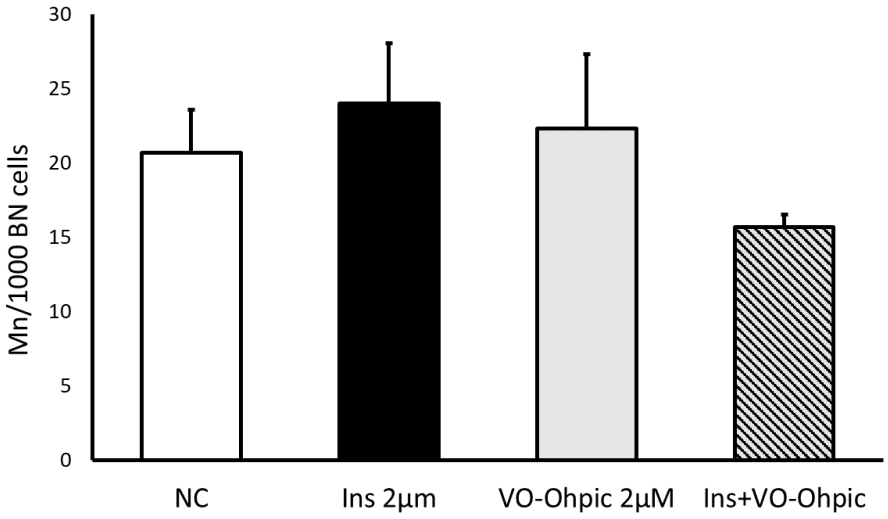

Figure 26. Micronucleus induction in Hela-H2B-GFP cells with insulin 2µM and VO-Ohpic 2µM and their combination

Hela-H2B-GFP cells were treated for 30min with the PTEN inhibitor VO-Ohpic 2µM and then for 4h with insulin 2µM, followed by the addition of cytochalasin B 3µg/mL for 20-22h and the micronucleus number was counted per 1000 binucleated cells. No statistical significance was observed. Ins = insulin.

We then used live cell microscopy to observe the induction of micronuclei, apoptosis, and multipolar mitosis in the Hela-H2B-GFP cells. In Figure 27, it was seen that the treatment with insulin 2µM and MMS 200µM showed a higher induction of micronuclei as compared to the untreated control in 1000 live cells. The treatment with insulin also showed a 3-fold increase in multipolar mitosis as compared to the

control and the MMS. Then, scoring for the cells going into apoptosis showed that the insulin treated cells had a lower apoptosis number as compared to that of the control and the MMS treatment.

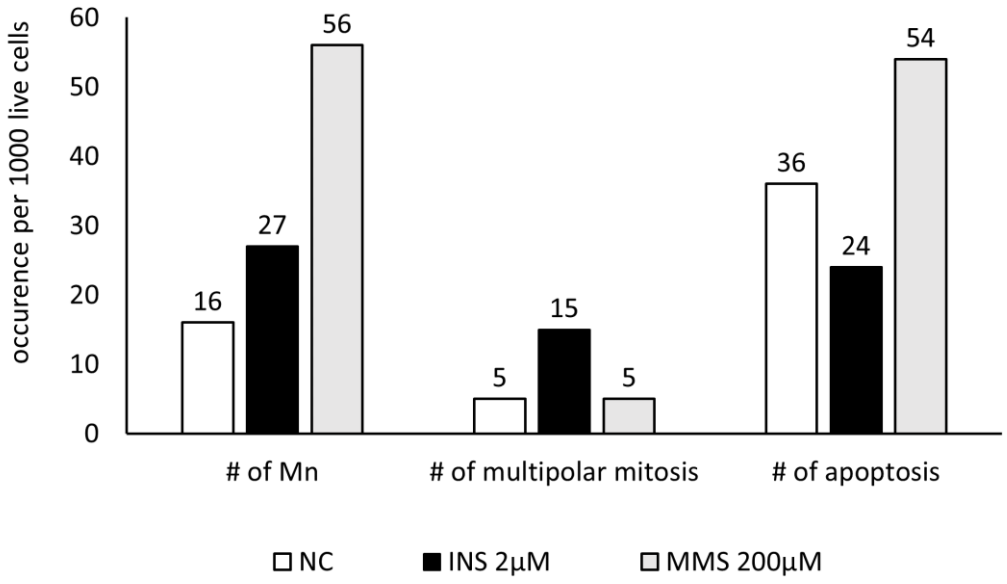

Figure 27. Live cell imaging and scoring micronuclei in Hela-H2B-GFP treated with insulin 2µM and MMS 200µM as positive control

The graph shows the occurrence of micronuclei, multipolar mitosis and apoptosis counted from 1000 live cells, which were added up from three experimental runs. The images were recorded at every 10min interval for a duration of 24h using fluorescence microscopy. Ins = insulin, MMS = methyl methane sulfonate.

Because of the increase in MN induction and the multipolar mitosis, we next measured the duration of mitosis after the treatment with insulin and MMS. The results showed that the insulin treated cells had a shorter duration of mitosis as compared to the control and MMS. The MMS treatment, which is the positive control for micronucleus induction had the longest duration of mitosis (Figure 28).

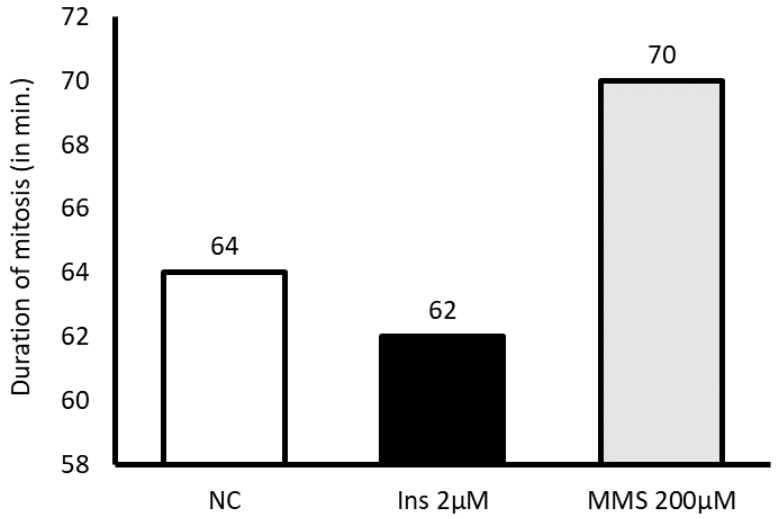

Figure 28. Scoring the period of mitosis in Hela-H2B-GFP treated with insulin 2µM and MMS 200µM as positive control

The graph shows the mean duration of mitosis in minutes after being treated with insulin 2µM and MMS 200µM occurring among 1000 live cells, which were added up from three experimental runs. The images were recorded at every 10min interval for a duration of 24h using fluorescence microscopy. Ins = insulin, MMS = methyl methane sulfonate.

We then evaluated the total number of mitoses occurring per 1000 live cells within 24h of observation. The insulin treated cells showed a 11% higher occurrence of mitosis and the MMS treated cells showed a 24.8% lower occurrence of mitosis as compared to the control in the Hela-H2B-GFP cells (Figure 29). The observation of more than 1000 mitoses indicates the occurrence of more than one cell division within the 24h duration and the decrease indicates a delay/arrest in cell cycle of the treated cells.

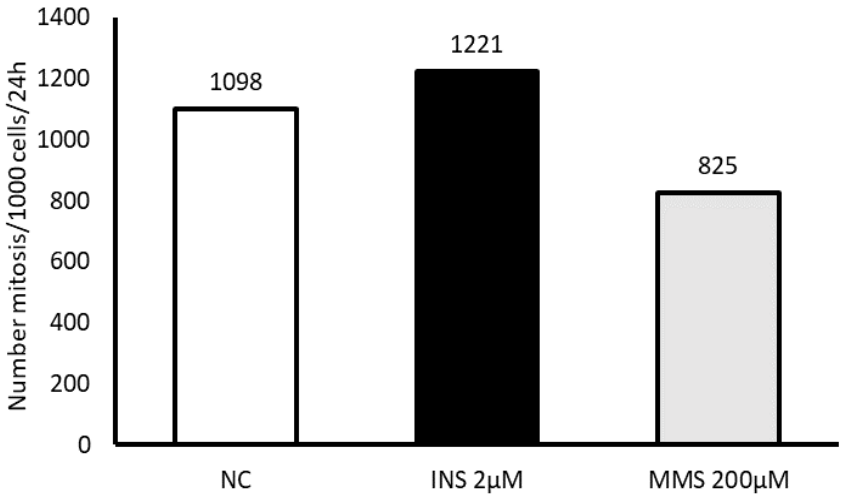

Figure 29. The total number of mitosis in Hela-H2B-GFP treated with insulin 2µM and MMS 200µM as positive control

The graph shows the total number of mitosis after being treated with insulin 2µM and MMS 200µM occurring among 1000 live cells, which were added up from three experimental runs. The images were recorded at every 10min interval for a duration of 24h using fluorescence microscopy. Ins = insulin, MMS = methyl methane sulfonate.

We calculated the mean for the duration taken by the cells to complete one mitosis i.e., from the prophase to the end of the telophase when the daughter nuclei had reached their final distance after division. To identify the mitotic phase which may be responsible for the faster progression of insulin treated cells, we watched the duration taken by the cells to proceed through the different stages of the mitosis. This was now done with a much higher temporal resolution, taking pictures every 2 minutes. The results showed that, like previously seen, the insulin treated cells had a significantly lower duration of mitosis as compared to the control, especially the duration from the beginning of metaphase to the end of anaphase. However, from the beginning of prophase to metaphase and from anaphase to telophase the insulin treated cells exhibited a significantly longer duration than the untreated controls (Figure 30).

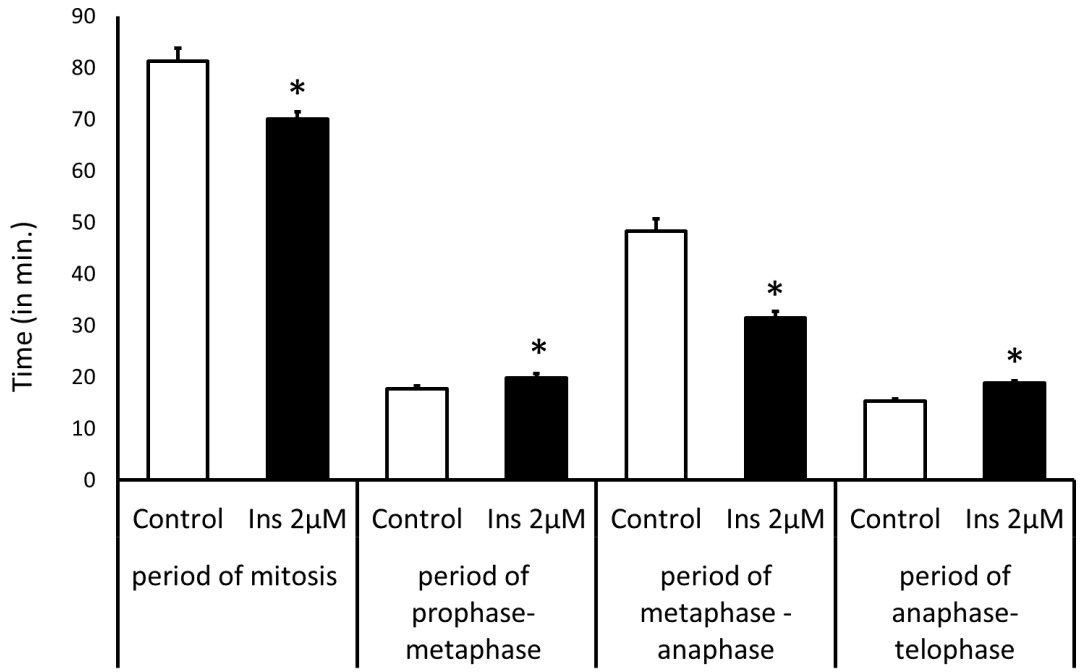

Figure 30. Live imaging of the different stages of mitosis after treatment with insulin 2µM and solvent control

*The graph shows the period taken for the total mitosis, from prophase to metaphase, metaphase to anaphase and from anaphase to telophase for 24h. The images were recorded at every 2min interval for a duration 24h using fluorescence microscopy. * significantly different from control with p≤.05. Ins = insulin.*

Further, we wanted to see whether the accelerated proliferation had any effect on scratch wound healing using live cell microscopy. Therefore, we treated the Hela-H2B-GFP cells with insulin and observed its effect in scratch healing by measuring the change in scratch width and area every 30min over a duration of 24h. The results from comparing the width of the scratch from the start (time 0h) to after 24h showed an increased difference in scratch width after insulin treatment (which shows a faster closure of the wound) as opposed to the effect seen by the control and the PTEN inhibitor VO-Ohpic. The combination of insulin and VO-Ohpic also showed a further decrease in the length of the scratch (Figure 31). Similarly, there was an increase in the difference in the scratch area in the insulin treated cells as compared to VO-Ohpic, their combination and the control (Figure 32). These results show that the insulin

treated cells undergo a faster wound closure after 24h as compared to the untreated control and the treatment with VO-Ohpic.

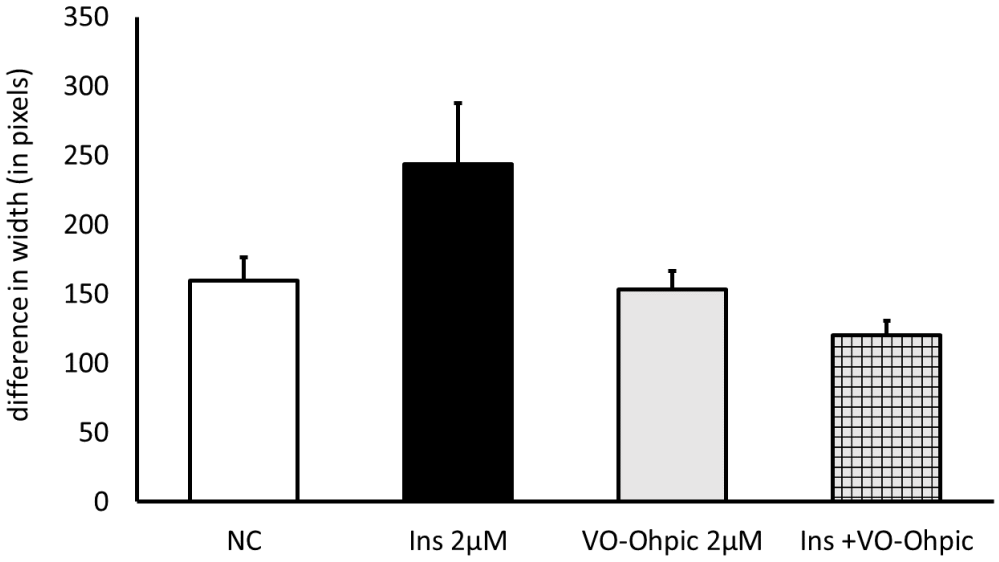

Figure 31. Live imaging of scratch wound healing in Hela-H2B-GFP cells with insulin 2µM and VO-Ohpic 2µM and their combination

The graph shows the difference in scratch width after treatment with insulin 2µM, VO-Ohpic 2µM and their combination, which was observed after 24h. The results are from 3 independent experiments and no statistical significance was seen. Ins = insulin.

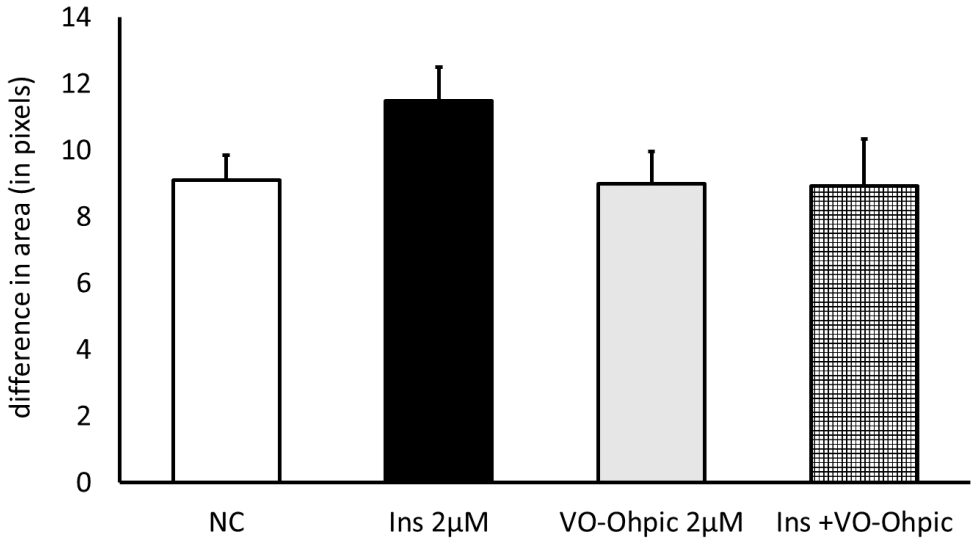

Figure 32. Live imaging of scratch wound healing in Hela-H2B-GFP cells with insulin 2µM and VO-Ohpic 2µM and their combination

The graph shows the difference in scratch area after treatment with insulin 2µM, VO-Ohpic 2µM and their combination, which was observed after 24h. The results are from 3 independent experiments and no statistical significance was seen. Ins = insulin.

We were then interested in counting the number of micronuclei induced in the scratch region, among the cells which had migrated and/or divided into the scratch area. We performed this by manual counting of micronuclei present in 1000 cells within the original scratch region. The results showed a slight non-significant increase in the number of micronuclei after insulin, VO-Ohpic and their combined treatment as compared to the control (Figure 33). We also observed the number of mitotic cells present in the area and clearly, the insulin treated cells had an increase in the number of mitosis as compared to the control and VO-Ohpic treated cells in the scratch region (Figure 34).

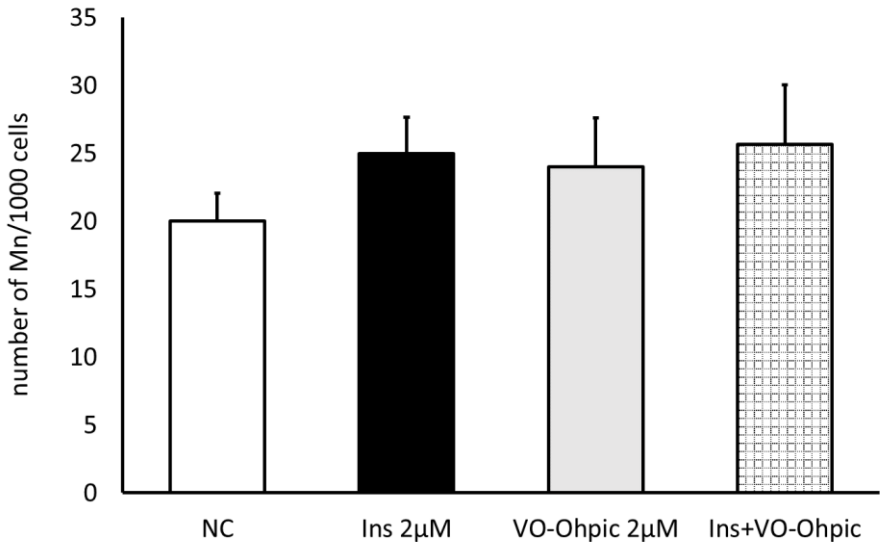

Figure 33. Live imaging of scratch wound healing in Hela-H2B-GFP cells with insulin 2µM and VO-Ohpic 2µM and their combination

The graph shows the number of micronuclei counted in the scratch area in 1000 mononucleated cells, after treatment with insulin 2µM, VO-Ohpic 2µM and their combination, which was observed after 24h. The results are from 3 independent experiments and no statistical significance was seen. Ins = insulin.

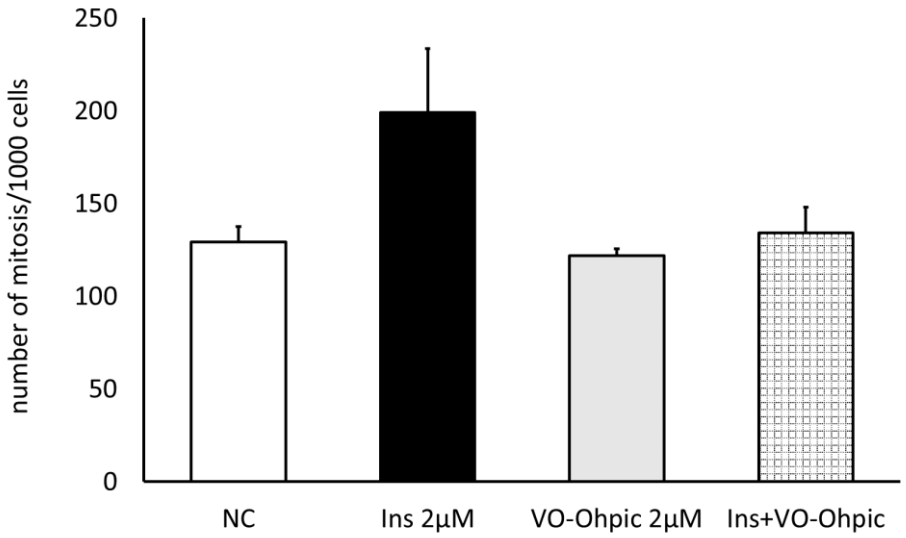

Figure 34. Live imaging of scratch wound healing in Hela-H2B-GFP cells with insulin 2µM and VO-Ohpic 2µM and their combination

The graph shows the number of mitosis which occurred among 1000 mononucleated cells, counted in the scratch area, after treatment with insulin 2µM, VO-Ohpic 2µM and their combination, which was observed after 24h. The results are from 3 independent experiments and no statistical significance was seen. Ins = insulin.

Then we wanted to test the effect of ROS depletion by the antioxidant N-acetyl cysteine (NAC) on insulin mediated proliferation and wound healing using the scratch assay to identify a possible role of ROS-related signalling in these events. The results showed a significant increase in MN with the insulin treated cells in the scratch area followed by a clear reduction in the number of micronuclei after treatment with NAC (Figure 35).

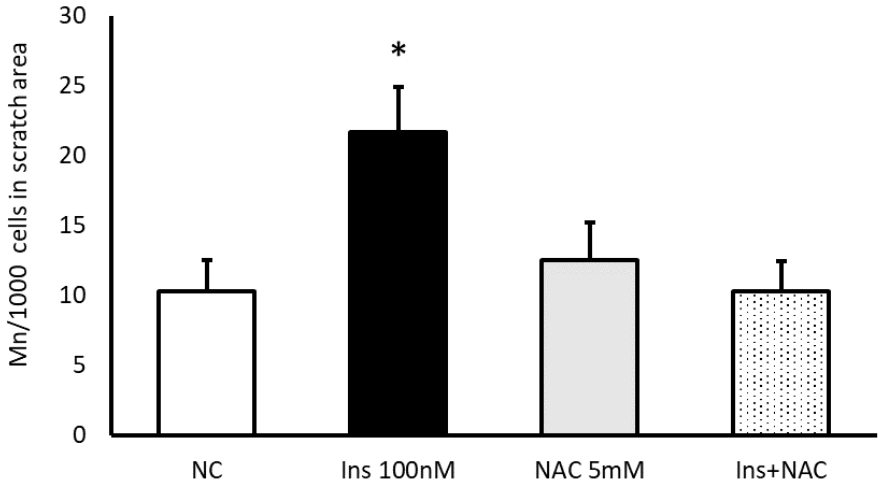

Figure 35. Live imaging of scratch wound healing in Hela-H2B-GFP cells with insulin 2µM and NAC 5mM and their combination

*The graph shows the number of micronuclei counted in the scratch area in 1000 mononucleated cells, after treatment with insulin 2µM, NAC 5mM and their combination, which was observed after 24h. The results are from 3 independent experiments. * significantly different from control with p≤.05. Ins = insulin, NAC = N-acetylcysteine.*

Similarly, the scratch assay showed an increase in the number of mitosis observed in the scratch region as compared to the control and this was reduced after combining with the NAC (Figure 36).

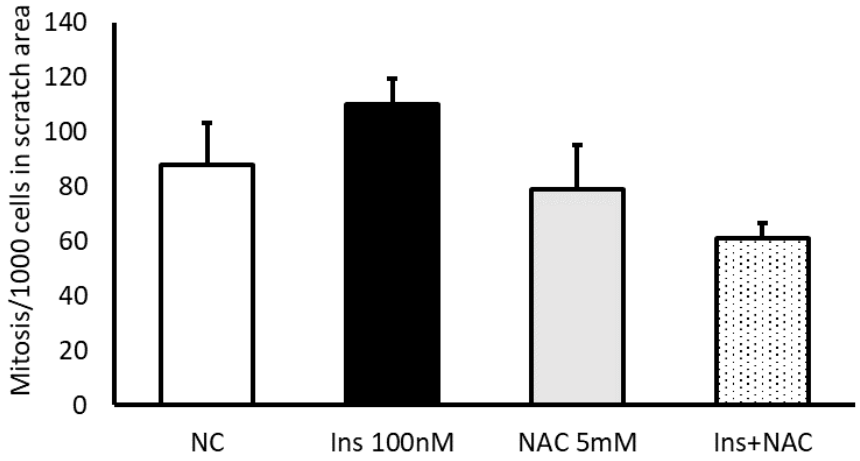

Figure 36. Live imaging of scratch wound healing in Hela-H2B-GFP cells with insulin 2µM and NAC 5mM and their combination

The graph shows the number of mitosis which occurred among 1000 mononucleated cells, counted in the scratch area, after treatment with insulin 2µM, NAC 5mM and their combination, which was observed after 24h. The results are from 3 independent experiments and no statistical significance was seen. Ins = insulin, NAC = N-acetylcysteine.

We measured the induction of oxidative stress by measuring ROS through DHE fluorescence in Hela-H2B-GFP cells treated with insulin, VO-Ohpic and their combination. Antimycin A was used as the positive control for ROS induction (Figure 37A). The results showed a significant increase in ROS induction after insulin treatment. The treatment with VO-Ohpic alone did not show an increase in ROS and it also prevented the ROS induction by insulin in the combination (Figure 37B).

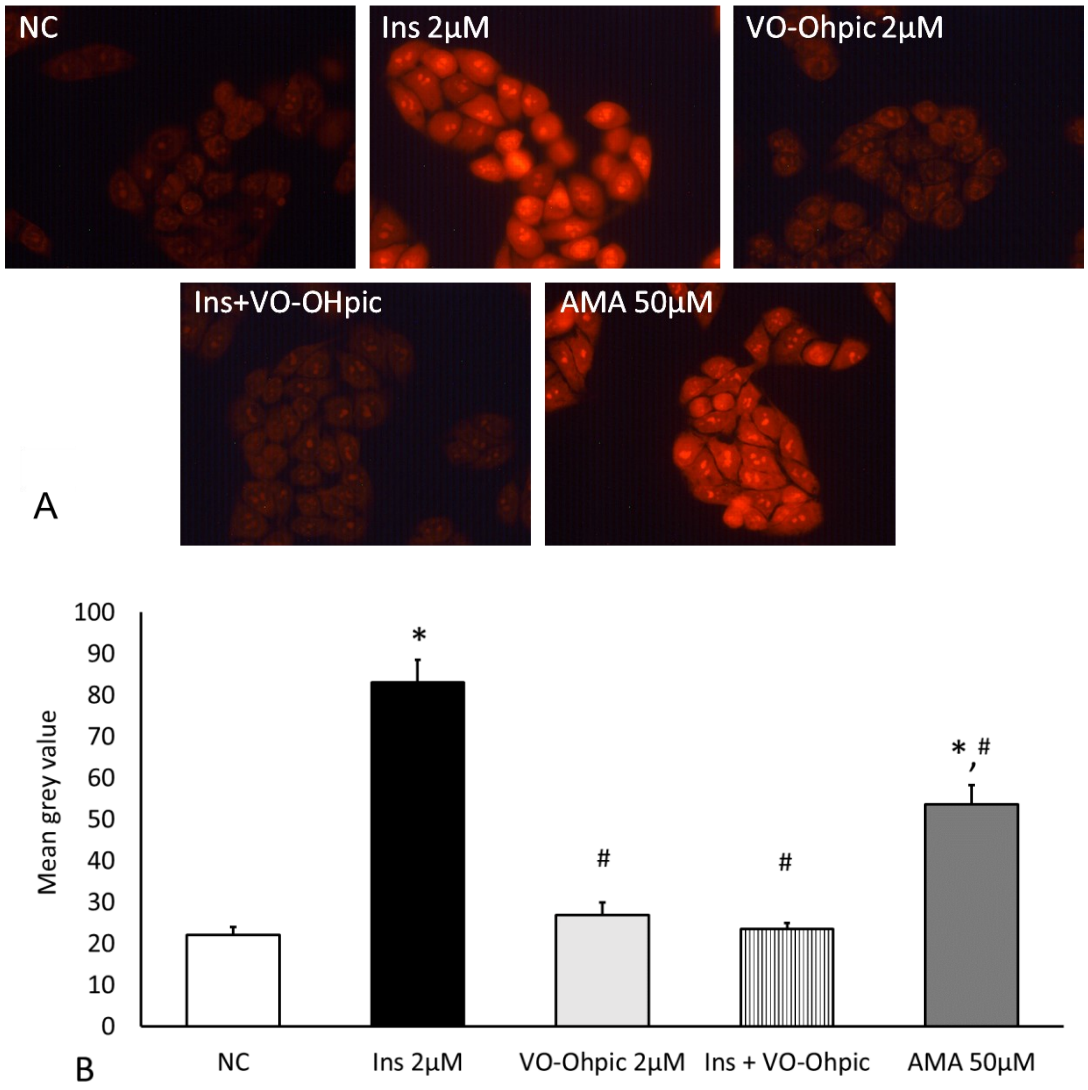

Figure 37. DHE fluorescence to measure the ROS induction in Hela-H2B-GFP cells treated with insulin 2µM and VO-Ohpic 2µM and their combination

A. Hela-H2B-GFP cells were treated for 30min with the PTEN inhibitor VO-Ohpic 2µM and then for 30min with insulin 2µM, along with 10µM DHE dye. Antimycin A 50µM was used as the positive control.

*B. The graph shows the DHE fluorescence measured as the mean grey value using the Image J software. * significantly different from control, # significantly different from insulin, *# different from both control and insulin with p≤.05. Ins = insulin, AMA = antimycin A*

We then tested the depolarization of the mitochondria by staining the Hela-H2B-GFP cells treated with insulin, VO-Ohpic and their combination by staining with TMRE dye (Figure 38A). The results showed only a slight reduction in mitochondrial membrane

potential in the insulin treated cells. The VO-Ohpic treatment alone and its combination with insulin also showed a slightly lower mitochondrial membrane potential compared to the control (Figure 38B). Here we again used antimycin A as a positive control for mitochondrial toxicity.

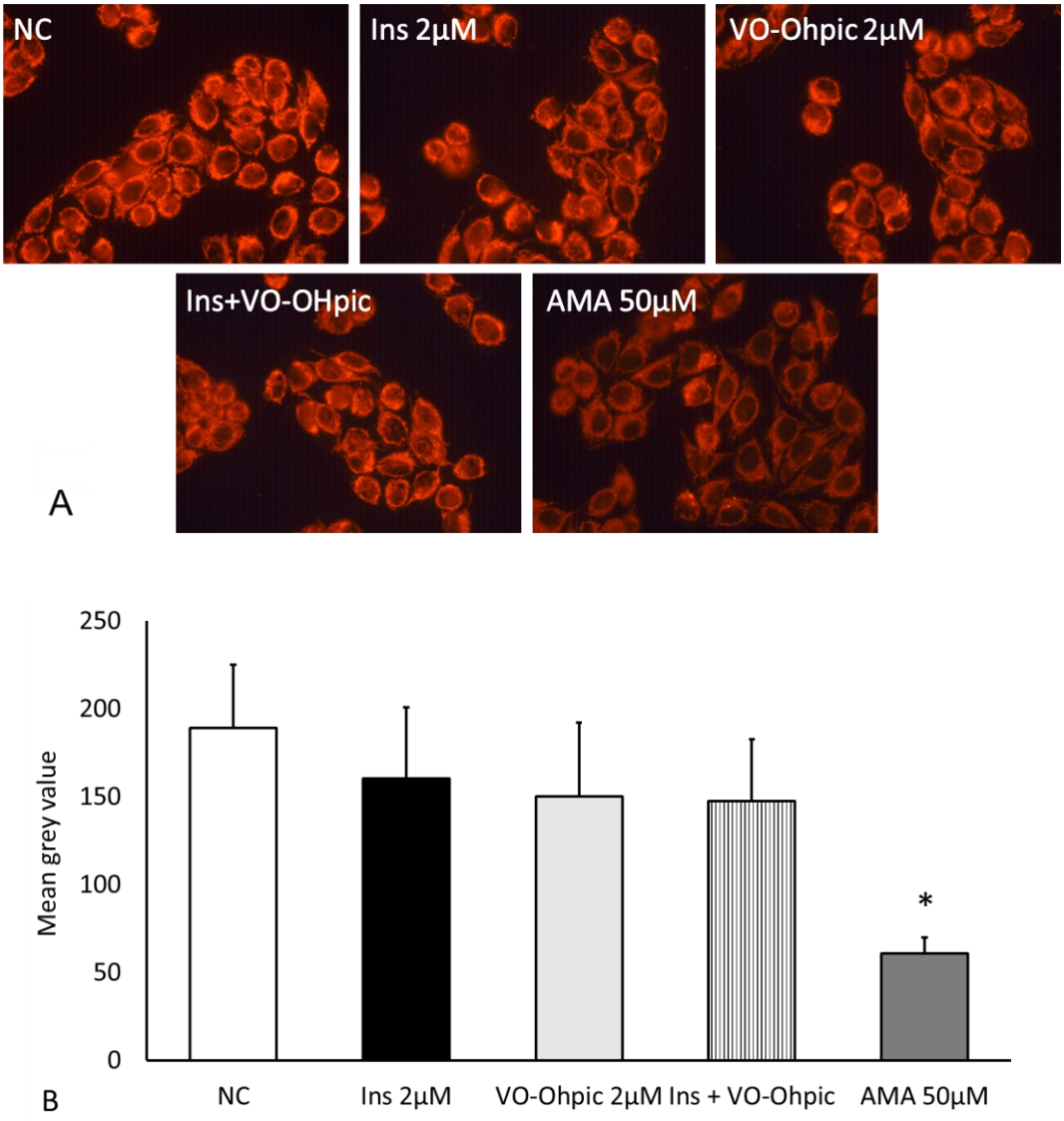

Figure 38. TMRE fluorescence to measure the ROS induction in Hela-H2B-GFP cells treated with insulin 2µM and VO-Ohpic 2µM and their combination

A. Hela-H2B-GFP cells were treated for 30min with the PTEN inhibitor VO-Ohpic 2µM and then for 30min with insulin 2µM, along with 10nM TMRE dye. Antimycin A 50µM was used as the positive control.

*B. The graph shows the TMRE fluorescence measured as the mean grey value using the Image J software. * significantly different from control with p≤.05. Ins = insulin, AMA = antimycin A.*

4.4. Genotoxic outcomes in obese patients with diabetes

To study the influence of obesity and T2DM in causing genomic damage, we used peripheral blood monocytes and plasma from the blood of obese patients and healthy controls. Height, weight, age, gender and bodyweight of the study subjects were recorded (Table 2) along with their history of comorbidities, if present, by the Department of Surgery and Endocrinology, University Hospital of Wuerzburg. The levels of glycated haemoglobin were also recorded in these subjects (Table 3). Prior permission had been obtained from the journal *Mutation Research – Genetic Toxicology and Environmental Mutagenesis* for the work co-authored and published by the author of this thesis, to use the contents of the publication [84] in this dissertation (permission attached in Appendix).

Type	**Gender**	**Mean of**			
		Body weight [kg]	**Height [cm]**	**BMI [kg/m^2]**	**Age [years]**
Control	Female = 8	64.13	169.00	22.39	35
	Male = 2	84.10	183.00	25.11	28
Patients	Female = 23	135.98	165.70	49.65	44
	Male = 4	166.23	178.25	52.51	51

Table 2. Characteristics of subjects used in the human study.

Glycated haemoglobin (HbA1c)		
	< 6%	**> 6%**
Number	n = 15	n = 12
Mean	5.39	7.00

Table 3. Glycated hemoglobin HbA1C levels in obese subjects.

We compared the body weight between the healthy controls and obese patients, along with their sub-distribution based on the different co-morbidities [Insulin resistance (IR) (n = 6), Type 2 diabetes mellitus (T2DM) (n = 4), non-insulin resistant and Type 2 diabetes mellitus (nIR/T2DM) (n = 3)]. Although this overall patient group was described already in a paper by our group [84], the parameters shown here are

recalculated for the precise subgroup of patients studied, which resulted from the availability of samples from the previous larger group and some additional parameters were calculated. The results clearly showed that the obese patients had a 2-fold higher bodyweight and had a difference based on their co-morbidities. All sub-groups had a higher weight as compared to the controls and the sub-group, which were non-insulin resistant and Type-2 diabetes mellitus, had the highest body weight as compared to the controls (Figures 39, 40).

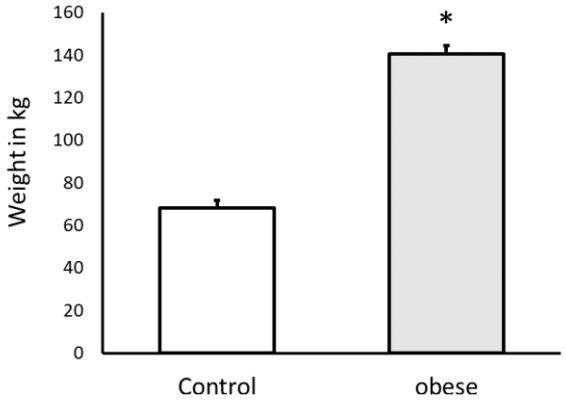

Figure 39. The graph shows the bodyweight distribution (in kg) of control and obese patients used in this study, n = 10 and n = 27, respectively.

** significantly different from control with p≤.05*

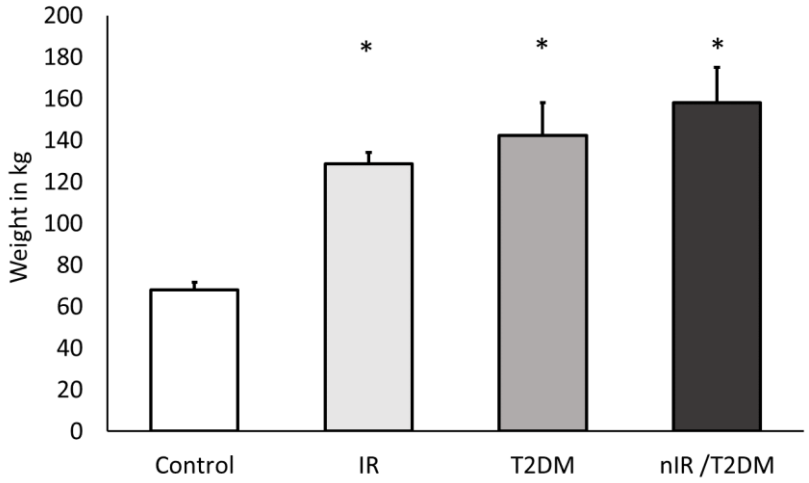

Figure 40. Bodyweight distribution (in kg) of control and obese patients with pre-existing conditions used in this study.

The graph shows the bodyweight (in kg); control (n = 10) and for different pre-existing conditions such as insulin resistance (IR) (n = 6), type-2 diabetes mellitus (T2DM) (n = 4), non-

*insulin resistant and type-2 diabetes mellitus nIR/T2DM (n = 3). * significantly different from control with p≤.05.*

We also compared the body mass index (BMI) between the healthy controls and obese patients, along with their sub-distribution based on the different co-morbidities [Insulin resistance (IR) (n = 6), Type 2 diabetes mellitus (T2DM) (n = 4), non-insulin resistant and Type 2 diabetes mellitus (nIR/T2DM) (n = 3)]. The results showed that the obese patients had a 2-fold higher BMI and a difference based on their co-morbidities. All of them had a higher BMI as compared to the controls and the sub-group, which had type-2 diabetes mellitus, had the highest BMI as compared to the controls (Figure 41, 42).

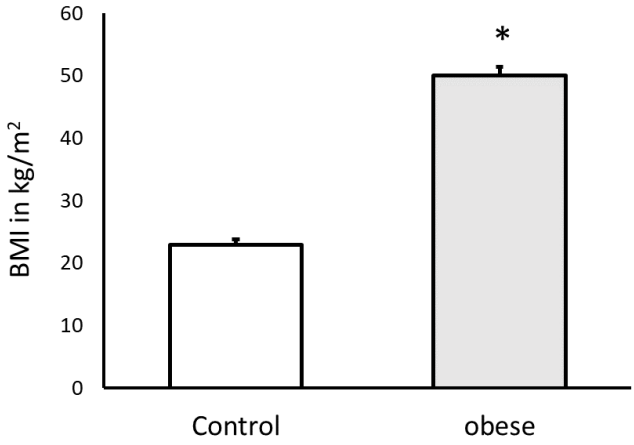

Figure 41. The graph shows the body mass index (BMI) distribution (in kg/m^2) of control and obese patients used in this study, n = 10 and n = 27, respectively.

** significantly different from control with p≤.05.*

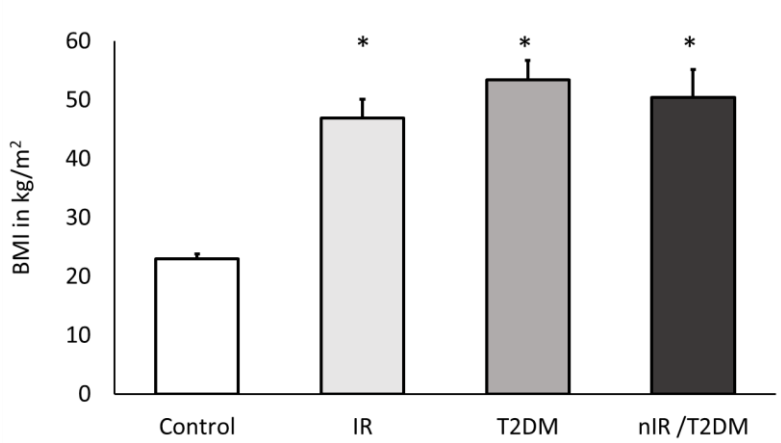

Figure 42. Body mass index (BMI) distribution (in kg/m^2) of control and obese patients with pre-existing conditions used in this study.

*The graph shows the body mass index (BMI) (in kg/m^2); control (n = 10) and for different pre-existing conditions such as insulin resistance (IR) (n = 6), type-2 diabetes mellitus (T2DM) (n = 4), non-insulin resistant and type-2 diabetes mellitus nIR/T2DM (n = 3). * significantly different from control with p≤.05.*

The peripheral blood mononuclear cells were collected from healthy controls and obese patients, and the alkaline comet assay was performed. The results showed a significantly higher level of DNA damage among the obese patients (n = 27), as compared to the healthy controls (n = 10), detected as percentage of tail DNA (Figure 43). When the patients with high levels of glycated hemoglobin (HbA1c ≥6%) were selected (n = 12), once again, significantly higher levels of DNA damage was detected as compared to the healthy controls (n = 10) (Figure 44). We then performed a correlation analysis to compare the relationship between the bodyweight, BMI, glycated hemoglobin and the percentage of DNA damage, but we did not find a positive correlation among them (data shown in Table 3 and Figure 48 of the Appendix).

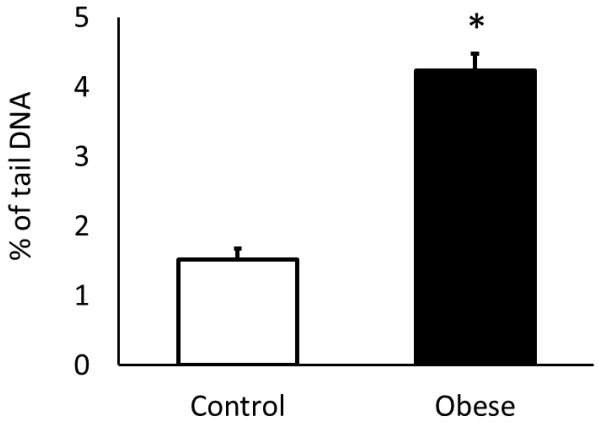

Figure 43. Genotoxicity assessment by alkaline comet assay in peripheral blood mononuclear cells of the control and obese patients, n = 10 and n = 27, respectively.

** significantly different from control with p≤.05*

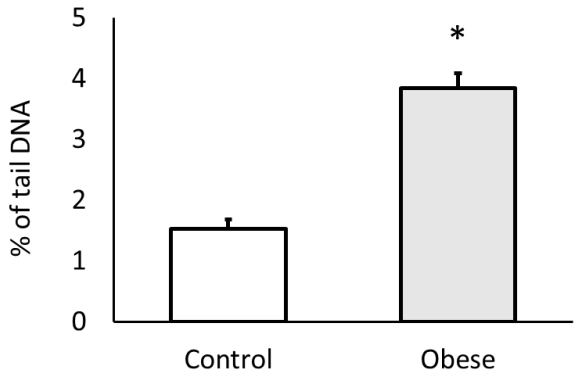

Figure 44. Genotoxicity assessment by comet assay in peripheral blood mononuclear cells of the control and obese patients with glycated hemoglobin (HbA1C) levels higher than 6

*The graph shows the percentage of DNA damage, detected by alkaline comet assay among the control (n = 10) and obese patients (n = 12). * significantly different from control with p≤.05*

We then sorted the DNA damage outcomes in those obese patients based on their pre-existing disease conditions [Insulin resistance (IR) (n = 6), Type 2 diabetes mellitus (T2DM) (n = 4), non-insulin resistant and Type 2 diabetes mellitus (nIR/T2DM) (n = 3)]. The results showed that the obese patients with the different co-morbidities had increased DNA damage as compared to healthy controls. Among the different co-morbidities, the insulin resistant (IR) group had the highest level of DNA damage. (Figure 45)

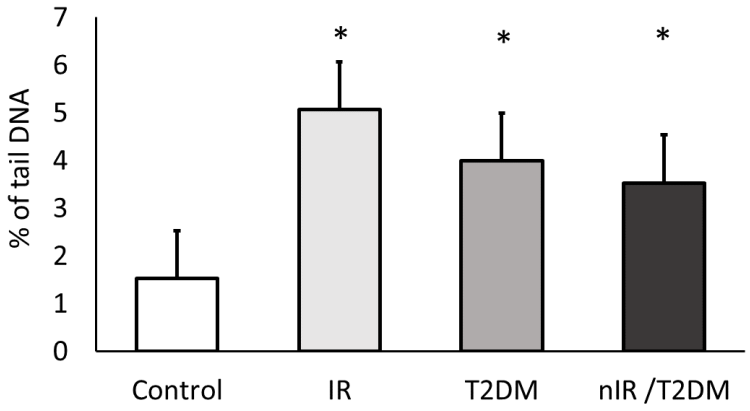

Figure 45. Genotoxicity assessment by alkaline comet assay in peripheral blood mononuclear cells of the control and obese patients with different pre-existing conditions.

*The graph shows the percentage of DNA damage detected by alkaline comet assay among the control (n = 10) and for the different pre-existing conditions such as insulin resistance (IR) (n = 6), type-2 diabetes mellitus (T2DM) (n = 4), non-insulin resistant and type-2 diabetes mellitus nIR/T2DM (n = 3). * significantly different from control with p≤.05.*

We then measured the advanced oxidative protein products (AOPP) found bound to the plasma of the healthy controls and obese patients. The results confirmed that the obese patients had a significantly higher (3.5-fold) increase in oxidative products detected in their plasma as compared to the controls (Figure 46). When we further tested this based on the co-morbidities [IR (n = 6), T2DM (n = 4), nIR/T2DM (n = 3)], we found that the sub-group with IR and nIR/T2DM had higher levels of AOPP's found in their plasma as compared to the controls (Figure 47).

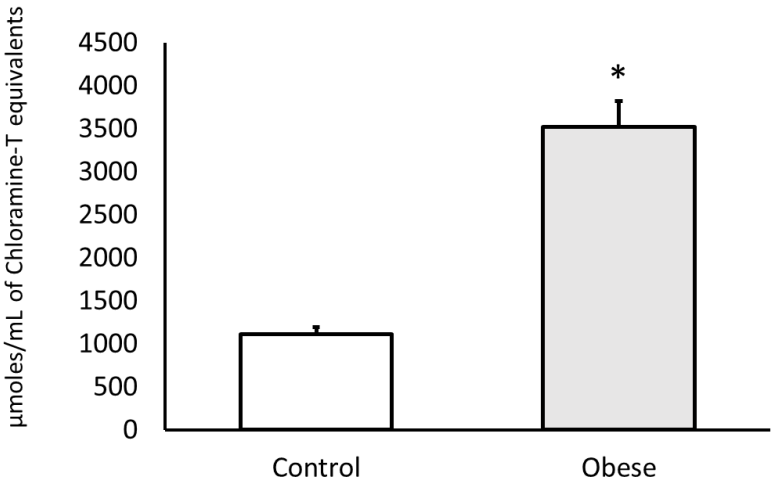

Figure 46. Detection of advanced oxidation protein products as µmoles/mL equivalents of Chloramine-T in the plasma of the control and obese patients used in this study, n = 10 and n = 27, respectively

** significantly different from control with p≤.05*

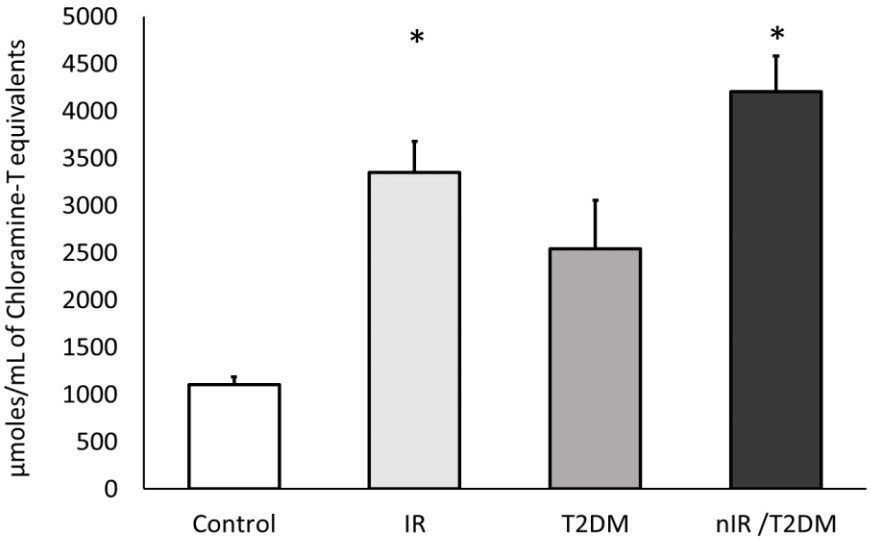

Figure 47. Detection of advanced oxidation protein products as µmoles/mL equivalents of Chloramine-T in the plasma of the control and obese patients used in this study with pre-existing conditions

*The graph shows the advanced oxidation protein products measured as µmoles/mL equivalents of Chloramine-T; control (n = 10) and for the different pre-existing conditions such as insulin resistance (IR) (n = 6), type-2 diabetes mellitus (T2DM) (n = 4), non-insulin resistant and type-2 diabetes mellitus nIR/T2DM (n = 3). * significantly different from control with p≤.05.*

5. Discussion

5.1. *In vitro* genotoxicity of insulin in combination with adrenaline

The cytokinesis block MN assay confirmed previous findings [6, 85] that both hormones - insulin and adrenaline, had a genotoxic potential at high concentrations. High non-physiological concentrations from the saturation dose range of the individual dose response relationships were chosen for a combination experiment. The simultaneous treatment of HL60 cells with insulin and adrenaline did not show any additive increase in MN induction, although the combination of insulin with the alkylating agent MMS [86], yielded an additive effect. This showed that achieving an additive response was possible in this test model. Additive increase in MN induction could be expected because of the difference in the mechanism of action between insulin and MMS, through oxidative stress induction and DNA alkylation, respectively.

The lack of additivity after the combination of insulin and adrenaline at high concentrations was hypothesized to be due to the exhaustion of an overlapping point in the intracellular signalling pathway of the two hormones. Therefore, we looked for a mechanistic overlap, and based on available literature we investigated the role of AKT, a known activator of the insulin signalling pathway [41]. With regards to adrenaline, published studies had shown that there was a cell type specific inhibitory or activating effect on AKT through the cAMP signalling pathway [25]. The results from the western blotting showed that, in the HL60 cells used here, only insulin, but not adrenaline, led to an increase of phosphorylated AKT over total AKT. The combination of insulin and adrenaline also did not induce an additive increase in AKT phosphorylation, while the combination of insulin and MMS showed an additive increase. To further investigate the potential role of AKT activation in MN induction by insulin, we combined the insulin treatment with the total AKT inhibitor MK-2206 [87] and observed a significant decrease in MN formation. Thus, AKT was involved in the insulin-induced MN formation, but was not involved in the adrenaline-induced MN formation in our test model.

Hormone signalling is known to begin at the site of the membrane bound receptors to which the hormone is bound. Therefore, we used the hormone receptor specific blockers HNMPA $(AM)_3$ and propranolol to block the insulin receptor and β-adrenergic receptor, respectively [85, 88]. This prevented the MN induction by each of the hormones. Thus, in the case of insulin, the genomic damage causing events began with its interaction to the membrane bound receptor, followed by the phosphorylation of the AKT protein and further induction of MN. Whereas in the case of adrenaline, signalling also started with the receptor-binding, but circumvented the AKT protein to cause the DNA damage. Therefore, AKT phosphorylation and activation did not represent the mechanistic overlap between the two hormones regarding the induction of MN.

Increased AKT signalling was associated with high ROS and oxidative stress [89], and previous studies had shown that oxidative stress was involved in the induction of genomic damage by both the hormones [6, 90-92]. Therefore, the antioxidant substance N-acetyl-cysteine was used to test if cellular ROS scavenging could cause a reduction in the MN formation [93]. For both the hormones, a reduction in the induction of MN was observed. Thus, we hypothesized that the ROS producing source could be the overlapping signalling part, which was exhausted by each of the hormones in its response-saturated dose range and could not produce more ROS upon application of the hormone combination.

The two most important cellular sources of this ROS production were the mitochondria and the NADPH enzyme complex (NOX) [91, 94]. Of the different NOX isoforms, the HL60 cells used here showed a predominant expression of the NOX 2 isoform [23]. To study which of the two ROS sources were crucial for the hormone-induced MN, we used rotenone (a mitochondrial complex I inhibitor) [95] and total NOX inhibitor VAS2870 (a general NOX enzyme assembly blocker) [96]. The use of rotenone caused the blockage of electron transfer from the mitochondrial complex I to the following complexes, which led to the absence of ROS leakage from the complex III. The combination of insulin and adrenaline with rotenone led to the reduction in the genomic damage, indicating that the mitochondrial ROS was involved in the

induction of MN. The combination of the hormones with VAS2870, a general NOX blocker, also effectively decreased the induction of MN. Therefore, the inhibition of the mitochondrial and NOX 2 related ROS production yielded a reduction in the MN formation.

Mitochondria and NOX were known to perform cross talk, thereby, regulating the overall cellular ROS production [33, 95]. MN tests with the mitochondrial complex III inhibitor antimycin A, which was known to cause a leakage of mitochondrial superoxide due to the blockage of electron transfer across the electron transport chain [97, 98], showed no MN formation but an increase in cytotoxicity with higher concentrations. The treatment with antimycin A may have increased the uncoupling of the mitochondria which led to the enhanced release of mitochondrial superoxide, a negatively charged reactive molecule, which further led to the mitochondrial dysfunction and affected the cellular ROS regulation through the activation of TNFα and IL-1 signalling cascades [99]. From previous studies [99], it has been observed that the mitochondrial oxidative stress affected the cellular ability to produce energy and redox signalling. Also, the increased release of mitochondrial ROS into the cytoplasm may have led to the activation of the apoptotic signalling cascade before the ROS reached the nucleus and caused the DNA damage. Therefore, the location of ROS production and mitochondrial antioxidant scavenging system could also be a reason why high levels of antimycin A stimulation did not cause an increase in genomic damage induction. At high concentrations, antimycin A may have triggered a cell death response but this confirmed that the mitochondrial ROS alone were not sufficient for the induction of micronuclei and the combination with NOX activation may be essential for ROS-mediated genomic damage induction.

From literature [91, 99], it has been known that the NOX 2 produced superoxide outside the cellular membrane, that was converted to hydrogen peroxide immediately, which could then re-enter the cell and cause DNA damage. In other cell lines, we previously demonstrated that the NOX 1 or the NOX 4, but not the NOX 2, was responsible for genomic damage induction [82, 92]. However, it could be that this effect was always produced by the predominant cellular NOX-isoform, which was the

NOX 2 isoform in the HL-60 cells. Since mitochondria could produce enough ROS for the cells to go into apoptosis, it was unlikely that each of the hormones exhausted their capacity. The more likely explanation for the non-additive effect was that the NOX 2 capacity in the HL-60 cells was exhausted by each of the hormones, pointing to the NOX 2 as the mechanistic overlap between insulin- and adrenaline-induced genomic damage.

Regarding *in vivo* physiological conditions, where the hormones are present at lower levels, it must be pointed out that the non-additivity observed here may not occur. If concentrations occurred at levels that were not already in the saturation range of the dose response relationship, their combination could cause an additive effect even if the same cellular ROS source (or other overlapping mechanism) was involved. This should be considered further for situations like T2DM, where the pancreatic β-cells could become dysfunctional and exhaust their cellular antioxidant capacity. [100] In this case, the pathophysiological concentrations of insulin and adrenaline could still lead to an additive increase in genomic damage.

5.2. Effect of PTEN inhibition on insulin induced genotoxicity

The PTEN gene was involved in the regulation of the insulin-AKT signalling pathway and its dysregulation could lead to the development of insulin resistance, obesity and cancer. Diabetic patients showed a higher risk of developing a chronic kidney disease and kidney cancer. [101] A special situation was the Cowden syndrome, which was a hereditary cancer syndrome having germline mutations in the PTEN gene leading to many cancers including renal cell carcinoma [102]. According to [103], a high fat diet induced hypersecretion of pancreatic insulin, led to hyperinsulinemia and obesity. Also, in another study [64], mice deficient in 8-oxoguanine DNA glycosylase (OGG1) (Ogg1−/−), when exposed to a high fat diet, had an increase of adiposity, hepatic steatosis, higher insulin levels and impaired glucose tolerance.

The kidney tissue of a PTEN haplodeficient knockout (Ko) mouse model and wild-type controls were available to us through a collaboration and allowed the further analysis of the PTEN relevance in the ROS-related pathways of insulin action. In addition to normal diet (ND), a high fat diet (HFD) had been applied, which was known to induce hyperinsulinemia in this C57BL/6 mice model [104, 105]. Hence, we used this high fat diet fed mouse model in our study to test for oxidative stress markers.

The results showed an increased expression of the oxidative stress protein HSP70 [106] and of the antioxidant response enzyme HO-1 [107] in the kidneys of the PTEN Ko mice, as compared to the wildtype mice. A slight increase in oxidative stress was observed between the ND and the HFD in the wildtype mice, but no such difference was observed in the PTEN Ko mice. The high fat diet group of mice, known to have signs of hyperinsulinemia and insulin resistance [108, 109], did not give any conclusive evidence of the PTEN deletion effect on oxidative stress. Overall, the results from this rodent model supported the hypothesis of PTEN being a relevant step in the signalling between insulin and oxidative stress, which could probably lead to genomic damage induction, but by itself did not provide any clear and conclusive evidence.

Therefore, we performed further experiments to test for genomic damage and oxidative stress using cultured kidney cell lines, NRK cells (rat) and pig kidney proximal

tubule LLCPK1 cells (pig). The MN tests with insulin treatment and the combination of insulin with pharmacological PTEN inhibition with VO-Ohpic in NRK cells showed a clear increase in genomic damage, when compared to the control. This showed that, before the insulin mediated MN induction went through the AKT signalling pathway, the blocking of its regulator protein PTEN led to the overactivation of AKT and caused an increase in genomic damage. This was also previously shown in the liver tissue and *in vitro* hepatic cell lines [77]. From the DHE fluorescence measurement, we detected no increase in intracellular ROS production after the pharmacological PTEN inhibition with VO-Ohpic alone and also after its combination with insulin treatment. This was probably due to the overwhelmed endogenous ROS production from the insulin treatment, and this exhaustion was known to cause a total disruption of mitochondrial function, which could lead to reduced mitochondrial ROS production and tumorigenesis. [110] TMRE staining for the mitochondrial membrane depolarization showed that the insulin treatment caused a significantly lower fluorescence, similar to the combination with VO-Ohpic. Overall, the *in vitro* results in NRK cells revealed the depletion of mitochondrial function and consequently a reduced ROS production after PTEN inhibition and insulin treatment.

Another aspect was that, both the NOX 1 and the NOX 4 enzyme-derived ROS formation regulated the PTEN function through the oxidative inhibition of AKT and increased cell proliferation, through the hyperactivation of the AKT signaling pathway [110]. For example, the dissertation work by [111] had shown that the kidney cell line HK2 expressed high levels of the NOX 2 and the NOX 4 isoforms, and the increased ROS production from the high levels of insulin treatment caused an increase in DNA oxidation damage. Similarly, in the LLCPK1 pig kidney cells, we observed a slight increase in MN number, DHE fluorescence for ROS detection and mitochondrial membrane depolarization after treatment with insulin and VO-Ohpic, as compared to the insulin treatment alone. Therefore, our results showed that the pharmacological inhibition of PTEN had an influence in the increase in insulin induced genotoxicity and the exhaustion of mitochondrial ROS production, which caused an oxidative stress mediated genomic damage induction.

The mitochondrial oxidative metabolism and insulin resistance were closely related to each other and there was evidence of a low mitochondrial oxidative capacity in T2DM and obesity [112]. Many studies had shown that chronic inflammation, T2DM and obesity were important factors in chronic kidney disease and injury [113, 114]. It was also proven that there was reduced mitochondrial activity, overall mitotic content and biogenesis in the diabetic kidney [113, 115]. The kidney tissue in humans expressed high levels of the NOX 2 and the NOX 4 isoforms, which could internally regulate the PTEN function via ROS [116]. The high insulin levels in T2DM and obesity, along with the subsequent increased ROS production could be of significant importance under the conditions of failed antioxidant scavenging defence and PTEN deletion. Especially for the *in vivo* conditions, where the physiological insulin levels could not yet be saturated, the endogenous ROS sources could still be functional and at that point, the presence of PTEN mutations of either sporadic or hereditary origin could influence the initiation of genomic damage and promotion of cancer.

In summary, we now know that the AKT signalling and its regulation via the PTEN gene had implications on the insulin-induced increase in oxidative stress and MN induction.

5.3. Effect of proliferative stress on micronucleus induction

Replicative stress could lead to MN formation if the P53 gene becomes defective [52]. The P53 gene protects the cells against oxidative stress, regulates the action of the cell cycle checkpoints and the DNA repair mechanisms and also initiates cell death response [55]. Hela cells were known to have an intact insulin signalling pathway through the cell surface insulin receptor [117] and an insulin mediated AKT phosphorylation, which had mitogenic effects [118]. In the Hela cells where the P53 gene was known to be defective [119], the addition of high concentrations of insulin led to an increase in MN formation. This MN formation occurred in addition to the ROS mediated effects, as seen in the other cell lines. This could be due to a replicative stress caused by the proliferation enhancement through insulin treatment. Therefore, high insulin levels when presented along with defective P53 conditions could lead to the increased induction of MN and the accumulation of genomic damage.

Time-lapse live cell imaging showed that insulin induced an increase in the number of MN, mitosis and multipolar mitosis as compared to the untreated control, while a reduction in the number of apoptosis was observed. The insulin treatment not only yielded an increase in the number of mitotic cells but also exhibited an increased rate of mitosis, as compared to the untreated control. The positive control MMS, known to cause DNA alkylation, led to a high MN number but a relatively lower rate of mitosis. This longer duration of the cell cycle in MMS treatment could be due to the delay in cell cycle progression, in order to allow for DNA repair action. [120] We hypothesized that the accelerated mitosis due to insulin treatment could exert a mild proliferative stress, wherein, the cell cycle checkpoints were bypassed, and the cells divided with mitotic errors, which led to MN formation and genomic instability [53]. Similar observations were reported for the stimulation of proliferation and the induction of MN by estradiol treatment of breast and ovarian cancer cell lines [121, 122].

Out of the 1000 cells scored, the insulin treated cells had the shortest duration of mitosis and MMS treated group had the longest duration of mitosis; the long mitosis duration indicated cell cycle checks (G1/G2) and DNA repair activity [123]. The shorter

duration of mitosis occurring in the insulin treated cells could be exerted by the proliferation stimulus that insulin induced in many cell types. This allowed the cells to escape the mitotic checkpoint proteins and to result in abnormal mitosis, which we observed by the increase in multipolar mitosis in the insulin treated cells. The insulin treated cells had a higher number of cells in mitosis as compared to the MMS treated ones. This indicated that during the 24h observation period, a cell had undergone cell division more than once in the insulin treated group, as compared to the MMS treated group. This further confirmed that the growth stimulatory/proliferative signal exhibited by insulin in the Hela cells added to the genomic instability observed in these cells after insulin treatment, possibly in addition to ROS mediated damage. It could also be possible that genomic damage from proliferative stress and oxidative stress were inseparable from each other, in the sense that the enhanced proliferation could be mediated by the elevated ROS formation.

The results from the short interval time-lapse imaging also showed that the insulin treated cells had a shorter duration of mitosis and a shorter time span from metaphase to anaphase, as compared to the untreated control. In addition, the insulin treated cells had a longer duration from prophase to metaphase and from anaphase to telophase. It was already known that the tumor cells had defective, but not deficient, mitotic checkpoint regulators [124]. These checkpoint regulators delayed the progression through mitosis and rectified the errors to maintain the chromosome-spindle integrity and prevent the generation of aneuploidy that facilitated carcinogenesis [124, 125].

In the insulin treated vs the untreated control cells, the high levels of ROS from insulin treatment could have led to the accelerated proliferation signal while the defective P53 caused the bypassing of the inhibitory action of the anaphase promoting complex (APC). The main role of the APC was to inhibit the progression from metaphase to anaphase before all the kinetochores were tightly bound to the spindle apparatus. Thus, insulin used a mitotic checkpoint defect and spindle impairment, to generate anaphase lag chromosomes and missegregated chromosomes, which ended up as MN and led to genomic instability. Therefore, we showed for the first time that insulin

caused a mild replicative stress on cancer cells. In the case of healthy non-cancerous cells, the functional mitotic checkpoint proteins and antioxidant defense systems could counteract these events. However, in pre-cancerous or other pathological conditions with defective cell cycle machinery (e.g., PTEN deficiency syndromes), the effect from high insulin and other hormone levels could be relevant for the development of additional genomic damage and cancer progression.

We then used the scratch wound healing assay to test the potential of insulin to increase proliferation and to induce mitosis. The wound healing was characterized by cell proliferation and migration [80]. The non-significant increase in healing (change in scratch area and width) after insulin treatment along with an increase in mitosis and MN number, showed its relevance as a growth promoter as well as an inducer of mild replicative stress leading to MN formation. When the insulin treatment was combined with an antioxidant, there was a clear reduction in MN and mitosis. This indicated the influence of insulin-induced ROS in the enhancement of proliferative signals and the induction of MN formation. The results were in line with the replicative effect observed from the live imaging experiments.

To see the influence of PTEN-related signalling in the scratch wound healing, we combined the insulin treatment with the PTEN inhibitor VO-Ohpic. The results showed a clear increase in scratch healing with insulin treatment and a reduction after treatment with VO-Ohpic. The expected outcome was that the PTEN inhibition could increase the AKT activation and ROS production, thereby, enhancing the genotoxic effect of insulin. However, both results from the scratch wound healing (change in scratch area, width, mitosis and MN number) and the above-discussed *in vitro* results from oxidative stress and mitochondrial depolarization, showed conflicting outcomes. This could be a result of overactivation of the AKT signalling pathway in Hela cells, due to the P53 defect and a pharmacological PTEN inhibition, that could have activated an alternate negative feedback regulation through the mTORC1 signalling. [126]

5.4. Genotoxic outcomes in obese patients with diabetes

The increase in genomic damage among obese patients was a consistent outcome and has been well documented [66, 68, 127]. However, the factors influencing this outcome are still under scrutiny. Oxidative stress and inflammation were commonly occurring pathologies of obesity that caused DNA repair defects and genomic instability. Different factors such as the body weight, body mass index (BMI), glycated haemoglobin (HbA1C) levels served as biomarkers in the context of obesity. Some of these biomarkers had been correlated to the genomic damage induction via MN, nucleoplasmic buds and bridges, and the development of 8-hydroxy-2'-deoxyguanosine (8-OHdG) bases [128]. Here, the results of alkaline comet assay in the PBMC's of control vs obese subjects showed a 2-fold significant increase in DNA damage. Obesity and insulin resistance (IR) are interrelated processes due to the involvement of oxidative stress and redox signalling. Chronic inflammation markers were increased during obesity and T2DM, which could lead to insulin resistance. [68, 84] The AOPP's are chronic biomarkers of plasma oxidation products especially in T2DM, which depended on oxidative/antioxidative metabolic regulation [129]. The measurement of plasma oxidation products was significantly higher in the obese patients as compared to the respective healthy controls. This outcome was consistent with the increased DNA damage observed in alkaline comet assay. Therefore, the results explained the link between oxidative stress and genotoxicity present in obesity. When we categorize the data according to the different comorbidities present in the test subjects, we found that the IR and non-insulin resistance/type-2 diabetes mellitus (nIR/T2DM) subgroups had the highest AOPP levels.

It was well-known that hyperinsulinemia and T2DM led to high HbA1c levels as compared to the controls [130]. Here, we used a cut-off level (≥6%) HbA1c, which was representative of the pre-diabetic state and diabetes, according to the American Diabetes Association. The sub-group of patients with (≥6%) HbA1c levels had a 2-fold increase in DNA damage as compared to the healthy controls. Studies had already indicated a correlation between HbA1c and oxidative stress through low antioxidant capacity and high lipid peroxidation status in diabetic individuals [131]. Despite the

elevated levels of DNA damage and oxidative stress on a group level, a correlation analysis on an individual level did not show a positive correlation between these markers and BMI or HB1Ac, which could be due to the small sample size.

We then classified the data from DNA damage according to the different comorbidities of obesity, namely insulin resistance and type 2 diabetes mellitus with or without insulin-resistance. All the sub-groups with and without insulin resistance showed increased DNA damage levels. This finding complemented our main hypothesis that high insulin levels were associated with increased DNA damage. The DNA damage in the diabetic groups were lower, which could be due to the medical treatment in these groups that may lower the insulin levels. High insulin levels were found in obese, pre- and early T2DM patients, which could lead to insulin resistance and these insulin resistant groups tend to have increased DNA damage. [127, 132] This could then contribute to the accumulation of mutations and the elevated cancer incidence in obesity.

On one hand, it explained the hypothesis that insulin resistance led to an increased oxidative stress and thereafter, higher DNA damage. On the other hand, patients without insulin resistance but with an impaired β-cell function and insulin secretion (which could lead to T2DM), also had a high risk of oxidative stress and genotoxicity. Nevertheless, in both the cases, high HbA1c levels and hyperinsulinemia could be present [133], which could increase the potential to develop oxidative stress and genomic damage. The antioxidant defense and DNA repair mechanisms were known to be altered in obesity and T2DM. [134] However, this is also a reversible damage that can improved by physical exercise, dietary intervention and weight loss in the case of obese patients [84, 135]. The overall oxidative stress and its defense are key players in determining the genotoxic outcome in obese patients. Early hyperinsulinemia and insulin resistance further increase the oxidative stress and genomic damage burden in these patients.

5.5. Conclusion

Overall, we conclude that under *in vitro* conditions, high insulin levels caused DNA damage through the induction of oxidative stress. This could have an additive effect in inducing DNA damage (under pathophysiological conditions), when presented along with other hormonal imbalances, such as high adrenaline levels, which could also cause an increase in oxidative stress and genomic damage. *In vitro* PTEN inhibition along with insulin treatment showed an increase in oxidative stress and DNA damage. In the case of diseases where the PTEN regulatory gene is mutated/deleted, a dysregulated insulin signalling could lead to the accumulation of DNA damage and increase the pre-disposition to cancer formation. Defective insulin signalling mechanism caused genomic damage through the induction of high levels of endogenous ROS and a possible replicative stress, which led to an increased micronucleus formation. Finally, obese and T2DM patients, with or without insulin resistance, showed an increase in DNA damage and plasma protein oxidation levels as compared to the healthy subjects. Thus, from our studies, we have shown that high insulin levels are in fact involved in causing DNA damage through the induction of oxidative stress and this could lead to the accumulation of deleterious mutations and cancer formation.

6. Summary

In vitro genotoxicity studies with high concentrations of insulin and its combination with adrenaline showed no additive increase in MN formation. The insulin mediated genomic damage involved mainly the insulin receptor and the AKT signaling pathway. The endogenous ROS sources, mitochondria and NOX, were involved in insulin mediated DNA damage. High levels of mitochondrial ROS alone, caused by a mitochondrial complex III inhibitor, led to cytotoxicity but not to an increase in genomic damage. The NOX enzyme mediated ROS production seemed to be the shared component of the genotoxic signaling pathway between insulin and adrenaline. The overstimulation of this NOX could have led to the saturation and lack of additivity in genomic damage induction. This could, however, be different under physiological conditions, where the hormone levels could be lower and the ROS sources are yet to be exhausted, thereby, increasing the possibility of an additive genomic damage.

The effect of AKT signaling in insulin mediated genomic damage was well established and the function of its negative regulator protein, PTEN, was studied here. The results showed that the PTEN inhibition not only caused increased genotoxicity via MN induction, but also led to the depletion of mitochondrial function. Although no actual increase in ROS was observed after PTEN inhibition, the mitochondrial dysfunction could have been sufficient to cause a metabolic imbalance and led to the increase in genomic damage. This may be particularly significant in patients with certain PTEN associated syndromes and cancers, with defective PTEN functions, such as dysfunctional tumor suppression, DNA repair and antioxidant defense mechanisms. When these patients are affected by hyperinsulinemia, it could enhance the accumulation of genomic damage and the risk of developing cancer.

The mechanism of genomic damage induction through insulin has been mostly associated with DNA oxidation but rarely through mitogenic signaling. Here the mitogenic potential of insulin along with the generated oxidative stress accelerated

the cell division, causing a mild replicative stress. This mild replicative stress could have escaped the scrutiny of the mitotic checkpoint proteins and led to mitotic errors, which ended up as lagging chromosomes and chromosome breaks. In case of cancerous Hela cells, this mitotic error could have formed the multipolar spindles and micronuclei. Under healthy conditions, the cellular defense mechanisms could counteract this effect. But high insulin mediated genomic damage presented along with other comorbidities such as PTEN syndromes, metabolic syndrome or obesity could lead to the accumulation of deleterious genomic damage.

Finally, the genotoxic outcomes studied in obese patients showed an increase in DNA damage and oxidative stress as compared to the healthy controls. The increase in DNA damage was also the highest amongst the subgroup of patients with insulin resistance. Thus, high insulin levels presented the risk of increased oxidative stress and genomic damage, especially when combined with comorbidities.

Limitations in clearly understanding these multifactorial interrelationships was the interplay of oxidative stress and its cellular regulation in many physiological, as well as pathophysiological processes. Along with this, the detection of the low effect range of the insulin mediated genomic damage was challenging. Further studies into the complex insulin mediated genomic damage pathway will be necessary to better characterize the possible risks posed by hyperinsulinemia in conditions like metabolic disease, early type 2 diabetes and obesity.

Zusammenfassung

In-vitro-Genotoxizitätsstudien mit hohen Konzentrationen von Insulin und die Kombination mit Adrenalin zeigten keinen additiven Anstieg der Mikrokernzahl. Der Insulinrezeptor und der AKT-Signalweg waren in den insulinvermittelten Genomschaden involviert. Die endogenen ROS-Quellen, Mitochondrien und NOX, waren an dem insulinvermittelten DNA-Schaden beteiligt. Hohe Konzentrationen von mitochondrialen ROS allein, verursacht durch einen Komplex III Mitochondrien-Inhibitor, führten zu Zytotoxizität, aber nicht zu einer Zunahme des Genomschadens. Daher ist die durch das NOX-Enzym vermittelte ROS-Produktion wahrscheinlich der gemeinsame Faktor des genotoxischen Signalweges von Insulin und Adrenalin. Die Überstimulation des NOX-Enzyms führte zu einer Sättigung der zellulären biologischen Effekte und fehlender Additivität bei der Induktion von Genomschaden. Dies könnte jedoch unter physiologischen Bedingungen anders sein, da die Hormonspiegel niedriger sind und die ROS-Quellen nicht durch jedes einzelne der Hormone bereits maximal genutzt und daher erschöpft werden. Damit könnte die Möglichkeit eines additiven Genomschadens *in vivo* bestehen.

Die Rolle des AKT-Signalwegs bei der Insulin-vermittelten genomischen Schädigung ist bereits etabliert und hier wurde nun die Funktion des negativen Regulatorproteins PTEN untersucht. Die Ergebnisse zeigten, dass die PTEN Inhibierung nicht nur zu einer erhöhten Genotoxizität durch MN-Induktion führte, sondern auch zur Beeinträchtigung der mitochondrialen Funktion. Obwohl kein Anstieg von ROS nach PTEN-Inhibierung beobachtet wurde, könnte die mitochondriale Dysfunktion zur metabolischen Imbalance sowie zur Zunahme des Genomschadens führen. Dies könnte insbesondere bei Patienten mit bestimmten PTEN-assoziierten Syndromen und Krebserkrankungen, die eine defekte PTEN-vermittelte Tumorsuppressorfunktion, DNA-Reparaturdefekte und kompromittierte antioxidative Abwehrmechanismen aufweisen, eine wichtige Rolle spielen. Wenn diese Patienten zusätzlich von Hyperinsulinämie betroffen sind, könnte eine Akkumulation von Genomschaden erfolgen und das Risiko zur Krebsentstehung wäre erhöht.

Der Mechanismus der Genomschadensinduktion durch Insulin wurde bisher mit einer ROS-vermittelten DNA-Oxidation in Verbindung gebracht, aber noch nicht mit der mitogenen Signalgebung. Bei dieser beschleunigte das mitogene Potential des Insulins die Zellteilung und verursachte einen leichten replikativen Stress. Der milde replikative Stress könnte der Kontrolle durch die mitotischen Checkpoint-Proteine entgehen und zu Chromosomen-Fehlverteilungen und Chromosomenbrüchen führen. Dieser Effekt wurde in der Krebszelllinie Hela in Form von multipolaren Spindeln und Mikronuklei beobachtet und es ist nicht klar ob normale Zellen mit effizienterer Kontrolle dies verhindern könnten. Insgesamt könnte ein durch hohe Insulinspiegel vermittelter Schaden im Kontext anderer Komorbiditäten wie etwa PTEN Syndromen, metabolischem Syndrom oder Adipositas zu einer Akkumulation von DNA-Schäden führen.

Schließlich zeigte die Analyse von Proben adipöser Patienten eine Zunahme von DNA-Schaden und oxidativem Stress im Vergleich zu den gesunden Kontrollen. Der Anstieg des DNA-Schadens war am höchsten in der Untergruppe der Patienten mit Insulinresistenz. Hoher Insulinspiegel bedeutet somit ein Risiko vom erhöhten oxidativen Stress und Genomschaden, insbesondere in Kombination mit Komorbiditäten.

Erschwert wird das Verständnis dieser multifaktoriellen Zusammenhänge durch das komplexe Zusammenspiel von oxidativem Stress und seiner zellulären Regulation in vielen physiologischen sowie pathophysiologischen Prozessen. Daneben ist es eine Herausforderung, Genomschäden bei den geringen Wirkspiegeln hormoneller Effekte zu detektieren. Weitere Untersuchungen der komplexen Insulin-vermittelten Genomschadenswege werden notwendig sein, um mögliche Risiken der Hyperinsulinämie bei Erkrankungen wie Stoffwechselkrankheiten, Diabetes Typ 2 und Adipositas besser zu charakterisieren.

7. Bibliography

1. Phillips, D.H. and V.M. Arlt, *Genotoxicity: damage to DNA and its consequences*, in *Molecular, Clinical and Environmental Toxicology: Volume 1: Molecular Toxicology*, A. Luch, Editor. 2009, Birkhäuser Basel: Basel. p. 87-110.
2. Luzhna, L., P. Kathiria, and O. Kovalchuk, *Micronuclei in genotoxicity assessment: from genetics to epigenetics and beyond.* Frontiers in Genetics, 2013. **4**(131).
3. Ye, C.J., et al., *Micronuclei and Genome Chaos: Changing the System Inheritance.* Genes (Basel), 2019. **10**(5).
4. Das, D. and S. Arur, *Conserved insulin signaling in the regulation of oocyte growth, development, and maturation.* Mol Reprod Dev, 2017. **84**(6): p. 444-459.
5. Yang, H.R., et al., *Obesity induced by estrogen deficiency is associated with hypothalamic inflammation.* Biochem Biophys Rep, 2020. **23**: p. 100794.
6. Djelic, N., et al., *Evaluation of cytogenetic and DNA damage in human lymphocytes treated with adrenaline in vitro.* Toxicology In Vitro, 2015. **29**(1): p. 27-33.
7. Othman, E.M., et al., *Insulin-mediated oxidative stress and DNA damage in LLC-PK1 pig kidney cell line, female rat primary kidney cells, and male ZDF rat kidneys in vivo.* Endocrinology, 2013. **154**(4): p. 1434-1443.
8. Højlund, K., *Metabolism and insulin signaling in common metabolic disorders and inherited insulin resistance.* 2014.
9. Krizanova, O., P. Babula, and K. Pacak, *Stress, catecholaminergic system and cancer.* Stress, 2016. **19**(4): p. 419-428.
10. Cheng, Z., Y. Tseng, and M.F. White, *Insulin signaling meets mitochondria in metabolism.* Trends Endocrinol Metab, 2010. **21**(10): p. 589-98.
11. Wang, Q. and T. Jin, *The role of insulin signaling in the development of β-cell dysfunction and diabetes.* Islets, 2009. **1**(2): p. 95-101.
12. Parichatikanond, W., et al., *Prolonged stimulation of β2-adrenergic receptor with β2-agonists impairs insulin actions in H9c2 cells.* Journal of Pharmacological Sciences, 2018. **138**(3): p. 184-191.
13. Mangmool, S., et al., *β-Adrenergic Receptor and Insulin Resistance in the Heart.* Biomolecules & therapeutics, 2017. **25**(1): p. 44-56.
14. Sun, F., et al., *Adrenergic DNA damage of embryonic pluripotent cells via beta2 receptor signalling.* Sci Rep, 2015. **5**: p. 15950.

15. Wachter, S.B. and E.M. Gilbert, *Beta-Adrenergic Receptors, from Their Discovery and Characterization through Their Manipulation to Beneficial Clinical Application.* Cardiology, 2012. **122**(2): p. 104-112.
16. Meyts, P.D., *The Insulin Receptor and Its Signal Transduction Network.* 2016.
17. Kahn, B.B. and J.S. Flier, *Obesity and insulin resistance.* The Journal of Clinical Investigation, 2000. **106**(4): p. 473-481.
18. Grindel, A., et al., *Oxidative Stress, DNA Damage and DNA Repair in Female Patients with Diabetes Mellitus Type 2.* PLoS One, 2016. **11**(9): p. e0162082.
19. Sergi, D., et al., *Mitochondrial (Dys)function and Insulin Resistance: From Pathophysiological Molecular Mechanisms to the Impact of Diet.* Frontiers in Physiology, 2019. **10**(532).
20. Sangwung, P., et al., *Mitochondrial Dysfunction, Insulin Resistance, and Potential Genetic Implications: Potential Role of Alterations in Mitochondrial Function in the Pathogenesis of Insulin Resistance and Type 2 Diabetes.* Endocrinology, 2020. **161**(4).
21. Lutz, W.K., et al., *Different types of combination effects for the induction of micronuclei in mouse lymphoma cells by binary mixtures of the genotoxic agents MMS, MNU, and genistein.* Toxicological Sciences, 2005. **86**(2): p. 318-23.
22. Borgert, C.J., et al., *Can mode of action predict mixture toxicity for risk assessment?* Toxicology and Applied Pharmacology, 2004. **201**(2): p. 85-96.
23. Kodandaraman, G., E.E. Bankoglu, and H. Stopper, *Overlapping mechanism of the induction of genomic damage by insulin and adrenaline in human promyelocytic HL-60 cells.* Toxicology in Vitro, 2020. **66**: p. 104867.
24. Scholze, M., E. Silva, and A. Kortenkamp, *Extending the applicability of the dose addition model to the assessment of chemical mixtures of partial agonists by using a novel toxic unit extrapolation method.* PloS one, 2014. **9**(2): p. e88808-e88808.
25. Brennesvik, E.O., et al., *Adrenaline potentiates insulin-stimulated PKB activation via cAMP and Epac: implications for cross talk between insulin and adrenaline.* Cellular Signalling, 2005. **17**(12): p. 1551-9.
26. Jensen, J., et al., *GSK-3beta regulation in skeletal muscles by adrenaline and insulin: evidence that PKA and PKB regulate different pools of GSK-3.* Cell Signal, 2007. **19**(1): p. 204-10.
27. Wang, Q., et al., *Inhibiting Insulin-Mediated β2-Adrenergic Receptor Activation Prevents Diabetes-Associated Cardiac Dysfunction.* Circulation, 2017. **135**(1): p. 73-88.
28. Sager, G., et al., *The human promyelocytic leukemia cell (HL-60 cell) beta-adrenergic receptor.* Journal of Leukocyte Biology, 1988. **44**(1): p. 41-5.

29. Di Meo, S., et al., *Role of ROS and RNS Sources in Physiological and Pathological Conditions.* Oxidative medicine and cellular longevity, 2016. **2016**: p. 1245049-1245049.
30. Hekimi, S., Y. Wang, and A. Noë, *Mitochondrial ROS and the Effectors of the Intrinsic Apoptotic Pathway in Aging Cells: The Discerning Killers!* Frontiers in genetics, 2016. **7**: p. 161-161.
31. Bhatti, J.S., G.K. Bhatti, and P.H. Reddy, *Mitochondrial dysfunction and oxidative stress in metabolic disorders — A step towards mitochondria based therapeutic strategies.* Biochimica et Biophysica Acta (BBA) - Molecular Basis of Disease, 2017. **1863**(5): p. 1066-1077.
32. Kowluru, A. and R.A. Kowluru, *Phagocyte-like NADPH oxidase [Nox2] in cellular dysfunction in models of glucolipotoxicity and diabetes.* Biochem Pharmacol, 2014. **88**(3): p. 275-83.
33. Daiber, A., et al., *Crosstalk of mitochondria with NADPH oxidase via reactive oxygen and nitrogen species signalling and its role for vascular function.* British Journal of Pharmacology, 2017. **174**(12): p. 1670-1689.
34. Morino, K., et al., *Reduced mitochondrial density and increased IRS-1 serine phosphorylation in muscle of insulin-resistant offspring of type 2 diabetic parents.* The Journal of Clinical Investigation, 2005. **115**(12): p. 3587-3593.
35. Buvelot, H., V. Jaquet, and K.-H. Krause, *Mammalian NADPH Oxidases*, in *NADPH Oxidases: Methods and Protocols*, U.G. Knaus and T.L. Leto, Editors. 2019, Springer New York: New York, NY. p. 17-36.
36. Brandes, R.P., N. Weissmann, and K. Schröder, *Nox family NADPH oxidases: Molecular mechanisms of activation.* Free Radic Biol Med, 2014. **76**: p. 208-26.
37. Chalhoub, N. and S.J. Baker, *PTEN and the PI3-kinase pathway in cancer.* Annual review of pathology, 2009. **4**: p. 127-150.
38. Keniry, M. and R. Parsons, *The role of PTEN signaling perturbations in cancer and in targeted therapy.* Oncogene, 2008. **27**(41): p. 5477-5485.
39. Molinari, F. and M. Frattini, *Functions and Regulation of the PTEN Gene in Colorectal Cancer.* Frontiers in Oncology, 2014. **3**(326).
40. Koundouros, N. and G. Poulogiannis, *Phosphoinositide 3-Kinase/Akt Signaling and Redox Metabolism in Cancer.* Frontiers in Oncology, 2018. **8**(160).
41. Osaki, M., M. Oshimura, and H. Ito, *PI3K-Akt pathway: its functions and alterations in human cancer.* Apoptosis, 2004. **9**(6): p. 667-76.
42. Hou, S.-Q., et al., *PTEN in the maintenance of genome integrity: From DNA replication to chromosome segregation.* BioEssays : news and reviews in molecular, cellular and developmental biology, 2017. **39**(10): p. 10.1002/bies.201700082.

43. Álvarez-Garcia, V., et al., *Mechanisms of PTEN loss in cancer: It's all about diversity.* Seminars in Cancer Biology, 2019. **59**: p. 66-79.
44. Gao, Y., et al., *The Role of PTEN in Chronic Growth Hormone-Induced Hepatic Insulin Resistance.* PLOS ONE, 2013. **8**(6): p. e68105.
45. Grinder-Hansen, L., et al., *A common variation of the PTEN gene is associated with peripheral insulin resistance.* Diabetes Metab, 2016. **42**(4): p. 280-4.
46. Sun, Z., et al., *Deficiency of PTEN leads to aberrant chromosome segregation through downregulation of MAD2.* Molecular medicine reports, 2019. **20**(5): p. 4235-4243.
47. Chen, C.-Y., et al., *PTEN: Tumor Suppressor and Metabolic Regulator.* Frontiers in Endocrinology, 2018. **9**(338).
48. Nakanishi, A., et al., *Link between PI3K/AKT/PTEN Pathway and NOX Proteinin Diseases.* Aging and disease, 2014. **5**(3): p. 203-211.
49. Zeman, M.K. and K.A. Cimprich, *Causes and consequences of replication stress.* Nature Cell Biology, 2014. **16**(1): p. 2-9.
50. Wilhelm, T., M. Said, and V. Naim, *DNA Replication Stress and Chromosomal Instability: Dangerous Liaisons.* Genes (Basel), 2020. **11**(6).
51. Soto, M., et al., *Chromosomes trapped in micronuclei are liable to segregation errors.* Journal of cell science, 2018. **131**(13): p. jcs214742.
52. Utani, K.-i., et al., *Emergence of micronuclei and their effects on the fate of cells under replication stress.* PloS one, 2010. **5**(4): p. e10089-e10089.
53. Wilhelm, T., et al., *Mild replication stress causes chromosome mis-segregation via premature centriole disengagement.* Nature Communications, 2019. **10**(1): p. 3585.
54. Böhly, N., M. Kistner, and H. Bastians, *Mild replication stress causes aneuploidy by deregulating microtubule dynamics in mitosis.* Cell Cycle, 2019. **18**(20): p. 2770-2783.
55. Xu, B., et al., *Oxidative stress preferentially induces a subtype of micronuclei and mediates the genomic instability caused by p53 dysfunction.* Mutation research, 2014. **770**: p. 1-8.
56. Ruan, W., H.H. Lim, and U. Surana, *Mapping Mitotic Death: Functional Integration of Mitochondria, Spindle Assembly Checkpoint and Apoptosis.* Frontiers in Cell and Developmental Biology, 2019. **6**: p. 177.
57. Venkatachalam, G., U. Surana, and M.-V. Clément, *Replication stress-induced endogenous DNA damage drives cellular senescence induced by a sub-lethal oxidative stress.* Nucleic Acids Research, 2017. **45**(18): p. 10564-10582.
58. Wassmann, K. and R. Benezra, *Mitotic checkpoints: from yeast to cancer.* Current Opinion in Genetics & Development, 2001. **11**(1): p. 83-90.

59. Gorbsky, G.J., *The mitotic spindle checkpoint.* Current Biology, 2001. **11**(24): p. R1001-R1004.
60. Sivakumar, S., J.R. Daum, and G.J. Gorbsky, *Live-cell fluorescence imaging for phenotypic analysis of mitosis.* Methods in molecular biology (Clifton, N.J.), 2014. **1170**: p. 549-562.
61. Huang, Y., M. Fenech, and Q. Shi, *Micronucleus formation detected by live-cell imaging.* Mutagenesis, 2011. **26**(1): p. 133-138.
62. Lamiquiz-Moneo, I., et al., *Genetic predictors of weight loss in overweight and obese subjects.* Scientific Reports, 2019. **9**(1): p. 10770.
63. Manna, P. and S.K. Jain, *Obesity, Oxidative Stress, Adipose Tissue Dysfunction, and the Associated Health Risks: Causes and Therapeutic Strategies.* Metabolic syndrome and related disorders, 2015. **13**(10): p. 423-444.
64. Concha Cerdá, C.S., Benjamín Climent, Antonio Vázquez, Antonio Iradi, Fátima El Amrani, Ana Bediaga, Guillermo T. Sáez, *Oxidative Stress and DNA Damage in Obesity-Related Tumorigenesis.* In: Camps J. (eds) Oxidative Stress and Inflammation in Non-communicable Diseases - Molecular Mechanisms and Perspectives in Therapeutics. 2014, Advances in Experimental Medicine and Biology: Springer, Cham.
65. Senoner, T. and W. Dichtl, *Oxidative Stress in Cardiovascular Diseases: Still a Therapeutic Target?* Nutrients, 2019. **11**(9): p. 2090.
66. Setayesh, T., et al., *Impact of obesity and overweight on DNA stability: Few facts and many hypotheses.* Mutat Res, 2018. **777**: p. 64-91.
67. Ježek, J., K.F. Cooper, and R. Strich, *Reactive Oxygen Species and Mitochondrial Dynamics: The Yin and Yang of Mitochondrial Dysfunction and Cancer Progression.* Antioxidants (Basel, Switzerland), 2018. **7**(1): p. 13.
68. Włodarczyk, M. and G. Nowicka, *Obesity, DNA Damage, and Development of Obesity-Related Diseases.* International Journal of Molecular Sciences, 2019. **20**(5): p. 1146.
69. Broedbaek, K., et al., *Urinary 8-oxo-7,8-dihydro-2'-deoxyguanosine as a biomarker in type 2 diabetes.* Free Radic Biol Med, 2011. **51**(8): p. 1473-9.
70. Van Houten, B., G.A. Santa-Gonzalez, and M. Camargo, *DNA repair after oxidative stress: current challenges.* Current opinion in toxicology, 2018. **7**: p. 9-16.
71. Saha, S. and P.E.H. Schwarz, *Impact of glycated hemoglobin (HbA1c) on identifying insulin resistance among apparently healthy individuals.* Journal of Public Health, 2017. **25**(5): p. 505-512.
72. Hayder, A.A.-A. and F.J. Herbert, *Oxidative DNA damage and obesity in type 2 diabetes mellitus.* European Journal of Endocrinology, 2011. **164**(6): p. 899-904.

73. Klisic, A., et al., *Endocan and a novel score for dyslipidemia, oxidative stress and inflammation (DOI score) are independently correlated with glycated hemoglobin (HbA(1c)) in patients with prediabetes and type 2 diabetes.* Archives of medical science : AMS, 2019. **16**(1): p. 42-50.
74. Iris F. F. Benzie, a.J.J.S., *The Ferric Reducing Ability of Plasma (FRAP) as a Measure of ‘‘Antioxidant Power’’: The FRAP Assay.* Analytical Biochemistry, 1996. **239**: p. 70–76.
75. Crowley, L.C., M.E. Christensen, and N.J. Waterhouse, *Measuring Mitochondrial Transmembrane Potential by TMRE Staining.* Cold Spring Harb Protoc, 2016. **2016**(12).
76. Chen, J., S.C. Rogers, and M. Kavdia, *Analysis of kinetics of dihydroethidium fluorescence with superoxide using xanthine oxidase and hypoxanthine assay.* Annals of biomedical engineering, 2013. **41**(2): p. 327-337.
77. Bankoglu, E.E., et al., *Role of PTEN in Oxidative Stress and DNA Damage in the Liver of Whole-Body Pten Haplodeficient Mice.* PloS one, 2016. **11**(11): p. e0166956-e0166956.
78. Dummler, B., et al., *Life with a Single Isoform of Akt: Mice Lacking Akt2 and Akt3 Are Viable but Display Impaired Glucose Homeostasis and Growth Deficiencies.* Molecular and Cellular Biology, 2006. **26**(21): p. 8042.
79. Reimann, H., H. Stopper, and H. Hintzsche, *Long-term fate of etoposide-induced micronuclei and micronucleated cells in Hela-H2B-GFP cells.* Archives of Toxicology, 2020. **94**(10): p. 3553-3561.
80. Riahi, R., et al., *Advances in Wound-Healing Assays for Probing Collective Cell Migration.* Journal of Laboratory Automation, 2012. **17**(1): p. 59-65.
81. Guntas, G., et al., *Evaluation of advanced oxidation protein products, prooxidant-antioxidant balance, and total antioxidant capacity in untreated vitiligo patients.* Ann Dermatol, 2015. **27**(2): p. 178-83.
82. Othman, E.M., A. Leyh, and H. Stopper, *Insulin mediated DNA damage in mammalian colon cells and human lymphocytes in vitro.* Mutation Research/Fundamental and Molecular Mechanisms of Mutagenesis, 2013. **745-746**: p. 34-9.
83. Cabarkapa, A., et al., *Protective effect of dry olive leaf extract in adrenaline induced DNA damage evaluated using in vitro comet assay with human peripheral leukocytes.* Toxicol In Vitro, 2014. **28**(3): p. 451-6.
84. Bankoglu, E.E., et al., *Influence of bariatric surgery induced weight loss on oxidative DNA damage.* Mutation Research/Genetic Toxicology and Environmental Mutagenesis, 2020. **853**: p. 503194.

85. Othman, E.M., H. Hintzsche, and H. Stopper, *Signaling steps in the induction of genomic damage by insulin in colon and kidney cells.* Free Radical Biology and Medicine, 2014. **68**: p. 247-57.
86. Lundin, C., et al., *Methyl methanesulfonate (MMS) produces heat-labile DNA damage but no detectable in vivo DNA double-strand breaks.* Nucleic Acids Research, 2005. **33**(12): p. 3799-811.
87. Li, Z., et al., *Combination of an allosteric Akt Inhibitor MK-2206 with etoposide or rapamycin enhances the antitumor growth effect in neuroblastoma.* Clinical Cancer Research, 2012. **18**(13): p. 3603-15.
88. Popovic, W.J., J.E. Brown, and J.W. Adamson, *The Influence of Thyroid Hormones on In Vitro Erythropoiesis: mediation by a receptor with beta adrenergic properties.* The Journal of Clinical Investigation, 1977. **60**(4): p. 907-913.
89. Schieber, M. and N.S. Chandel, *ROS function in redox signaling and oxidative stress.* Curr Biol, 2014. **24**(10): p. R453-62.
90. Loft, S. and H.E. Poulsen, *Cancer risk and oxidative DNA damage in man.* Journal of Molecular Medicine, 1996. **74**(6): p. 297-312.
91. Bedard, K. and K.-H. Krause, *The NOX Family of ROS-Generating NADPH Oxidases: Physiology and Pathophysiology.* Physiological Reviews, 2007. **87**(1): p. 245-313.
92. Othman, E.M., et al., *Insulin-mediated oxidative stress and DNA damage in LLC-PK1 pig kidney cell line, female rat primary kidney cells, and male ZDF rat kidneys in vivo.* Endocrinology, 2013. **154**(4): p. 1434-43.
93. Ezerina, D., et al., *N-Acetyl Cysteine Functions as a Fast-Acting Antioxidant by Triggering Intracellular H2S and Sulfane Sulfur Production.* Cell Chemical Biology, 2018. **25**(4): p. 447-459 e4.
94. Martin, K.R. and J.C. Barrett, *Reactive oxygen species as double-edged swords in cellular processes: low-dose cell signaling versus high-dose toxicity.* Human & Experimental Toxicology, 2002. **21**(2): p. 71-75.
95. Rathore, R., et al., *Hypoxia activates NADPH oxidase to increase [ROS]i and [Ca2+]i through the mitochondrial ROS-PKCepsilon signaling axis in pulmonary artery smooth muscle cells.* Free Radical Biology and Medicine, 2008. **45**(9): p. 1223-31.
96. Panday, A., et al., *NADPH oxidases: an overview from structure to innate immunity-associated pathologies.* Cellular and Molecular Immunology, 2015. **12**(1): p. 5-23.
97. Rieske, J.S., et al., *Factors Affecting the Binding of Antimycin A to Complex III of the Mitochondrial Respiratory Chain.* Journal of Biological Chemistry, 1967. **242**(21): p. 4888-4896.

98. Lanju, X., et al., *Induction of apoptosis by antimycin A in differentiated PC12 cell line.* Journal of Applied Toxicology, 2014. **34**(6): p. 651-7.
99. Dikalov, S., *Cross talk between mitochondria and NADPH oxidases.* Free radical biology & medicine, 2011. **51**(7): p. 1289-1301.
100. Karunakaran, U. and K.-G. Park, *A Systematic Review of Oxidative Stress and Safety of Antioxidants in Diabetes: Focus on Islets and Their Defense.* Diabetes Metab J, 2013. **37**(2): p. 106-112.
101. Habib, S.L., et al., *Diabetes and risk of renal cell carcinoma.* J Cancer, 2012. **3**: p. 42-8.
102. Shuch, B., et al., *Germline PTEN mutation Cowden syndrome: an underappreciated form of hereditary kidney cancer.* J Urol, 2013. **190**(6): p. 1990-8.
103. Mehran, Arya E., et al., *Hyperinsulinemia Drives Diet-Induced Obesity Independently of Brain Insulin Production.* Cell Metabolism, 2012. **16**(6): p. 723-737.
104. Lang, P., et al., *Effects of different diets used in diet-induced obesity models on insulin resistance and vascular dysfunction in C57BL/6 mice.* Scientific Reports, 2019. **9**(1): p. 19556.
105. Dittmann, A., et al., *High-fat diet in a mouse insulin-resistant model induces widespread rewiring of the phosphotyrosine signaling network.* Molecular systems biology, 2019. **15**(8): p. e8849-e8849.
106. Kurashova, N.A., I.M. Madaeva, and L.I. Kolesnikova, *Expression of HSP70 Heat-Shock Proteins under Oxidative Stress.* Advances in Gerontology, 2020. **10**(1): p. 20-25.
107. Araujo, J., M. Zhang, and F. Yin, *Heme Oxygenase-1, Oxidation, Inflammation, and Atherosclerosis.* Frontiers in Pharmacology, 2012. **3**: p. 119.
108. Yuzefovych, L.V., et al., *Mitochondrial DNA damage and dysfunction, and oxidative stress are associated with endoplasmic reticulum stress, protein degradation and apoptosis in high fat diet-induced insulin resistance mice.* PLoS One, 2013. **8**(1): p. e54059.
109. Fraulob, J.C., et al., *A Mouse Model of Metabolic Syndrome: Insulin Resistance, Fatty Liver and Non-Alcoholic Fatty Pancreas Disease (NAFPD) in C57BL/6 Mice Fed a High Fat Diet.* J Clin Biochem Nutr, 2010. **46**(3): p. 212-23.
110. Helfinger, V. and K. Schröder, *Redox control in cancer development and progression.* Molecular Aspects of Medicine, 2018. **63**: p. 88-98.
111. Sholkamy, E.M.O., *<Diss_Eman_Maher.pdf>*.
112. Goodpaster, B.H., *Mitochondrial deficiency is associated with insulin resistance.* Diabetes, 2013. **62**(4): p. 1032-1035.

113. Sharma, K., *Obesity and Diabetic Kidney Disease: Role of Oxidant Stress and Redox Balance.* Antioxidants & redox signaling, 2016. **25**(4): p. 208-216.
114. Irazabal, M.V. and V.E. Torres, *Reactive Oxygen Species and Redox Signaling in Chronic Kidney Disease.* Cells, 2020. **9**(6).
115. Abhijit, S., et al., *Hyperinsulinemia-induced vascular smooth muscle cell (VSMC) migration and proliferation is mediated by converging mechanisms of mitochondrial dysfunction and oxidative stress.* Mol Cell Biochem, 2013. **373**(1-2): p. 95-105.
116. Sedeek, M., et al., *NADPH oxidases, reactive oxygen species, and the kidney: friend and foe.* Journal of the American Society of Nephrology : JASN, 2013. **24**(10): p. 1512-1518.
117. Anne L. Frattali, J.L.T., and Jeffrey E. Pessine, *Transmembrane Signaling by the Human Insulin Receptor Kinase.* The Journal of Biological Chemistry, 1992. **267**(September 25): p. 19521-19528.
118. Nagarajan, A., et al., *MARCH1 regulates insulin sensitivity by controlling cell surface insulin receptor levels.* Nature communications, 2016. **7**: p. 12639-12639.
119. Ajay, A.K., A.S. Meena, and M.K. Bhat, *Human papillomavirus 18 E6 inhibits phosphorylation of p53 expressed in HeLa cells.* Cell & Bioscience, 2012. **2**(1): p. 2.
120. Robertson, A.B., et al., *DNA repair in mammalian cells: Base excision repair: the long and short of it.* Cell Mol Life Sci, 2009. **66**(6): p. 981-93.
121. Stopper, H., et al., *Increased cell proliferation is associated with genomic instability: elevated micronuclei frequencies in estradiol-treated human ovarian cancer cells.* Mutagenesis, 2003. **18**(3): p. 243-247.
122. Fischer, W.H., et al., *Increased formation of micronuclei after hormonal stimulation of cell proliferation in human breast cancer cells.* Mutagenesis, 2001. **16**(3): p. 209-212.
123. Barnum, K.J. and M.J. O'Connell, *Cell cycle regulation by checkpoints.* Methods in molecular biology (Clifton, N.J.), 2014. **1170**: p. 29-40.
124. Kops, G.J.P.L., B.A.A. Weaver, and D.W. Cleveland, *On the road to cancer: aneuploidy and the mitotic checkpoint.* Nature Reviews Cancer, 2005. **5**(10): p. 773-785.
125. Lara-Gonzalez, P., Frederick G. Westhorpe, and Stephen S. Taylor, *The Spindle Assembly Checkpoint.* Current Biology, 2012. **22**(22): p. R966-R980.
126. Manning, B.D. and A. Toker, *AKT/PKB Signaling: Navigating the Network.* Cell, 2017. **169**(3): p. 381-405.
127. Bankoglu, E.E., et al., *Decreased Chromosomal Damage in Lymphocytes of Obese Patients After Bariatric Surgery.* Sci Rep, 2018. **8**(1): p. 11195.

128. Donmez-Altuntas, H., et al., *Evaluation of chromosomal damage, cytostasis, cytotoxicity, oxidative DNA damage and their association with body-mass index in obese subjects.* Mutation Research/Genetic Toxicology and Environmental Mutagenesis, 2014. **771**: p. 30-36.
129. Piwowar, A., M. Knapik-Kordecka, and M. Warwas, *AOPP and its relations with selected markers of oxidative/antioxidative system in type 2 diabetes mellitus.* Diabetes Research and Clinical Practice, 2007. **77**(2): p. 188-192.
130. Bennett, C.M., M. Guo, and S.C. Dharmage, *HbA1c as a screening tool for detection of Type 2 diabetes: a systematic review.* Diabetic Medicine, 2007. **24**(4): p. 333-343.
131. Palem, S.P. and P. Abraham, *A Study on the Level of Oxidative Stress and Inflammatory Markers in Type 2 Diabetes Mellitus Patients with Different Treatment Modalities.* Journal of clinical and diagnostic research : JCDR, 2015. **9**(9): p. BC04-BC7.
132. Othman, E.M., et al., *Metformin Protects Kidney Cells From Insulin-Mediated Genotoxicity In Vitro and in Male Zucker Diabetic Fatty Rats.* Endocrinology, 2016. **157**(2): p. 548-59.
133. Gerich, J.E., *Insulin Resistance Is Not Necessarily an Essential Component of Type 2 Diabetes1.* The Journal of Clinical Endocrinology & Metabolism, 2000. **85**(6): p. 2113-2115.
134. Picu, A., et al., *Markers of Oxidative Stress and Antioxidant Defense in Romanian Patients with Type 2 Diabetes Mellitus and Obesity.* Molecules, 2017. **22**(5).
135. Bankoglu, E.E., et al., *Decreased Chromosomal Damage in Lymphocytes of Obese Patients After Bariatric Surgery.* Scientific reports, 2018. **8**(1): p. 11195-11195.

Acknowledgements

With palms together, I would like to extend my gratitude to all my colleagues, friends and family for enabling me in completing this doctoral dissertation successfully.

My sincere thanks to Prof. Dr. Helga Stopper for giving me a platform to nurture my research interest in Genetic Toxicology. Opportunity being the key to success, I am ever thankful to you for having the confidence in me and guiding me in developing my knowledge and career in Science. You have been so friendly and patient with me throughout the project, and your professional demeanour has been a good learning experience. I am truly happy to have been a part of your working group. Not only did you give me a chance to learn, but also showed me a way to present the knowledge acquired through international conferences and helped me gain some valuable contacts in the field of Toxicology.

Thank you Dr. Ezgi Eylül Bankoglu (Eylül), for your indispensable support from the time I started at our lab. You have helped me in understanding concepts and learning new techniques. Your amicable and encouraging spirit made it a wonderful learning experience, I thank you very much. Every morning coffee and the deep discussions about Science and beyond, truly made it a lively working environment.

I would like to thank the members of the thesis committee (Prof. Dr. Thomas Haaf and Dr. Robert Hock) for the productive and interesting scientific discussions.

I thank all my colleagues in the lab and at the institute who helped me with my work and enabled the successful completion of this doctoral dissertation work. Thank you, Jonas, Hauke, Heike, Emily, Jana, Lea, Katharina, Franziska, Vanessa, Johanna for the friendly and lively work environment. Thank you, Gaby (Frau. Gabriele Curtaz-Wolz), for taking interest and making me speak in German and offering support during my time in the lab and afterwards.

A big thanks to my family for your support and encouragement. Thank you, Uncle, Aunty and Ranju for being there and encouraging me at every milestone of this work.

Raahul, your moral support and love is my constant lifeline. Last but never the least to my parents, Mrs. Mythili and Mr. Kodandaraman, I dedicate this work to you. I will always try my best to live up to your expectations and fulfil your dreams. Dad be with me always and guide me through.

Thank you

Appendix

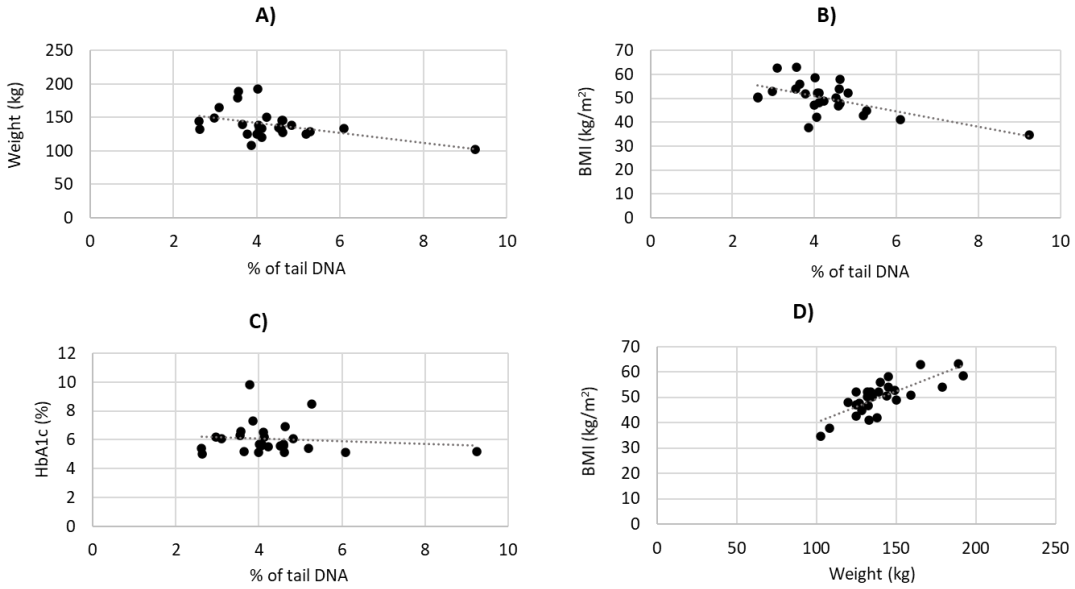

Figure 48. Correlation analysis performed in obese patients between:

A) the body weight and the percentage of DNA damage

B) the body mass index (BMI) and the percentage of DNA damage

C) the percentage of glycated hemoglobin (HbA1c) levels in the blood and the DNA damage

D) the body weight and body mass index (BMI).

The number of subjects tested is 27. Statistical test information given below in Table 3.

	Number of subjects	**Correlation coefficient**	**Remarks**	**P-value**	
Weight [kg] vs DNA damage	n = 27	-0.447	negative correlation	0.0193	*
BMI vs DNA damage	n = 27	-0.594	negative correlation	0.0011	*
HbA1c vs DNA damage	n = 27	-0.110	negative correlation	0.5850	
BMI vs HbA1c	n = 27	0.010	no correlation	0.9597	
Weight [kg] vs BMI	n = 27	0.773	positive correlation	0.0000	*

Table 4. Correlation analysis performed between the physiological characteristics and the DNA damage levels among the obese patients used in the human study.

*The number of subjects used is 27. * Statistically significant correlation with p≤.05*

Permissions for the use of published data in this dissertation

I. Permission acquired from the journal to use contents of the research article published in the journal Toxicology in vitro for the paper: **G. Kodandaraman**, E. E. Bankoglu and H. Stopper (2020). "Overlapping mechanism of the induction of genomic damage by insulin and adrenaline in human promyelocytic HL-60 cells." Toxicology in Vitro 66: 104867

Dear Geema Kodandaraman,

We hereby grant you permission to reprint the material below at no charge in your thesis subject to the following conditions:

1. If any part of the material to be used (for example, figures) has appeared in our publication with credit or acknowledgement to another source, permission must also be sought from that source. If such permission is not obtained, then that material may not be included in your publication/copies.

2. Suitable acknowledgment to the source must be made, either as a footnote or in a reference list at the end of your publication, as follows:

“This article was published in Publication title, Vol number, Author(s), Title of article, Page Nos, Copyright Elsevier (or appropriate Society name) (Year).”

3. Your thesis may be submitted to your institution in either print or electronic form.

4. Reproduction of this material is confined to the purpose for which permission is hereby given.

5. This permission is granted for non-exclusive world English rights only. For other languages please reapply separately for each one required. Permission excludes use in an electronic form other than submission. Should you have a specific electronic project in mind please reapply for permission.

6. As long as the article is embedded in your thesis, you can post/share your thesis in the University repository.

7. Should your thesis be published commercially, please reapply for permission. This includes permission for the Library and Archives of Canada to supply single copies, on demand, of the complete thesis. Should your thesis be published commercially, please reapply for permission.

This includes permission for UMI to supply single copies, on demand, of the complete thesis. Should your thesis be published commercially, please reapply for permission.

8. Posting of the full article/ chapter online is not permitted. You may post an abstract with a link to the Elsevier website www.elsevier.com, or to the article on ScienceDirect if it is available on that platform.

Regards,
Kaveri

ELSEVIER | Permissions Granting Team

II. Permission acquired from the journal to use contents of the research article published in the journal Mutation Research/Genetic Toxicology and Environmental Mutagenesis for the paper:
Bankoglu, E. E., J. Gerber, **G. Kodandaraman**, F. Seyfried and H. Stopper (2020). "Influence of bariatric surgery induced weight loss on oxidative DNA damage." Mutation Research/Genetic Toxicology and Environmental Mutagenesis 853: 503194

Dear Geema Kodandaraman,

Thank you for your query.

Please note that, as one of the authors of this article, you retain the right to reuse it in your thesis/dissertation. You do not require formal permission to do so. You are permitted to post this Elsevier article online if it is embedded within your thesis. You are also permitted to post your Author Accepted Manuscript online.

However, posting of the final published article is prohibited.

"As per our Sharing Policy, authors are permitted to post the Accepted version of their article on their institutional repository – as long as it is for internal institutional use only.

It can only be shared publicly on that site once the journal-specific embargo period has lapsed. For a list of embargo periods please see: Embargo List.

You are not permitted to post the Published Journal Article (PJA) on the repository."

Please feel free to contact me if you have any queries.

Regards,
Kaveri

ELSEVIER | Permissions Granting Team

Publications

Publications relevant for the thesis

1. **G. Kodandaraman**, E. E. Bankoglu and H. Stopper (2020). "Overlapping mechanism of the induction of genomic damage by insulin and adrenaline in human promyelocytic HL-60 cells." Toxicology in Vitro 66: 104867
2. Bankoglu, E. E., J. Gerber, **G. Kodandaraman**, F. Seyfried and H. Stopper (2020). "Influence of bariatric surgery induced weight loss on oxidative DNA damage." Mutation Research/Genetic Toxicology and Environmental Mutagenesis 853: 503194

Other publications

3. M. Naseem, E. Othman, F. AlRemeithi, **G.Kodandaraman**, H. Stopper, E. Bencurova, D. Vlachakis, T. Dandekar, M. Fathy, J. Iqbal, F. Howari (2020). "Integrated structural and functional analysis of the protective effects of kinetin against oxidative stress in mammalian cellular systems." Scientific Reports, July. (accepted)
4. Bankoglu, E. E., **G. Kodandaraman** and H. Stopper (2019). "A systematic review of the use of the alkaline comet assay for genotoxicity studies in human colon-derived cells." Mutation Research/Genetic Toxicology and Environmental Mutagenesis 845: 402976

CV / Resume

Affidavit

I hereby confirmed that my thesis entitled “Influence of insulin-induced oxidative stress in genotoxicity and disease” is the result of my own work. I did not receive any help or support from commercial consultants. All sources and / or materials applied are listed and specified in the thesis.

Furthermore, I confirm that this thesis has not yet been submitted as part of another examination process neither in identical nor in similar form.

Wuerzburg, 2021 Geema Kodandaraman